University of Pardubice

Faculty of Chemical Technology

Department of Physical Chemistry

Nucleation and Crystal Growth in Chalcogenide Amorphous Materials

DOCTORAL THESIS

Author: Ing. Simona Martinková

Supervisor: prof. Ing. Jiří Málek, DrSc.

Supervisor specialist: Ing. Jana Shánělová, Ph.D.

2018

I hereby declare:

This thesis was prepared separately. All the literary sources and the information I used in the thesis are listed in the bibliography. I got familiar with the fact that the rights and obligations arising from the Act No. 121/2000 Coll., Copyright Act, apply to my thesis, especially with the fact that the University of Pardubice has the right to enter into a license agreement for use of this thesis as a school work pursuant to § 60, Section 1 of the Copyright Act, and the fact that should this thesis be used by me or should a license be granted for the use to another entity, the University of Pardubice is authorized to claim a reasonable contribution from me to cover the costs incurred during making of the thesis, according to the circumstances up to the actual amount thereof. I am aware that my thesis will be accessible to the public in the University Library and via the Digital Library of the University of Pardubice in agreement with the article 47b of the Act No. 111/1998 Coll., on Higher Education Institutions, and on the Amendment and Supplement to some other Acts (the Higher Education Act), as subsequently amended, and with the University Pardubice's directive no. 9/2012.

In Pardubice on 5 August 2018

I would like to thank to my supervisor Professor Jiří Málek for his patience, valuable advice and help during my study. I really appreciate the opportunity for a yearlong stay in National Institute for Material Science (NIMS, Japan), that he gave me.

I would like to express my gratitude to Dr. Hiroyo Segawa (NIMS, Japan) and her coworkers for the opportunity to operate interesting apparatuses (SEM, XRD), support, guidance and hospitality during my stay in NIMS. Part of my presented work was supported by International Cooperative Graduate Program between University of Pardubice and NIMS.

I would like to thank to my supervisor specialist and other colleagues from Málek group for their scientific help, fruitful discussions and friendship.

And last but not least, I thank to my boyfriend Jan and my family for their patience and support during my studies.

Annotation

The presented doctoral thesis deals with the study of nucleation and crystal growth in chalcogenide glasses. Although a lot of papers have been published about nucleation and crystal growth during past decades and many theories have been suggested, there is still a need for more information about these complicated processes in chalcogenide glasses, in particular with respect to their indispensable technological applications. It should be noted that the essential portion of the present knowledge on nucleation in glasses comes from the studies in oxide glasses. This thesis extends the understanding of crystal nucleation and growth behavior in chalcogenide glasses. The thesis consists from 5 papers supplemented with the theoretical insight into the crystallization process and the summary of main goals of the work.

The first objective of the thesis was the study of nucleation kinetics in chalcogenide glass and testing of the applicability of so far proposed theories and their improvements for description of steady-state and transient nucleation. The study on nucleation was performed in $Ge_{1.8}Sb_{36.8}S_{61.4}$ thin films of 1 μm thickness using isothermal in-situ annealing and optical microscopy. The time evolution of nuclei number at different temperatures revealed transient behavior, which was described by Shneidman theory that provides values of steady-state nucleation rate, induction period and time-lag. The nucleation rate data were discussed in terms of classical nucleation theory (CNT). Some predictions and improvements of CNT were tested and applied.

The second objective of the thesis was the extension of studies on crystal growth kinetics in chalcogenide glasses using direct (optical and electron microscopy) and indirect (X-ray diffraction, differential scanning calorimetry, thermomechanical analysis) analytical methods. The combination of more approaches gave better insight into the crystal growth process. The studies were performed in both, bulk glasses and thin films, for the following glassy systems: Se-Te, Ge-Sb-Se and As-Se. The results were described on the basis of standard and corrected growth models.

Keywords: nucleation, crystal growth, chalcogenide glass, microscopy, CNT, crystal growth models

Annotation in Czech

Předložená disertační práce se zabývá studiem nukleace a růstu krystalů v chalkogenidových sklech. Ačkoli již bylo během uplynulých desetiletí publikováno mnoho prací zabývajících se nukleací a růstem krystalů a mnoho teorií bylo navrženo, nadále přetrvává potřeba získání více informací o těchto komplikovaných procesech a to s ohledem na nepostradatelné technologické aplikace chalkogenidových skel. Je důležité zmínit, že převážná část doposud známých znalostí o nukleaci pochází ze studií prováděných na oxidických sklech. Tato disertační práce obsahuje další poznatky o nukleaci a růstu krystalů v chalkogenidových sklech. Práce se skládá z pěti článků, které jsou doplněny teorií týkající se krystalizace a souhrnem hlavních cílů.

Prvním cílem disertační práce bylo studium kinetiky nukleace v chalkogenidovém skle a ověření platnosti doposud navržených teorií a jejich zlepšení pro popis ustálené a neustálené nukleace. Nukleace byla studována v tenkých vrstvách systému $Ge_{1.8}Sb_{36.8}S_{61.4}$ o tloušťce 1 μm za pomoci isotermních in-situ temperací a optického mikroskopu. Závislost počtu nukleí na čase pro různé temperační teploty odhalila neustálené chování, které bylo popsáno Shneidmanovou teorií za účelem získání hodnot ustálené rychlosti nukleace, indukční doby a časového zpoždění (tzv. time-lag). Nukleační data byla popsána pomocí klasické nukleační teorie (CNT). Některé předpoklady a vylepšení klasické nukleační teorie byly testovány a aplikovány.

Druhým cílem disertační práce bylo rozšíření a pokračování ve studiu kinetiky růstu krystalů v chalkogenidových sklech pomocí přímých (optická a elektronová mikroskopie) a nepřímých (rentgenová difrakce, diferenciální skenovací kalorimetrie, termomechanická analýza) metod. Kombinací více přístupů je možné získat lepší náhled na proces růstu krystalů. Studie zahrnující jak objemová skla, tak tenké vrstvy byly provedeny v systémech: Se-Te, Ge-Sb-Se a As-Se. Výsledky byly popsány na základě standardních a korigovaných růstových modelů.

Klíčová slova: nukleace, růst krystalů, chalkogenidové sklo, mikroskopie, CNT, růstové modely

LIST OF PAPERS

Paper I

Transient Nucleation in Ge-Sb-S Thin Films

S. Martinková, J. Shánělová, J. Barták, J. Málek

Cryst. Growth Des. **18** (2018) 4562 – 4570.

Paper II

Crystal Growth Kinetics in Se-Te Bulk Glasses

J. Barták, S. Martinková, J. Málek

Cryst. Growth Des. **15** (2015) 4287 – 4295.

Paper III

Crystal Growth in $Se_{70}Te_{30}$ Thin Films Followed by SEM and In Situ XRD

S. Martinková, J. Barták, J. Málek, H. Segawa

J. Appl. Phys. **120** (2016) 145301-1 – 145301-7.

Paper IV

Extended Study on Crystal Growth and Viscosity in Ge-Sb-Se Bulk Glasses and Thin Films

S. Martinková, J. Barták, P. Košťál, J. Málek, H. Segawa

J. Phys. Chem. B **121** (2017) 7978 – 7986.

Paper V

Crystal Growth Velocity in As_2Se_3 Supercooled Liquid

J. Málek, J. Shánělová, S. Martinková, P.Pilný, P. Košťál

Cryst. Growth Des. **17** (2017) 4990 – 4999.

TABLE OF CONTENTS

SYMBOLS

A_0	interface area of growing crystal
A_N	pre-exponential term of the equation for the steady-state homogeneous nucleation rate
C, Z	parameters of 2D surface nucleated growth model
c_1, c_2	shape factors of evolving nucleus
D	effective diffusion coefficient
E_1	exponential integral
E_G	activation energy of crystal growth
f	fraction of preferred growth sites at the interface
h	Planck constant
I	nucleation rate
$I(t)$	non-steady-state nucleation rate
I_{st}	steady-state nucleation rate
k	constant involving concentration terms
K	rate constant
k_B	Boltzmann constant
m	Avrami exponent
m_η	fragility
N	number of nuclei
n_S	number of structural units in contact with the catalyzing surface
N_S	number of formula units per unit area of interface
n_V	number of structural units per unit volume
q	cooling rate
r	radius of nucleus
R	gas constant
r^*	size of critical nucleus
T	temperature
t	time
T_D	development temperature
T_g	glass transition temperature

$t_i(r)$	size-dependent "relaxation time" which is defined as the time when the nucleation rate has reached 1/e of its steady-state value
t_{ind}	induction period
T_m	temperature of melting
T_{max}	temperature where nucleation rate is maximum
T_N	nucleation temperature
T_p	temperature of crystallization peak on DSC/DTA curve
u	crystal growth rate
u_{kin}	kinetic part of crystal growth rate
U_R	reduced crystal growth rate
V_m	molar volume
W	work of nucleus formation
W^*	thermodynamic barrier for nucleation
W^*_{het}	thermodynamic barrier for heterogeneous nucleation
α	crystallized fraction
γ	Euler's constant
Γ	gamma function
ΔC_p	heat capacity difference between supercooled liquid and crystalline phase
ΔG	thermodynamic driving force for crystallization
ΔG_D	kinetic barrier for nucleation
ΔH_m	melting enthalpy
ΔS_m	melting entropy
ΔT	undercooling
η	viscosity
θ	wetting angle
λ	size of structural unit; diameter of the diffusing molecules; jump distance
ξ	kinetic exponent expresses the extent of decoupling between crystal growth rate and viscosity
σ	crystal-liquid surface energy
τ	time-lag in nucleation
ϕ	parameter depending on the value of wetting angle

ABBREVIATIONS

C-K equation	Collins-Kashchiev equation
CNT	classical nucleation theory
DSC	differential scanning calorimetry
DTA	differential thermal analysis
E equation	Eyring equation
EM	electron microscopy
JMA model	Johnson-Mehl-Avrami nucleation-growth model
OM	optical microscopy
PCM	phase-change memory
SE equation	Stokes-Einstein equation
SEM	scanning electron microscopy
SPM	scanning probe microscopy
TEM	transmission electron microscopy
TMA	thermomechanical analysis
XRD	X-ray diffraction analysis

1 GLASS

Glasses are important materials for modern technology, however, they have been known for centuries. Most people associate the word "glass" with traditional oxide glasses but there are also some relatively novel inorganic and organic glasses, such as chalcogenide ones. Chalcogenide glasses are non-oxide materials which contain one or more of the chalcogen elements: S, Se, or Te. Researchers are interested in glassy alloys of chalcogen elements due to their unique structural, electronic, optical and thermal properties and hence technologically attractive applications. Chalcogenide glasses are good transmitters in the infrared spectral region (3-20 μm), they are bandgap semiconductors and have high refractive index[1]. These heavy-anion glasses (S, Se, Te) are generally less mechanically strong, less thermally stable and more weakly bonded materials than the more familiar oxide glasses[2]. The last named property is reflected in the possibility of light-induced changes such as photocrystallization and photopolymerization.

Chalcogenide glasses allow the fabrication of molded optics for infrared cameras and fibers. Such optical components are used in thermal imaging systems or integrated optical waveguides devices for laser power delivery, temperature sensors, chemical sensing, medical diagnostics and telecommunications[1,3,4]. These applications call for the perfect and stable glass, where it is essential to avoid the crystallization process. Another important property of chalcogenide glasses is the difference in either optical reflectivity and/or electrical resistivity between the amorphous and crystalline states[5]. This is utilized in phase-change memories that store information in the amorphous and crystalline phases by reversible switching between the phases, using an appropriate external voltage or laser pulse[6-8]. The requirements for phase-change memory such as optical and electrical contrast, fast crystallization and high crystallization temperature are fulfilled by some chalcogenide glasses. Novel phase-change materials with higher switching speed and data transfer are still investigated. The last important product of chalcogenide glasses is glass-ceramics, which can be obtained by controlled nucleation and crystal growth[9,10]. Glass-ceramics is a modern material composed of one or more glass and crystal phases with low or zero thermal expansion, high mechanical strength and chemical durability, which finds the use in nose cones of high-performance aircraft, mirrors of astronomical telescopes, household market (cooktops, cookware), medical applications, just to name a few.

Although many studies on structural ordering, thermal properties and nucleation and crystal growth in chalcogenide glasses have been performed, there is still a need for more detailed information.

1.1 DEFINITION AND FORMATION OF GLASS

Researchers proposed several different definitions of glass in past decades[11]. One of the recent detailed definitions of glass published by Zanotto and Mauro is[11]: "*Glass is a nonequilibrium, non-crystalline condensed state of matter that exhibits a glass transition. The structure of glasses is similar to that of their parent supercooled liquids, and they spontaneously relax toward the supercooled liquid state. Their ultimate fate, in the limit of infinite time, is to crystallize."*

Glass can be theoretically prepared from any kind of material provided sufficiently high cooling rate of liquid[12]. In order to avoid the crystallization, the cooling rate must be high enough to ensure negligible nucleation or crystal growth. The temperature dependence of liquid's volume which can crystallize and form a glass is depicted in Figure 1. Crystallization can occur if the liquid is cooled below the temperature of melting T_m with low cooling rate. In such case, the slow cooling results in the molecules being rearranged into the regular crystalline structure. Crystallization is the first-order phase transition which usually results in a decrease in volume. In the case when the cooling rate is high enough so that the nucleation and crystal growth are avoided, the uncrystallized liquid-like material below T_m is called supercooled liquid. Further cooling of supercooled liquid is accompanied by slowing-down of viscous flow and thus inhibiting the molecular motions. At certain temperature the molecules move so slowly that they cannot rearrange into adequate configurations in the available time allowed by the cooling rate. The resulting structure of material which appears "frozen" in comparison with the laboratory timescale is denoted as glass. This transformation is manifested in the temperature dependence of volume's liquid as a continuous slow-down of the dV/dT dependence, which occurs in a narrow range of temperatures. Temperature corresponding to the intersection of extrapolated temperature dependences of volume in glassy and supercooled liquid states is called the glass transition temperature T_g. As can be seen in Figure 1, the glass transition temperature changes with cooling rate. The faster the liquid is cooled, the shorter time for molecular rearrangement is available, and hence the falling out of liquid-state equilibrium occurs at higher temperatures. Although the glass transition temperature is different for different cooling rates, the dependence of T_g on cooling rate is weak (the change in cooling rate by an order of magnitude results in the change of T_g by 3 – 5 °C) and therefore T_g is an important material characteristic[13,14].

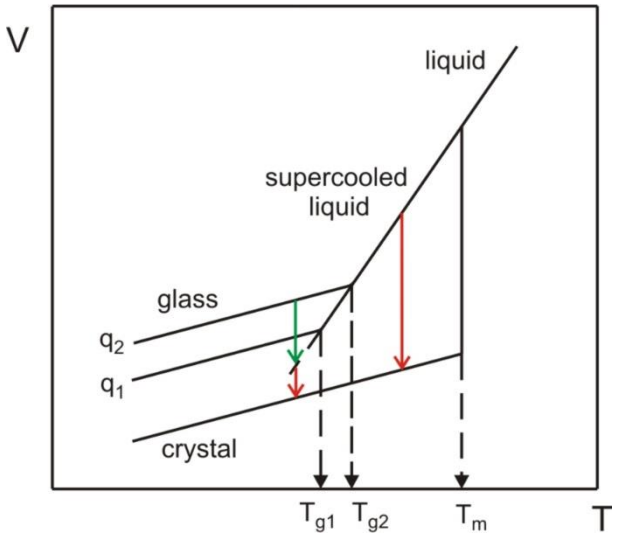

Figure 1: The dependence of liquid's volume on temperature. A slower cooling rate q_1 leads to a glass transition at T_{g1}, a faster cooling rate q_2 results in a glass transition at T_{g2}.

From the thermodynamic point of view[11], glass is an unstable state which over longer times spontaneously relaxes towards equilibrium. It is usually assumed that such equilibrium corresponds to the extrapolated supercooled liquid state (indicated by the green arrow in Figure 1). Finally, upon heating or at infinitely long times at any nonzero temperature, most glasses pass into the thermodynamically stable crystal state for $T < T_m$ (red arrow in Figure 1). The supercooled liquid is a metastable state, nevertheless if no nuclei are present, it can be considered an equilibrium state. A thermodynamic barrier exists, that is necessary to be overcome so that the nucleation event can occur. The supercooled liquids also tend to crystallize after certain time at any positive temperature (red arrows in Figure 1).

2 CRYSTALLIZATION

The importance of the study of crystallization mechanism and kinetics in chalcogenide amorphous materials arises from their applications such as optical and optoelectronic devices[15], glass-ceramics[9,10] and phase-change memories (PCM)[6]. On one hand, for many of these applications it is required to obtain perfect, stable, crystallization resistant glass and, on the other hand, there is also a need for controlled crystallization (glass-ceramics) and fast switching between amorphous and crystalline phases (PCM).

Crystallization is a process which results in the rearrangement of liquid or amorphous structure into the regular crystalline structure. The crystallization process involves two steps:

- Nucleation
- Crystal Growth.

At first the nucleation barrier must be overcome, hence the stable nuclei of critical size are formed and are capable of a further growth.

2.1 NUCLEATION

The first step of crystallization, the nucleation process, involves the formation of precursors of the crystalline phase which is connected with the overcoming of a potential barrier by thermal fluctuations. The process of nucleation may occur by different mechanisms which are commonly divided into[16]:

- Homogeneous – nuclei are formed stochastically with the same probability in volume (surface) of sample. The number of nuclei in non-crystalline sample volume increases with time.
- Heterogeneous – nucleation occurs at preferred places such as preexisting nuclei, impurities, defects. The number of nuclei is constant with time.

Depending on the position where nucleation takes place, one can distinguish volume and surface crystallization.

The classical nucleation theory (CNT), which is frequently used for the analysis of crystal nucleation in glass-forming liquids, is based on the thermodynamic description of heterogeneous systems evolved by Gibbs[17]. He was first to realize that the formation of new phase requires as a prerequisite the existence of small clusters of building units in the volume of ambient phase (vapor, melt, solution) and considered the properties of nuclei and corresponding bulk phase to be the same[18]. Volmer and Weber[19] constructed the first complete theory of nucleation by using Gibb's idea. Becker and Döring[20] argued that the equilibrium

distribution, which was chosen by Volmer and Weber, is inappropriate, suggesting instead the steady-state distribution. Other progresses in description of nucleation including the derivation of nucleation kinetics for crystallization in condensed systems and first systematic studies are summarized in works by Turnbull and Fisher[21], Turnbull[22]. Other approaches to nucleation theory are collected e.g. in the work of Kelton[23].

2.1.1 Homogeneous Nucleation

According to the classical nucleation theory (CNT), the steady-state homogeneous nucleation rate I_{st} at temperature T can be written as[16,24,25]:

$$I_{st} = A_N exp\left(-\frac{W^* + \Delta G_D}{k_B T}\right) \quad (1)$$

where W^* is the thermodynamic barrier for nucleation (i.e. increase in the free energy of a system due to the formation of a critical nucleus with size r^*), ΔG_D is the kinetic barrier for nucleation (i.e. activation free energy for move of structural units from liquid to nucleus), k_B is the Boltzmann constant and A_N is the pre-exponential term which is weakly temperature dependent compared to the exponential term. In the temperature range used for nucleation measurements A_N can be approximated by[26]:

$$A_N = \frac{n_V k_B T}{h} \quad (2)$$

where $n_V \sim 1/\lambda^3$ is the number of structural units, with a size λ, per unit volume and h is the Planck constant.

The size of critical nucleus r^* and hence the thermodynamic barrier for nucleation W^* can be estimated from the following condition[16,25]:

$$\frac{\partial W}{\partial r} = 0, \qquad W = c_1 r^2 \sigma - c_2 r^3 \Delta G_V \quad (3)$$

where W is the work of nucleus formation, c_1 and c_2 are the shape factors of evolving nucleus, σ is the crystal-liquid surface energy, r is the radius of nucleus and $\Delta G_V = \Delta G / V_m$ with ΔG being the thermodynamic driving force for crystallization (i.e. the free energy difference

between crystalline phase and supercooled liquid) and V_m being the molar volume. The first term in Eq. 3 is denoted as the surface term, which reflects the energy barrier for the creation of an interface, and the second term is denoted as the volume term. The dependence of work of nucleus formation W on nucleus size r is depicted in Figure 2 along with the situation for the temperature of melting T_m where the volume term is equal to zero, σ is always positive, hence W increases monotonically with increasing r and no crystallization can occur in the system. At temperatures below T_m the nuclei with $r < r^*$ are dissolved, whereas the nuclei with $r > r^*$ grow spontaneously up to macroscopic dimensions according to the thermodynamic evolution criteria [2,27,28].

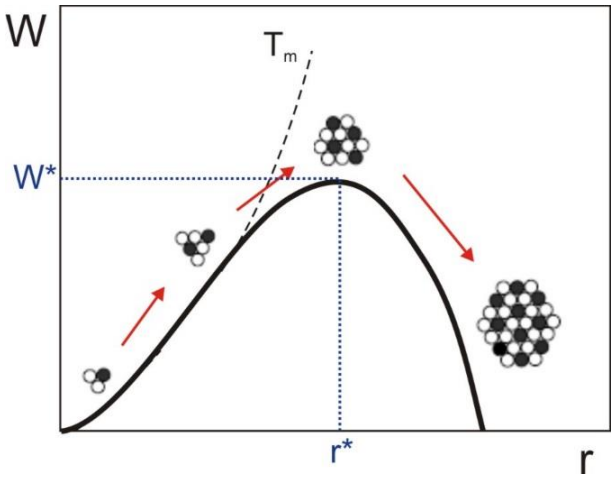

Figure 2: The work of nucleus formation W as a function of nucleus size r as it is assumed in the classical nucleation theory[27].

For a spherical nucleus, the critical nucleus size r^* and the thermodynamic barrier for nucleation W^* are given by[16,25]:

$$r^* = \frac{2\sigma V_m}{\Delta G} \tag{4}$$

$$W^* = \frac{16\pi\sigma^3 V_m^2}{3\Delta G^2} \tag{5}$$

With the knowledge of heat capacities of crystalline phase and supercooled liquid, the thermodynamic driving force for crystallization ΔG can be calculated via equation:

$$\Delta G = \Delta H_m \frac{\Delta T}{T_m} + \int_T^{T_m} \Delta C_p dT - T \int_T^{T_m} \Delta C_p \frac{dT}{T} \quad (6)$$

where ΔH_m is the melting enthalpy, ΔT is undercooling ($\Delta T = T_m - T$) and ΔC_p is the heat capacity difference between crystalline phase and supercooled liquid at constant pressure ($\Delta C_p = C_p^{cr} - C_p^m$). Due to the often found absence of experimental data on heat capacities, several approximations of ΔG were proposed[22,29-31]. One of the most used expressions is assigned to Turnbull[22] who assumed $\Delta C_p = 0$:

$$\Delta G = \Delta H_m \frac{\Delta T}{T_m} = \Delta S_m \Delta T \quad (7)$$

where ΔS_m is the melting entropy of the crystalline phase.

Regarding the kinetic barrier for nucleation, ΔG_D is usually related to the readily available experimentally obtained transport parameter, viscosity η[26]. It is assumed that the molecular transport for crystallization process is controlled by diffusion and can be described in terms of an effective diffusion coefficient *D*:

$$D = \frac{k_B T \lambda^2}{h} exp\left(-\frac{\Delta G_D}{k_B T}\right) \quad (8)$$

where λ is the diameter of the diffusing molecules (structural units) or jump distance. The measurement of diffusion is complicated, and the temperature dependence of diffusion coefficient is mostly not available, so *D* is usually expressed via the Stokes-Einstein (SE) or Eyring (E) equation[32]:

$$D = \frac{k_B T}{3\pi\lambda\eta} \quad \text{(SE)} \quad (9)$$

$$D = \frac{k_B T}{\lambda\eta} \quad \text{(E)} \quad (10)$$

Combining Eqs. 1, 2, 5, 7, 8, 9 one can obtain the expression for the steady-state homogeneous nucleation rate in the following form:

$$I_{st} = \frac{n_V k_B T}{3\pi\lambda^3\eta} exp\left(-\frac{16\pi\sigma^3 V_m^2}{3k_B T \Delta S_m^2 \Delta T^2}\right) \quad (11)$$

2.1.2 Heterogeneous Nucleation

The presence of preexisting nuclei, phase boundaries, dislocations, foreign solid particles may favor the nucleation process[16,24,25]. The thermodynamic barrier for heterogeneous nucleation is lower relative to that of homogeneous nucleation owing to a decrease of the surface energy contributions to the work of critical nucleus formation. The order of favorable sites with respect to the decreasing thermodynamic barrier is: nucleation on a boundary, on an edge and at a corner[16].

The thermodynamic barrier for heterogeneous nucleation for condensation on planar interface considering the convenient spherical-cap model can be expressed by[25]:

$$W_{het}^{*} = W^{*}\phi, \quad \phi = \frac{1}{2} - \frac{3}{4}cos\theta + \frac{1}{4}cos^{3}\theta \tag{12}$$

where ϕ is the parameter which can vary from zero to unity depending on the value of wetting angle θ. The formation of nucleus by heterogeneous nucleation mechanism is illustrated in Figure 3.

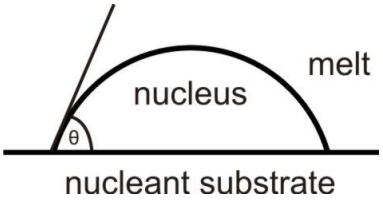

Figure 3: Heterogeneous nucleation taking place on a flat substrate. The new phase forms a spherical cap on nucleant substrate.

Using the similar assumptions that were employed in the derivation of the steady-state homogeneous nucleation rate, it is possible to express the equation for steady-state heterogeneous nucleation rate. The number of structural units per unit volume n_V, which can be found in pre-exponential term of Eq. 1, is replaced by the number of structural units in contact with the catalyzing surface n_S. Then, the steady-state heterogeneous nucleation rate is given by[25,33]:

$$I_{st}^{het} \cong n_S \frac{k_B T}{h} exp\left[-\frac{W^{*}\phi + \Delta G_D}{k_B T}\right] \tag{13}$$

2.1.3 Non-steady-state (Transient) Nucleation

Eq. 1 represents the classical model used to calculate a steady-state nucleation rate I_{st} which is independent of time. However, a lot of experiments in condensed systems indicate that the nucleation rates differ from the steady-state values in early stages of nucleation[16]. Such non-steady-state (transient) nucleation behavior can be seen in Figure 4 which shows typical time evolution of number of nuclei *N*. Some transient period is needed to build up the initial nuclei distribution toward the time independent distribution corresponding to the nucleation temperature *T*. Cooling rates used for glass formation via melt-quench process and the rates of heating a glass up to a temperature of interest, are usually too high to keep a steady-state distribution of nuclei. The time required to establish a steady-state nucleation rate is denoted as the time-lag in nucleation τ and can be determined with the knowledge of value of the induction period t_{ind}[24]. The experimental way of determination the values of I_{st} and t_{ind} is depicted in Figure 4. The slope of the linear part in *N*-*t* curve corresponds to the steady-state nucleation rate I_{st} at temperature *T* and the induction period t_{ind} can be found as the intercept of the extrapolated linear part with the time axis. One should consider that the selection of the linear part of *N*-*t* curve is a subjective procedure and that the phase transformation can be terminated prior to the establishment of the steady-state nucleation rate in the case of significantly overlapping nucleation and growth processes. Then a more accurate way for finding the values of I_{st}, t_{ind} and τ is by fitting the whole *N*-*t* curve using the appropriate model for transient nucleation.

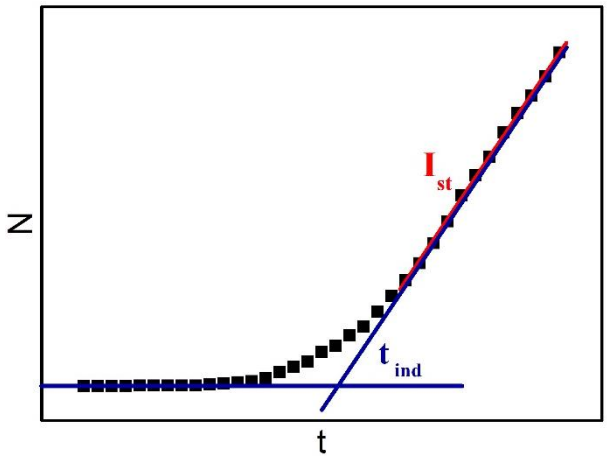

Figure 4: Time evolution of nuclei number *N* with marked experimental evaluation of induction period t_{ind} and steady-state nucleation rate I_{st}.

The first expression for transient nucleation proposed by Zeldovich[34] allows one to describe the time dependent nucleation rate and find the time-lag in nucleation. The Zeldovich equation fails mainly at large times of the time dependence of nuclei number[35], so many alternative analytical and numerical solutions[23] developed from the fundamental Frenkel-Zeldovich equation[16] were proposed for treatment of transient nucleation. Two successful analytical solutions for the description of transient nucleation in condensed systems are introduced in next paragraphs.

One of the most famous solutions for transient nucleation was proposed by Collins and Kashchiev[36,37]. The Collins-Kashchiev (C-K) equation is commonly used for the treatment of experimental *N*-*t* data to obtain the steady-state nucleation rate and time-lag in silicate glasses. Moreover, the C-K equation provides the values of I_{st} and τ, which are in a good agreement with those from numerical solutions[38]. The authors expressed the non-steady-state nucleation rate $I(t)$ as:

$$I(t) = I_{st}\left[1 + 2\sum_{m=1}^{\infty}(-1)^m exp\left(-m^2\frac{t}{\tau}\right)\right] \quad (14)$$

which results in the following equation for the time dependence of number of nuclei *N*:

$$N(t) = I_{st}\tau\left[\frac{t}{\tau} - \frac{\pi^2}{6} - 2\sum_{m=1}^{\infty}\frac{(-1)^m}{m^2}exp\left(-m^2\frac{t}{\tau}\right)\right] \quad (15)$$

Another analytical solution was suggested by Shneidman[39] for the time dependent nucleation rate for nuclei of sizes sufficiently larger than the critical size. According to Shneidman a double-exponential time-dependent nucleation rate $I(r,t)$ is given by:

$$I(r,t) = I_{st}exp\left[-exp\left\{-\frac{t-t_i(r)}{\tau}\right\}\right] \quad \text{with} \quad t_i(r) = t_{ind}(r) - \gamma\tau \quad (16)$$

where $t_i(r)$ is the size-dependent "relaxation time" which is defined as the time when the nucleation rate has reached 1/e of its steady-state value, γ is Euler's constant ($\gamma = 0.57721...$). In order to find the expression for the time dependence of number of nuclei *N*, Eq. 16 can be integrated:

$$N(r,t) = \tau I_{st}E_1[\exp(-z)] \quad \text{with} \quad z = [(t - t_{ind}(r))/\tau] + \gamma \quad (17)$$

where E_1 is the exponential integral.

2.2 CRYSTAL GROWTH

The second part of the crystallization process is the crystal growth. The crystal growth rate is affected by two quantities[40]:

- the probability of irreversible molecular attachment to the crystal (expressed in terms of the change of Gibbs free energy between the supercooled liquid and crystalline phase)
- the rate at which atoms/molecules can move from the liquid to the growing surface of crystal and can incorporate into the newly formed crystalline phase (u_{kin}).

The crystal growth rate can be controlled by three main processes[41]: diffusion in the liquid, flow of latent heat from the surface of the growing crystal and reaction at the crystal-liquid interface. If the rate controlling process is the diffusion in liquid, the crystal growth rate is given by:

$$u = k\left(\frac{D}{t}\right)^{1/2} \tag{18}$$

where k is the constant involving concentration terms and t is time. Therefore, the plot of crystal size vs square root of time yields a straight line. If flow of latent heat from the growing crystal surface is the slowest step (controlling process), the crystal-liquid interface has a cellular morphology and the crystal growth rate is time independent. In the case of the crystal growth controlled by the kinetics at the crystal-liquid interface, the crystal growth rate is time independent and the crystal size evolves linearly with time. This type of rate controlling process is the most common for crystal growth in glasses. The crystal growth rate can be expressed by the following equation[41]:

$$u = f\frac{D}{\lambda}\left[1 - exp\left(-\frac{\Delta G}{RT}\right)\right] \tag{19}$$

where f is the fraction of preferred growth sites at the interface which differs according to the crystal growth model, R is the gas constant. As was discussed above (Nucleation part), without the knowledge of heat capacity data the ΔG can be approximated by Turnbull equation

(Eq. 7) and, assuming the molecular motion controlling crystal growth similar to that controlling the viscous flow ($D = D_\eta$), the diffusion coefficient can be calculated via the Stokes-Einstein or the Eyring equation (Eqs. 9, 10).

2.2.1 Crystal Growth Models

Three standard phenomenological models are applicable for the description of the crystal growth which is controlled by the crystal-liquid interface kinetics[32,41]:

- Normal growth model
- Screw dislocation growth model
- 2D surface nucleated growth model.

The difference between the standard growth models is based on the nature of the crystal-liquid interface, i.e. the amount and type of available interfacial sites where atoms/molecules can attach to the surface of growing crystal.

Normal Growth Model

This type of growth[41-43] occurs at the atomically rough crystal-liquid interface, which is specific for the low value of melting entropy ($\Delta S_m < 2R$). Such crystal-liquid interface contains a lot of sites where atoms and molecules can be incorporated into or removed from the growing crystal surface. Moreover, all the sites at such interface are equivalent. Coefficient f (Eq. 19) related to the fraction of preferred growth sites at the interface is equal to one. Thus, the crystal growth rate at temperature T is expressed by equation:

$$u = \frac{D}{\lambda}\left[1 - exp\left(-\frac{\Delta G}{RT}\right)\right] \tag{20}$$

Screw Dislocation Growth Model

According to the screw dislocation model[41-43], the crystal-liquid interface is smooth, although imperfect on the atomic scale, characterized by high value of melting entropy ($\Delta S_m > 4R$). It is assumed that growth takes place at step sites provided by screw dislocations. The fraction of preferred growth sites f is given by:

$$f = \frac{\lambda \Delta G}{4\pi\sigma V_m} \tag{21}$$

With the use of the semi-empirical Skapski-Turnbull equation[22,44] for surface energy σ, Eq. 21 follows the form $f = \Delta T/2\pi T_m$ for small undercoolings. The temperature dependent crystal growth rate can be then expressed:

$$u = \frac{\Delta T}{2\pi T_m}\frac{D}{\lambda}\left[1 - exp\left(-\frac{\Delta G}{RT}\right)\right] \quad (22)$$

2D Surface Nucleated Growth Model

The 2D surface nucleated growth[41-43] assumes the atomically smooth and defect free crystal-liquid interface. In this case, the growth requires formation of two-dimensional nuclei on top of the primary crystals, which grow laterally. Number of nuclei and their impact on growth depend on the distribution of clusters at the crystal-liquid interface and on the frequency of nuclei development at the interface. The crystal growth rate is given by:

$$u = C\frac{D_u}{\lambda^2} exp\left(-\frac{Z}{T\Delta G}\right) \quad (23)$$

Parameters *C* and *Z* depend on the size of the secondary crystal and are different for the cases of "small" and "large" crystals[45]:

$$Z = \frac{\pi\lambda V_m\sigma^2}{\varepsilon k_B} \quad (24)$$

Herein, ε = 1 stands for the "small" crystal and ε = 3 stands for the "large" crystal, and σ is the surface edge energy of the 2D crystal for growth which is usually taken as the crystal-liquid surface energy. Parameter *C* is given by:

$$C = \lambda N_S A_0 \quad \text{"small" crystal} \quad (25)$$

$$C = \frac{\sqrt[3]{(\pi/3)N_S\lambda^5}}{\Gamma(4/3)}\left[1 - exp\left(-\frac{\Delta G}{RT}\right)\right]^{2/3} \quad \text{"large" crystal} \quad (26)$$

where A_0 is the interface area of the growing crystal, N_S is the number of formula units per unit area of interface and Γ is the gamma function. The "small" crystal case occurs when the primary crystals are much larger than the 2D crystals which grow on them. The crystal growth rate is

determined by nucleation rate. It means that times between nucleation events are long compared to the times for the growth of 2D crystals resulting in layer by layer growth (illustrated in Figure 5). Generally applied "large" crystal case refers to the situation, when 2D crystals have sizes similar to that of the primary crystals and the growth rate is determined by the nucleation rate and the rate of layer spreading. This results in the multi-nucleus growth (illustrated in Figure 5).

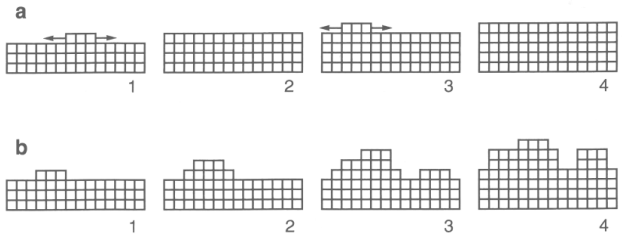

Figure 5: The schematic illustration of the 2D surface nucleated growth[32], a) "small" crystal case, layer by layer growth; b) "large" crystal case, multi-nucleus growth.

Reduced Crystal Growth Rate

Jackson[43] proposed a simple way for the estimation of the operative crystal growth model based on the dependence of reduced crystal growth rate U_R on supercooling ΔT. The reduced crystal growth rate can be expressed by equation:

$$U_R = \frac{u\eta}{1-exp\left(-\frac{\Delta G}{RT}\right)} \tag{27}$$

Temperature dependence of reduced crystal growth rate gives an information on the temperature dependence of the fraction of preferred growth sites f at the crystal-liquid interface. With the knowledge of crystal growth rates u and viscosity η at various temperatures T, the reduced crystal growth rate can be calculated and thus the appropriate growth mechanism for the description of crystal growth in the wide temperature range can be inferred.

The dependence of U_R on ΔT, depicted in Figure 6, results in a shape of horizontal line for the normal growth model, straight line with a positive slope for the screw dislocation growth model, or a curve with increasing positive slope for the 2D surface nucleated model.

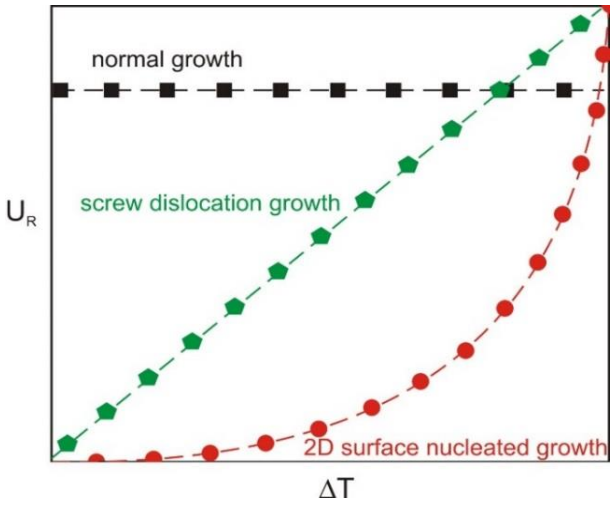

Figure 6: Dependence of the reduced crystal growth rate U_R on supercooling ΔT for the standard crystal growth models[46].

2.3 DECOUPLING OF VISCOSITY AND CRYSTALLIZATION PROCESSES

The classical nucleation theory (CNT) and standard growth models (see the Nucleation and Crystal Growth part for details) are based on the assumption that the molecular transport in nucleation and growth processes expressed by the diffusion coefficient can be described by temperature dependence of viscosity according to the Stokes-Einstein or Eyring relation SE/E (Eqs. 9, 10) ($D \approx \eta^{-1}$). This assumption was tested by several authors[40,47-53]. Ediger et al.[48] reported u_{kin} scaling with viscosity $\sim\eta^{-\xi}$ for a wide range of organic and inorganic materials with the exponent ξ smaller than unity. They proposed a simple way to test the decoupling which is based on a power law dependence of u_{kin} on the viscosity:

$$u_{kin} \propto \eta^{-\xi} \tag{28}$$

where u_{kin} is the kinetic part of crystal growth rate ($u_{kin} = u/[1 - exp(-\Delta G/RT)]$; defined using normal growth model) and the kinetic exponent $0 \leq \xi \leq 1$ expresses the extent of decoupling of crystal growth rate and viscosity. The slope of the dependence of log u_{kin} vs log η corresponds to the kinetic exponent ξ. In the work of Nascimento et al.[40] the comparison of u_{kin} with η^{-1} using the screw dislocation and 2D surface nucleated growth models was reported

and the normalized kinetic coefficients were proposed. The information about decoupling can also give a comparison of the effective diffusion coefficients calculated from the crystal growth data (Eq. 19) and from viscosity (using the SE/E equation)[49,50]. It was found that for strong glasses the SE/E equation describing the transport controlling crystal growth works well from T_m down to T_g, on the other hand the signs of a SE/E equation breakdown in fragile glasses were observed. With increasing supercooling the crystal growth can be slower compared to the prediction from the viscosity data, and the effective diffusivity and viscosity can decouple, which typically occurs below approximately 1.2 T_g. In the case of decoupling between the crystal growth and viscosity, the correction of growth models with the use of the kinetic exponent ξ ($D \approx \eta^{-\xi}$) is necessary[54-56] in order to achieve a good agreement between the experimental growth rate data and growth model.

Regarding the nucleation, Nascimento et al.[51] investigated the effects of decoupling of dynamics of crystal nucleation and growth from those of viscous flow in lithium disilicate glass using the effective diffusion coefficients estimated from nucleation time-lags, crystal growth rates, viscosity and experimental ionic diffusion coefficients of Li^+, O^{2-}, Si^{4+}. They found that the decoupling between nucleation rate and viscous flow occurs at lower temperature near T_g and that it is not so significant as that between the growth rate and viscous flow.

The possible explanation of the breakdown in scaling between the crystallization processes and viscosity is a manifestation of spatially dynamic heterogeneity in glass-forming liquids[48,51,57] which is connected with molecular motion. This means that during the cooling of liquids down to T_g the local relaxation occurs at different rates at different places within the supercooled liquid. The phenomenon of spatial dynamic heterogeneity is more pronounced for fragile liquids.

3 SUMMARY OF PAPERS

The presented dissertation thesis is focused on the study of nucleation and crystal growth in chalcogenide glasses with respect to the kinetics of the two processes. In order to obtain more details about crystallization, the direct microscopy observation was mainly used. Although many studies have been reported about crystallization in chalcogenide glasses during past decades, there is still a need for more detailed information about mechanism and kinetics of this process due to the unsolved problems and questions.

Chalcogenide glasses have received attention of researchers due to their unique structural, electronic, optical and thermal properties, which are utilized in applications such as glass-ceramics, phase-change memories and optical and optoelectronical components used in thermal imaging systems or integrated optical waveguides devices[1]. All of the mentioned applications are connected with the nucleation and crystal growth processes. For some applications it is essential to avoid crystallization, for other ones the controlled and very fast amorphous to crystalline phase transformation is required. Hence, the understanding and control of the crystallization process is fundamental for processing and development of the given materials (Figure 7). With the detailed knowledge of mechanisms, thermodynamics, and kinetics of crystal nucleation, growth and overall crystallization, one can predict the crystallization behavior, optimize the material composition and preparation methods to meet the prerequisites for specific application.

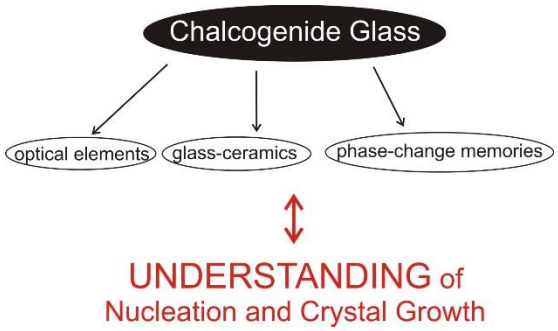

Figure 7: Schematically depicted the importance of study of crystal nucleation and growth.

There are several methods that can be used for the study of the crystallization process. The following methods can be distinguished:

- Direct – the observation of nucleation or crystal growth using various microscopic techniques, such as optical microscopy (OM), electron microscopy (EM), scanning probe microscopy (SPM).

- Indirect – based on the observation of macroscopic property change such as electrical conductivity, enthalpy (differential thermal analysis (DTA), differential scanning calorimetry (DSC)), structure (X-ray diffraction (XRD)), mechanical properties (thermomechanical analysis (TMA))

Both types of methods have their advantages and disadvantages and therefore it is always useful to combine more techniques to achieve a complex view on the crystallization process. In the case of direct methods, the main advantages are the possibility of study of nucleation and crystal growth kinetics separately. These methods also provide useful and important information about the crystal morphology and position in the sample (volume vs. surface crystallization). The optical microscopy (OM) utilizes the difference of transmittance or reflectance between amorphous and crystalline phase and it is usually possible to reliably measure objects larger than 1 μm. The higher resolution can be achieved using the scanning electron microscope and transmission electron microscope. The scanning electron microscopy (SEM) is based on the interaction of accelerated electrons and sample. However, electrons can penetrate only into small depth of sample and hence it is necessary to treat the sample surface by etching or polishing when the objects are far below the sample surface. Regarding the transmission electron microscopy (TEM), preparation of sample is quite complicated and time-consuming, and the sample can be influenced or destroyed using inappropriately applied electron beam. Although direct methods are convenient to study nucleation and crystal growth, in some glassy systems the processes are too fast to get reliable values of nucleation or growth rates in the whole temperature range up to T_m. In these cases, it is useful to follow crystallization kinetics by any of the indirect methods. The indirect measurements are fast and not so laborious in comparison with the direct measurements. One should keep in mind that usually the overall data on crystallization kinetics are obtained. Sometimes the change of macroscopic property cannot be detected if the process is too fast or too slow. The best result of the crystallization studies is achieved from combination of direct and indirect approaches.

The following text deals with the studies of crystal nucleation and growth in various chalcogenide glassy systems using mainly direct approaches which were supplemented with the results from indirect measurements. These studies were published in high-quality international journals in the form of 5 papers. Their main ideas and conclusions are summarized below in order to highlight the objectives of the presented thesis.

3.1 NUCLEATION

One of the aims of the presented thesis is the study of nucleation kinetics in chalcogenide glasses and testing the applicability of so far proposed theories (like CNT) and their improvements for the description of steady-state nucleation and analysis of transient models for nucleation. The crystal nucleation in glasses is studied for several decades, and many papers have been published that extend the understanding of the nucleation process and its description via classical nucleation theory (CNT). Some problems occurring in the quantitative description of nucleation rates were resolved in those papers. It should be noted that the essential portion of the present knowledge on nucleation in glass forming systems is based on studies in oxide glasses, especially in lithium disilicate glass which has been used as a model system[23,24,26,58]. As far as we know, only a few studies of nucleation have been performed in chalcogenide glasses, which were mostly qualitative without detailed information about nucleation kinetics and quantitative data on nucleation rates[59-68].

Measurement of nucleation kinetics is usually difficult and time-consuming. Special ways for studying nucleation kinetics using microscopy[24,59,60], differential scanning calorimetry/differential thermal analysis[69,70], and X-ray diffraction[71,72] were proposed in literature. Since the critical nuclei are undetectable using commonly available experimental techniques (OM, SEM) at undercoolings that correspond to the range of measurable nucleation rates in glasses, they have to be grown up to a detectable size. Then, it is possible to estimate the number of nuclei N as a function of time and hence the nucleation rate which is given by the equation $I = dN/dt$. Traditional optical microscopy methods are divided into two groups according to the overlapping of the nucleation $I(T)$ and crystal growth $U(T)$ rate curves (depicted in Figure 8): single-stage and double-stage method[24]. If the overlapping of nucleation and growth curves is weak, which means that crystal growth rates are low at temperatures corresponding to high nucleation rates, double-stage Tamman method[73] is employed to obtain the *N-t* dependence. The Tamman method starts with the sample heat treatment at a low nucleation temperature T_N, after which the crystals are grown up to microscopic sizes at higher development temperature T_D, which follows the conditions for nucleation and growth rates: $I(T_D) \ll I(T_N)$ and $U(T_D) \gg U(T_N)$. If the overlapping of nucleation and growth curves is considerable, the crystals are visible and can be counted after single-stage heat treatment. Simultaneous crystal nucleation and growth result in a wide distribution of crystal sizes. With the knowledge of crystal growth rates at various temperatures it is possible to calculate the "birth dates" of crystals belonging to every single size group and then plot the *N-t*

dependence. This method, which was originally proposed by Köster[74] for metallic glasses, is successful also in the study of heterogeneous nucleation with finite number of active sites that are depleted in a short time. Microscopy methods are based on counting of grown nuclei, so it is evident that they are laborious and time-consuming.

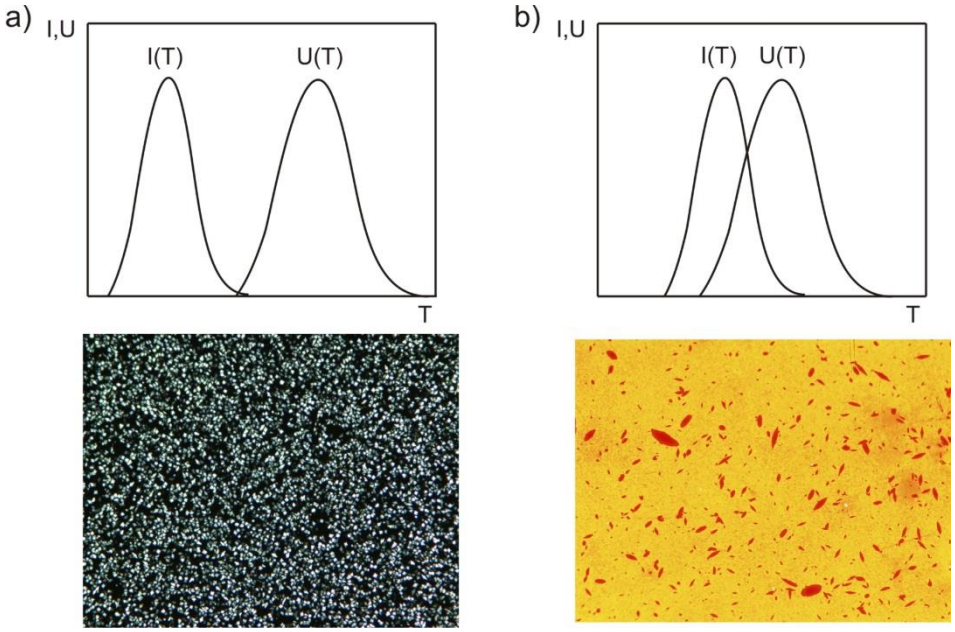

Figure 8: Temperature dependence of nucleation rate $I(T)$ and crystal growth rate $U(T)$; a) nucleation and growth region weakly overlap, crystals are of the same size; b) nucleation and growth region overlap significantly, wide distribution of crystal sizes is observed.

The indirect non-isothermal DSC/DTA measurements can be fast and provide accurate quantitative data, but it is necessary to have some preliminary information about nucleation and crystal growth from microscopy measurements. Indirect methods can be divided into two groups. The first type allows one to determine the temperature region of nucleation including the temperature T_{max} where nucleation rate is maximum on the basis of assumption that the inverse temperature of the crystallization peak $1/T_p$ on a DSC/DTA curve is proportional to the density of nuclei[69]. The higher the nuclei number the faster the crystallization kinetics is and, hence, the release of crystallization heat is detected at lower temperature. Therefore, a plot of $1/T_p$ versus temperature of nucleation heat treatment reflects the temperature dependence of nucleation rate. The second type of indirect method was proposed by Ray et al.[70] for the quantitative determination of steady-state nucleation rates at various temperatures. The method consists of a glass sample heat treatment used to induce partial crystallization, and

of the consequent estimation of the crystallized volume fraction via the decrease of the crystallization peak area obtained for the residual glass on a newly measured DSC/DTA heating scan.

As was mentioned in the theoretical part, nucleation can occur by homogeneous or heterogeneous mechanism in the volume or on the surface of the glass sample. Nevertheless, literature results give strong evidence that overwhelming majority of silicate glasses nucleate on free glass surface via defects such as scratches, tips, microcracks, compositional inhomogeneities, solid particles, etc[24,75]. The number of such sites is limited and depends on the degree of surface perfection and cleanness. Since there is a finite set of sites, the number of nuclei saturates with time, which often occurs at high pace, sometimes even before crystals become visible[16]. High surface nucleation rates are caused by the low interfacial energy between the contaminants and the nuclei[76]. Due to the fast nucleation and fast exhaustion of active sites, only constant numbers of nuclei *N* are typically observed for most glasses and various types of heat treatments. Therefore, the data on surface nucleation are mostly qualitative. Surface crystallization was studied mainly in cordierite glass ($2MgO\text{-}2Al_2O_3\text{-}5SiO_2$) which was chosen as model material because of the polymorphic course of crystallization and absence of volume crystallization[77-80]. Other systems where surface crystallization was followed, were soda-lime-silica glass and alkali-free silicates (anorthite $CaO\text{-}Al_2O_3\text{-}2SiO_2$; diopside $MgO\text{-}CaO\text{-}2SiO_2$)[75,81-83]. Both, volume homogeneous and surface heterogeneous nucleation can occur in lithium disilicate where annealing in the glass transition range gives rise to homogeneous nucleation, while at low degrees of supercooling the contact with Pt metal (container wall, particles) provokes heterogeneous nucleation[84]. Similar findings were observed in metallic[74,85] and chalcogenide glasses.

It was difficult to find chalcogenide glassy system where number of nuclei *N* changes with annealing time and temperature in order to test CNT, its improvements and analysis of transient models for nucleation. According to my observations, nucleation in chalcogenide glasses occurs mostly at sample surface via heterogeneous mechanism so it is difficult to obtain any quantitative result in the form of nucleation rates. The combination of volume and surface nucleation was observed in Se_xTe_{1-x} (x=0.1; 0.2; 0.3) bulk glass[61], volume nucleation was observed in $(GeS_2)_{0.9}(Sb_2S_3)_{0.1}$ bulk glass, where it seems that nucleation occurs at fixed athermal nuclei which were formed during the preparation of glass by melt-quench technique. In comparison with silicate glasses, the induction period and time-lag for nucleation are much more shorter and nucleation is faster, hence, maybe this is the reason why it is not possible to measure nucleation rates using DSC/DTA technique. Nevertheless, some compositions of

Ge-Sb-S system appear to be suitable for the quantitative study of nucleation. The Ge-Sb-S system was previously investigated by researchers from the thermodynamic and viscosity point of view[86,87]. These data are necessary for calculations of nucleation kinetics. The study of nucleation kinetics was made in $(GeS_2)_{0.9}(Sb_2S_3)_{0.1}$ thin films using double-stage heat treatment method and optical microscopy[62]. In **Paper I** included in the presented dissertation the opposite composition within the $(GeS_2)_x(Sb_2S_3)_{1-x}$ row was studied (schematically depicted in Figure 9). The crystal nucleation in $Ge_{1.8}Sb_{36.8}S_{61.4}$ thin films of 1 μm thickness, which is close to $(GeS_2)_{0.1}(Sb_2S_3)_{0.9}$ (= $Ge_{2.1}Sb_{37.5}S_{60.4}$), was observed in-situ using optical microscope coupled with a computer-controlled heating stage in the transmission mode. On the basis of our previously published results on crystal growth in the Ge-Sb-S system[88], where a broad distribution of crystal sizes was observed (Figure 9), the single-stage method was chosen as the appropriate one for the study of nucleation kinetics in these thin films. The crystals in thin films grew from randomly distributed nuclei in the volume of thin film, crystallization was not initiated at the surface and the numbers of grown nuclei increased during the isothermal heat treatment of the sample. All of the mentioned facts suggest the homogeneous mechanism of nucleation.

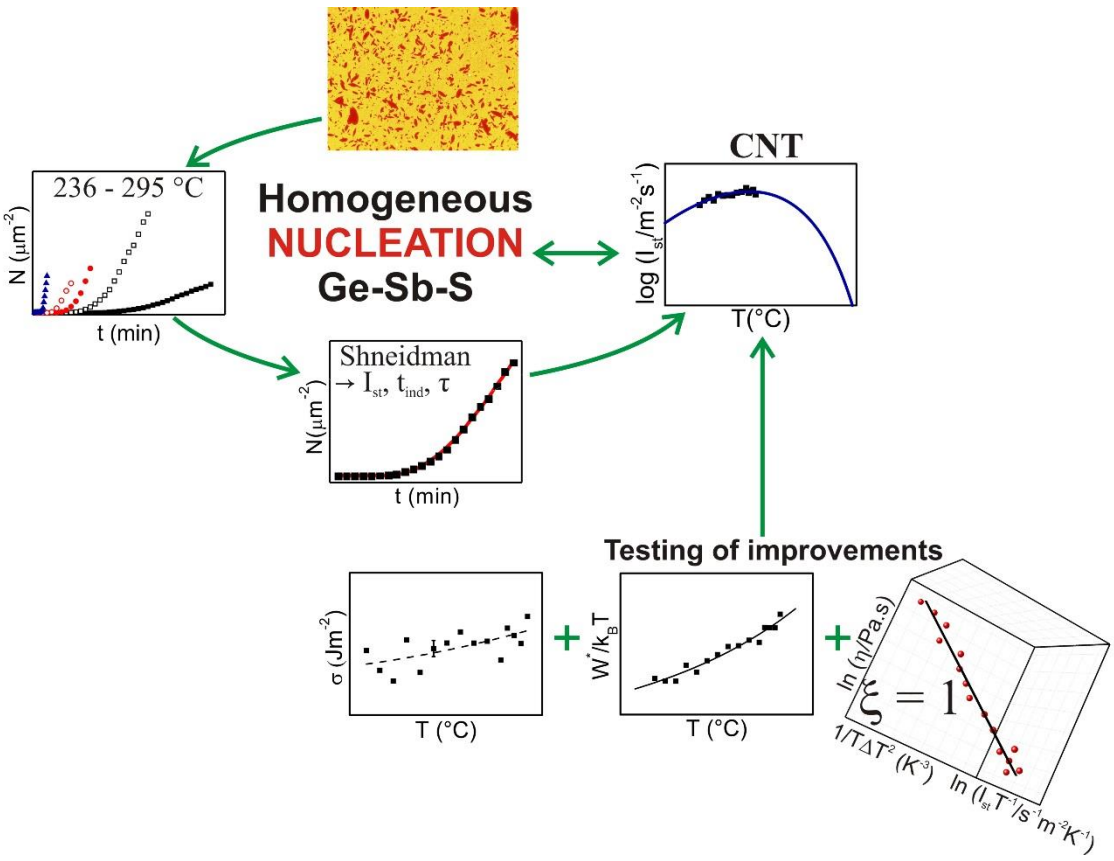

Figure 9: Procedure of the analysis of nucleation in $Ge_{1.8}Sb_{36.8}S_{61.4}$ thin films (**Paper I**).

Time evolutions of nuclei number N for various temperatures revealed non-steady-state (transient) behavior. The N-t curves were fitted using two successful theories for transient nucleation (Collins-Kashchiev[36,37] and Shneidman[39]) to find the quantities characterizing nucleation kinetics (steady-state nucleation rate I_{st}, induction period t_{ind}, time-lag τ). Collins-Kashchiev theory is the most famous and commonly used approach to the treatment of experimental N-t data in silicate glasses. Moreover, the obtained values of I_{st} and τ are in a good agreement with those from numerical calculations[38]. Nevertheless, it was shown that Collins-Kashchiev theory is not suitable for the description of transient nucleation in the studied thin films. Better description of N-t data and more realistic values of I_{st}, t_{ind} and τ were achieved using Shneidman theory, which was used for the final calculations.

Paper I also deals with the suitability of CNT for the description of found temperature dependence of the steady-state nucleation rate, so that the nucleation behavior could be described in a wide temperature range (from T_g to T_m). Sometimes it is not possible to measure nucleation in such wide temperature range due to a significant crystal growth at the temperatures where nucleation still occurs, i. e. sample is completely crystallized in a few seconds. It was shown in many studies on silicate glasses that CNT is convenient for description of nucleation, nevertheless, certain problems still persisted in case of several materials, thus various improvements of CNT were proposed. CNT is based on a number of assumptions that do not always have to be valid. One of these assumptions is the validity of the Stokes-Einstein relation for the description of molecular transport in nucleation process near the melting point T_m as well as in highly supercooled liquid down to T_g. Another assumption of CNT is that the crystal-liquid interface energy σ is treated as a macroscopic property with a value equal to that of a planar interface, which is known as capillarity approximation. It is well-known that CNT usually fails in calculation of I-T curve if a constant σ is used, so the temperature-dependent interfacial energies should be employed[26]. Third, CNT assumes that the thermodynamic properties of the critical cluster and the evolving macroscopic phase are equivalent. Following that and the validity of capillarity approximation, a monotonic decrease of the thermodynamic barrier for nucleation W^* with decreasing temperature is expected. An anomalous behavior of W^* was observed in silicate glasses, therefore, some additional corrections were introduced[89-92].

The test of validity of the mentioned assumptions for the studied $Ge_{1.8}Sb_{36.8}S_{61.4}$ thin films is included in **Paper I**. It was revealed that no anomalous behavior of W^* occurs in the studied temperature region and that the Stokes-Einstein relation is fulfilled as well near T_g ($\xi = 1$). The temperature dependence of crystal-liquid surface energy was found with the knowledge of

theoretical pre-exponential term of classical nucleation model for homogeneous steady-state nucleation and experimental nucleation rates for various temperatures. The found $\sigma(T)$ dependence was weak and nearly constant. Nevertheless, it was found that the model with incorporated $\sigma(T)$ took the experimental observations into better consideration and satisfactorily described nucleation behavior in a wide temperature range. The result of the study, in the form of normalized nucleation curve along with normalized crystal growth curve, is depicted in Figure 10. The strong overlap, with the maxima at 288 °C for nucleation and 309 °C for crystal growth, was found.

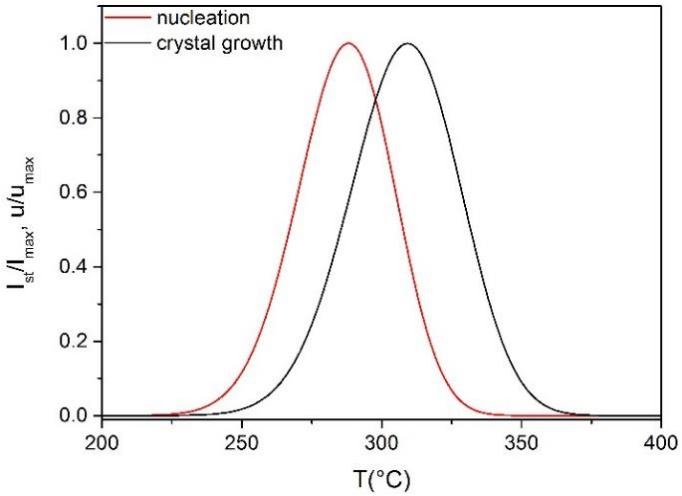

Figure 10: Calculated normalized crystal nucleation and growth curve ($I_{max} = 1.2 \cdot 10^{8}$ $m^{-2}s^{-1}$; $u_{max} = 9.9 \cdot 10^{-6}$ ms^{-1}).

A brief nucleation study in As_2Se_3 bulk glass was performed in **Paper V** using TMA, DSC and OM. This system shows quite complicated surface heterogeneous nucleation process which exhibits stochastic behavior and significantly long time-lags for nucleation (hours to days) in well prepared glass with minimum defects and stresses. Since the nucleation process is heterogeneous, density of formed nuclei can be modified by surface roughness, surface tension, contact with other materials, etc. Somewhat different behavior (shorter time-lag, higher nuclei density, minimized stochastic effects) was observed if the sample was sandwiched between two synthetic sapphire plates in TMA furnace with applied force during the nucleation heat treatment at temperature T_{max}, which corresponds to the maximum nucleation rate according to the study of Holubová et al.[93]. Formed nuclei were visualized by nonisothermal heat treatment in DSC furnace and observed and counted using optical microscope. The finite number of nuclei and nucleation rate at T_{max} were determined. These differences in nucleation behavior should

be considered during the preparation of molded lenses used in infrared optical systems where the glass is in contact with another material and under applied force.

3.2 CRYSTAL GROWTH

The second goal of the presented doctoral thesis was a study of crystal growth in selected chalcogenide materials, aiming to obtain further information about crystal morphologies, crystal growth behavior and kinetics of these materials. Crystal growth is the second part of the crystallization process and hence the mechanisms, thermodynamics, and kinetic aspects of crystal growth in glasses are some of the most significant features for understanding and controlling the vitrification and crystallization process.

As was mentioned earlier it is always useful to combine direct (microscopy) and indirect techniques for study of crystal growth, so that one can describe the growth behavior in a wide temperature range. The measurement of crystal growth kinetics in chalcogenide glasses is not so complicated relative to the measurement of nucleation kinetics. **Papers II – V** are focused on the description of crystal growth in a wide temperature range combining experimental data obtained mainly using different direct (OM, SEM) experimental techniques with those from indirect (XRD, DSC, TMA) experimental techniques.

Regarding the microscopic measurements (included in **Paper II – V**), bulk samples or thin films are first heat treated at selected temperatures for a specific amount of time in a computer-controlled furnace and then the micrographs with calibration line segment are taken by optical, infrared, or scanning electron microscope. The size of well-developed crystals can be measured as a length of crystal's long axis (**Papers III, IV**), as a thickness of the crystalline layer (**Papers IV, V**), or as a diameter of spherical crystal (**Paper II**), depending on the shape of formed crystals (Figure 11-a)). The mean crystal size is calculated as the average size of tens of crystals found in the sample. Figure 11-b) shows the set of micrographs with formed crystals in $Se_{70}Te_{30}$ thin film and the evaluation of crystal growth rate for a chosen temperature. Crystal growth rates for studied temperatures are determined as slopes of the linear time dependences of crystal sizes.

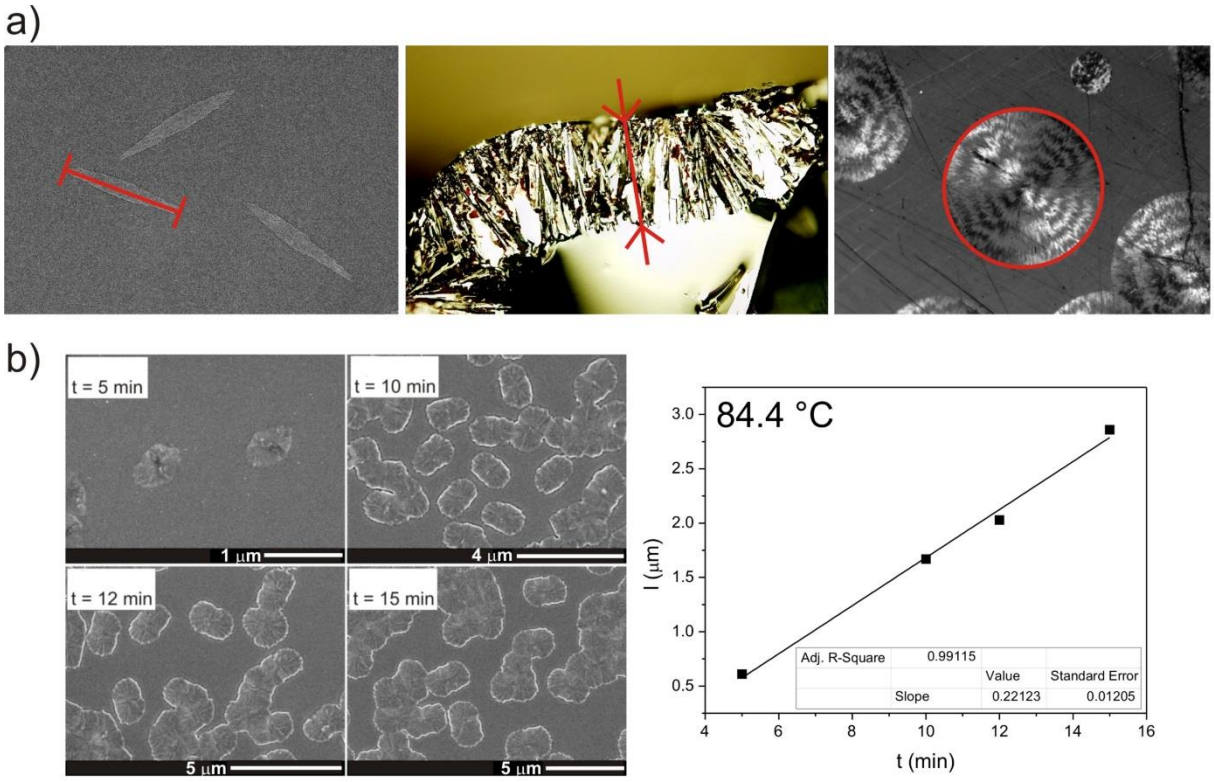

Figure 11: a) Ways of measurement of crystal sizes in various chalcogenide glasses; b) Evaluation of crystal growth rate in $Se_{70}Te_{30}$ thin films (**Paper III**); samples were heat treated at temperature 84.4 °C for various times.

The crystals grow linearly with time, which is typical for crystal growth controlled by crystal-liquid interface kinetics. As was mentioned in the theoretical part about crystallization, such type of crystal growth can be described by three phenomenological growth models (normal, screw dislocation, 2D surface-nucleated). These models are then used for description of crystal growth behavior in a wide temperature range (from T_g to T_m). The appropriate growth model is usually assessed using the dependence of reduced crystal growth rate on undercooling, according to Jackson[43]. The evaluation of activation energy of crystal growth E_G included in the papers is another part of the crystal growth analysis. E_G is usually estimated from the slope of linearized dependence of log u on $1/T$, provided a simple exponential dependence of crystal growth rate on temperature, which can be assumed in a narrow temperature range. All papers (**Paper II – V**) also include a detailed discussion about the proportionality of crystal growth rate to viscosity, which was tested mainly via Ediger's power law dependence of kinetic part of crystal growth rate u_{kin} on viscosity η. The standard crystal growth models assume validity of the Stokes-Einstein relation for description of molecular transport in the crystal growth process. If the decoupling of crystal growth and viscosity occurs in the system, the Stokes-Einstein

relation is not valid, and hence correction of the growth model is necessary to achieve better description of the experimental growth data. This is considered in each presented paper.

Paper II is focused on the isothermal study of crystal growth in the volume of $Se_{100-x}Te_x$ bulk glasses (x = 10, 20, and 30) using optical microscope equipped with infrared camera. The highlights of this paper are schematically depicted in Figure 12.

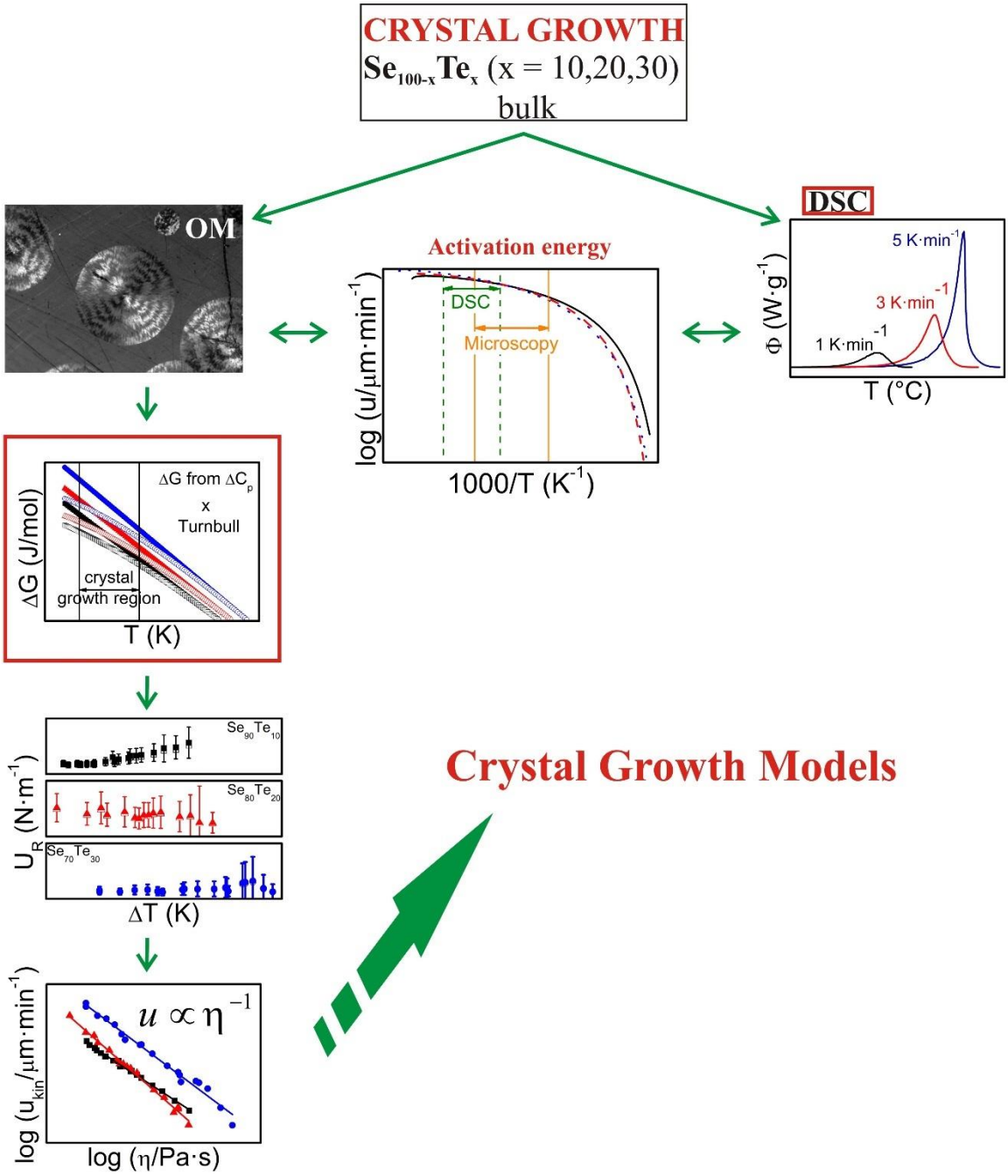

Figure 12: Procedure and highlights of the analysis of crystal growth in $Se_{100-x}Te_x$ (x = 10, 20, 30) bulk glasses (**Paper II**).

With the knowledge of crystal growth data from the microscopy measurements and temperature dependencies of η and Δ*G*, one can obtain the appropriate crystal growth model. Two different approaches for calculation of Δ*G* were analyzed in order to examine its influence on the determination of crystal growth model. The change in Gibbs free energy between supercooled liquid and crystalline phase Δ*G* is most often calculated using the approximation proposed by Turnbull due to the missing heat capacity data for chalcogenide glasses. The heat capacities of the crystalline and supercooled liquid phases are available for the Se-Te system[94], so Δ*G* could be calculated using both expressions (Eqs. 6, 7). It was found that with increasing supercooling the difference in Δ*G* calculated using the two approaches occurs. Nevertheless, Δ*G* can be substituted by simple Turnbull's expression, providing comparable results with respect to the modeling of the reduced crystal growth rate and operative crystal growth model. This is because the viscous flow controls the crystallization process in the region where difference in Δ*G* is observed. Regarding the decoupling of crystal growth rate and viscosity in the studied Se-Te compositions, the values of the kinetic exponent ξ (representing the extent of decoupling) are close to one even for such highly fragile system ($m_\eta \approx 76-88$). It can be assumed that the Stokes-Einstein relation is fulfilled even at higher undercoolings. In **Paper II** an alternative way to study the crystallization process using DSC is presented. Activation energies of the overall crystallization process evaluated from DSC measurements were compared within the activation energies of crystal growth calculated from the exponential dependence of crystal growth on temperature. One should note that such comparison of the activation energies is meaningful only in the same studied temperature range, because the dependence of log *u* on 1/*T* is highly nonlinear in a wider temperature region. Therefore, the activation energies of crystal growth were calculated in the temperature region where the DSC measurements were performed. It was found that this approach brought comparable values of the activation energies, which indicates that the crystal growth is the leading process in the overall crystallization process recorded by DSC, and that nucleation does not take place in the studied temperature region.

Paper III deals with the isothermal study of crystal growth kinetics in $Se_{70}Te_{30}$ thin films of thicknesses of 1 μm and 520 nm using the infrared and scanning electron microscopes, and in situ X-ray diffraction (XRD) measurements (Figure 13). This work continues in the crystal growth studies in Se-Te thin films[95]. The growth data obtained from the microscopy measurements were combined with the viscosity data and melting parameters, and the appropriate crystal growth model was assessed.

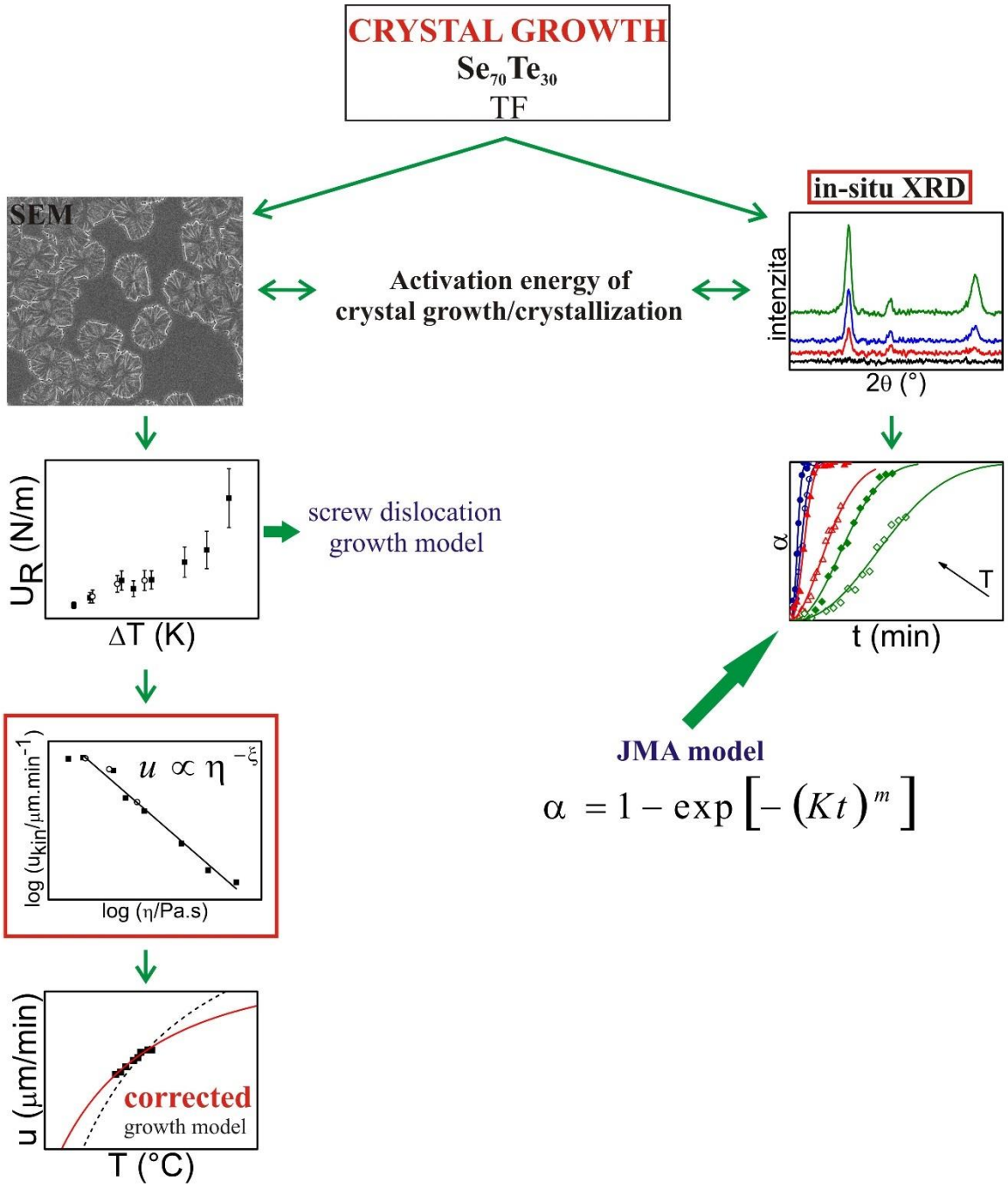

Figure 13: Procedure and highlights of the analysis of crystal growth in $Se_{70}Te_{30}$ thin films (**Paper III**).

It was found that the simple screw dislocation model (suitable according to the first estimation) does not fit the experimental data well because of the breakdown of the Stokes-Einstein relation ($\xi = 0.64$). Taking into account this fact, the correction of the standard growth model by incorporation of kinetic exponent ξ was suggested. This suggestion brought a new insight into the application of standard crystal growth model with respect to the $u - \eta$ relation. Besides

the study of crystal growth using the microscopic measurements, another approach to the study of crystallization kinetics was applied. The evolution of crystallization was studied using in situ XRD, which is based on the recording the changes in diffraction peaks during isothermal annealing. The measured crystallization data were interpreted using the Johnson-Mehl-Avrami (JMA) nucleation-growth model[96-99] which can be expressed by equation:

$$\alpha = 1 - exp[-(Kt)^m] \tag{29}$$

where α is the crystallized fraction at time *t*, *K* is the rate constant and *m* is the Avrami exponent reflecting the characteristics of nucleation and growth process. The average value of Avrami exponent indicated two-dimensional crystal growth, which was confirmed by direct observations. The results of XRD measurements were compared with the microscopic ones. The similar values of activation energies of the overall crystallization process (XRD) and crystal growth (SEM) can be explained in two ways: nucleation process has been finished and occurs in another temperature region; XRD technique is quite insensitive towards detecting nuclei and only crystal growth was followed.

Extended study on crystal growth, melting process, temperature dependence of viscosity and structure of crystalline phase in $Ge_{18}Sb_{28}Se_{54}$ bulk glasses and thin films, which is schematically depicted in Figure 14, is presented in **Paper IV**. The crystal growth rates in $Ge_{18}Sb_{28}Se_{54}$ bulk glasses and thin films were determined using optical and scanning electron microscopies under isothermal conditions. The compact crystalline layer growing from the surface into the amorphous core and needle-shape crystals were observed in bulk glass and thin films, respectively. The investigation of structure of crystallized bulk sample and thin films using XRD together with the measurements of crystallization and melting process of bulk sample using DSC under nonisothermal conditions was performed. The measurements revealed quite complex structure of the formed crystalline phase. With the knowledge of crystal growth, viscosity and melting data, the probable growth models were assessed. Regarding the decoupling of crystal growth rate and viscosity in $Ge_{18}Sb_{28}Se_{54}$ bulk glasses and thin films, similar findings as in Se-Te system (Papers II and III) were observed. Simple proportionality of crystal growth rate to inverse viscosity according to the Stokes-Einstein relation holds for the bulk material ($\xi = 0.98$) and is not fulfilled in the case of thin films ($\xi = 0.67$). Taking into account the possible decoupling, shape of dependence of U_R on ΔT and previously found results in Ge-Sb-Se system[100], experimental growth data of bulk glasses and thin films were fitted using two models. Unfortunately, it was not possible to distinguish which model is better for

the description of crystal growth in a wide temperature range, because the calculated models differ only in the region close to the melting, where the experimental growth data cannot be obtained with the used techniques. Although the appropriate crystal growth model was not found, this study provides a certain concept of growth behavior in $Ge_{18}Sb_{28}Se_{54}$ bulk glass and thin film.

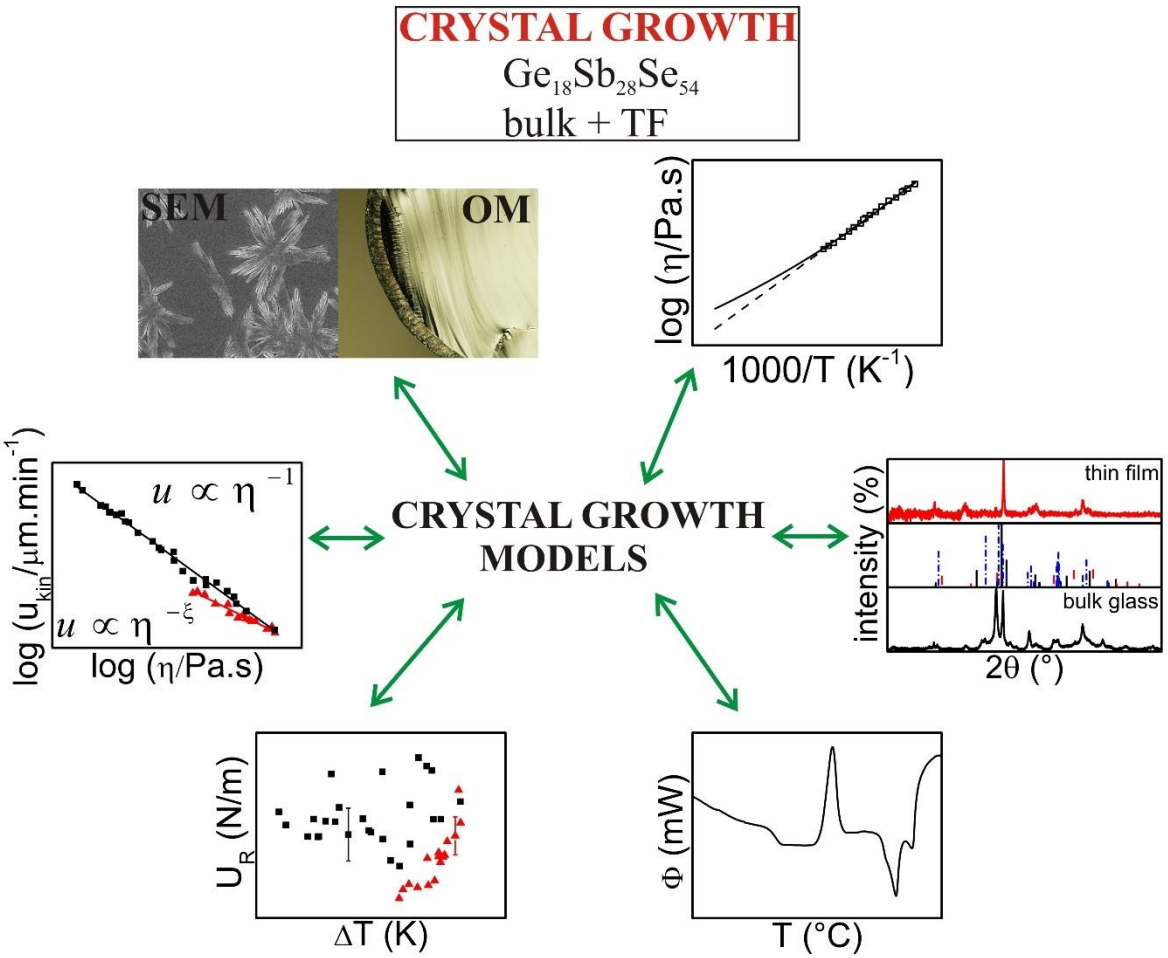

Figure 14: Procedure and highlights of the analysis of crystal growth in $Ge_{18}Sb_{28}Se_{54}$ thin films and bulk glasses (**Paper IV**).

The last introduced paper (**Paper V**) considerably extends the crystal growth rate data in As_2Se_3 material, which were published by Henderson and Ast[101], to higher temperatures up to the region close to melting point and completes the findings about the crystal growth behavior in As_2Se_3 bulk glass using optical microscopy and thermoanalytical measurements under isothermal and nonisothermal conditions (see Figure 15).

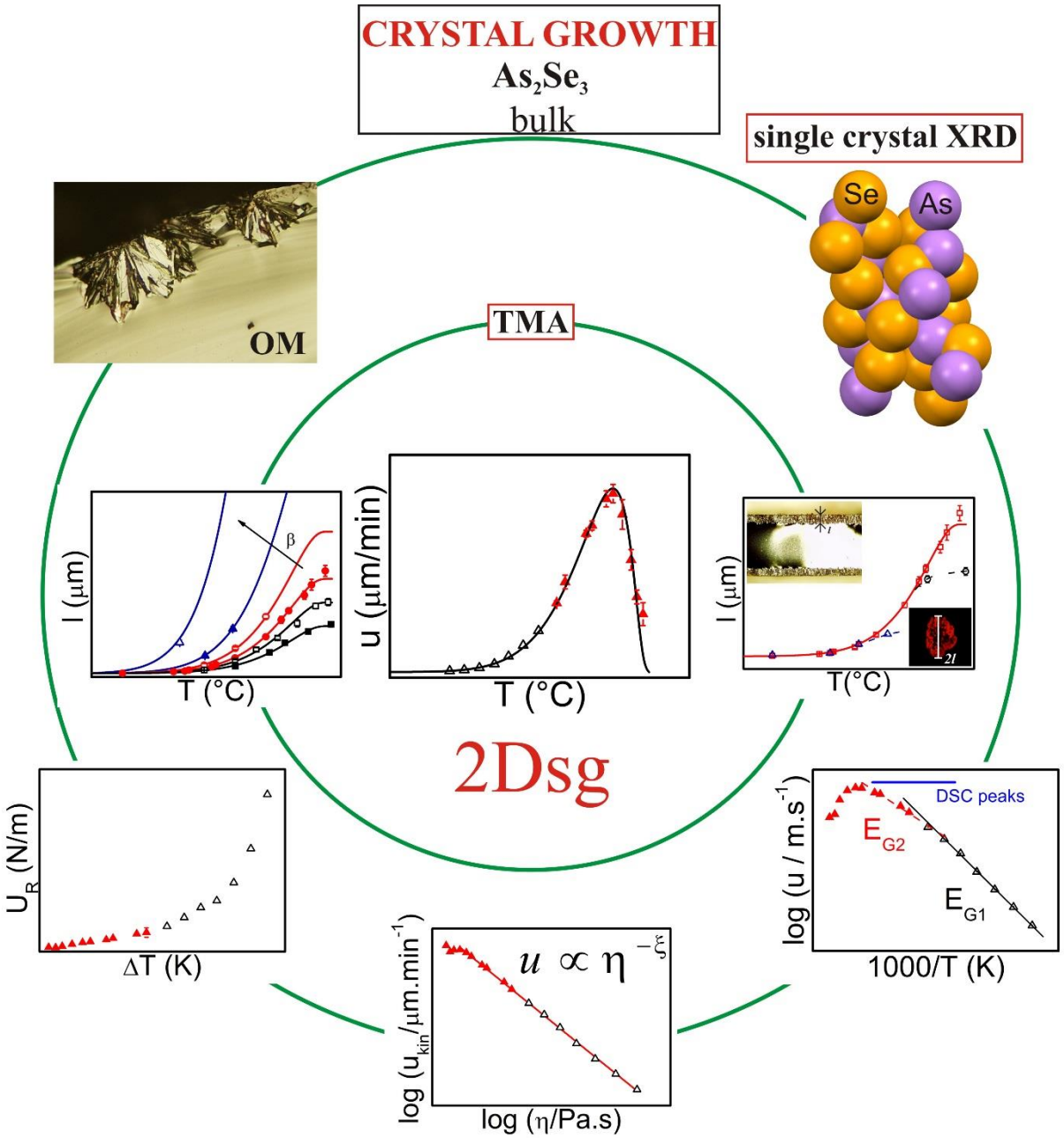

Figure 15: Procedure and highlights of the analysis of crystal growth in As_2Se_3 bulk glass (**Paper V**).

This system exhibits only surface crystallization, which is quite complicated, heterogeneous and totally stochastic process with significantly long time-lag for nucleation. Therefore, the samples were firstly nucleated to ensure higher nucleation density and make the study of crystal growth possible. It was proved that all isothermal crystal growth rate data can be well described by the kinetic exponent corrected 2D surface nucleated growth model. Regarding the decoupling of crystal growth rate and viscosity in this system, its extent was tested by three

different approaches: Ediger's approach (log u_{kin} vs log η); least square fit of linearized equation for 2D surface nucleated growth model with incorporated ξ in three-dimensional space; and ratio of the activation energy of crystal growth and the activation energy of viscous flow. All ways of testing provided values of kinetic exponent ξ that well correspond to each other within the combined error limits ($\xi = 0.69$). The corrected 2D surface nucleated crystal growth model also successfully describes the development of crystalline layer thickness and growth pattern at amorphous sample surface in nonisothermal conditions. In this paper, it was shown that one should pay attention to finding of the proper value of melting enthalpy with respect to the difference in values between the crystallization and melting enthalpies which indicates some uncrystallized amorphous phase in seemingly crystallized sample. Fully crystallized ingot of As_2Se_3 was prepared in a special way in order to find the proper melting enthalpy and examination of single crystal structure. Furthermore, the difficulty to obtain reliable values of ΔC_p due to the sublimation of crystalline As_2Se_3 and the volatility of its liquid was clearly demonstrated. This can be observed in many chalcogenide glassy systems and hence the approximations for ΔG calculation are applied.

The crystal growth studies presented in the thesis (**Paper II – V**) were performed in various chalcogenide glassy systems in the form of bulk glasses or thin films using many direct and indirect techniques. One of the important links between these studies was the relation of crystal growth and viscous flow with respect to their decoupling. Ediger et al.[48] demonstrated for numerous organic and inorganic glasses that the exponent ξ is linearly correlated with fragility m_η of the system: $\xi = 1.1 - 0.005 \cdot m_\eta$. Figure 16, which shows the dependence of exponent ξ on fragility m_η for the studied chalcogenide glasses, suggests that Ediger's relation might not be generally valid, especially in the case of chalcogenide glasses since they do not practically show any dependence of decoupling on fragility. It can be concluded that Ediger's assumption does not hold for chalcogenide glasses and it is necessary to deal with the viscosity-growth relation individually in every single study.

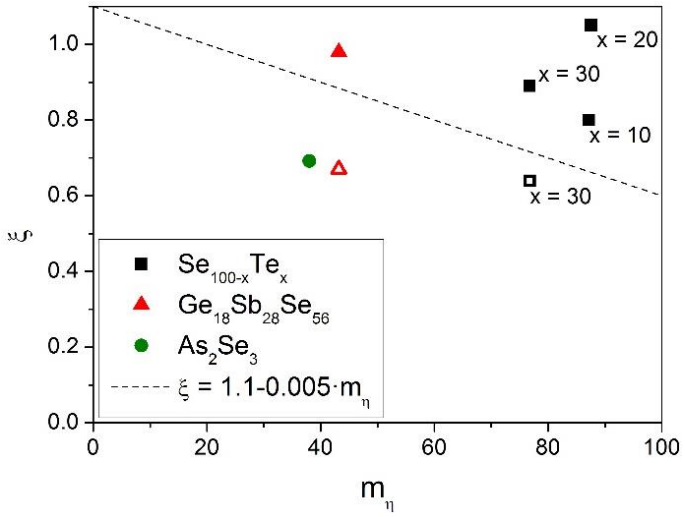

Figure 16: Dependence of kinetic exponent ξ expressing the extent of decoupling between crystal growth rate and viscous flow on fragility m_η of system for various chalcogenide systems; solid symbols correspond to bulk glass, empty symbols correspond to thin film.

3.3 CONCLUSIONS

Nucleation in chalcogenide glasses – the first aim of the doctoral thesis was to study nucleation kinetics and test the applicability of CNT and of its improvements for description of the steady-state nucleation and analysis of transient models for nucleation in chalcogenide glassy systems.

Experiments and findings:

- Nucleation in $Ge_{1.8}Sb_{36.8}S_{61.4}$ thin films of thickness 1 μm (isothermal in-situ single-stage annealing; optical microscope coupled with heating stage)
- Change of N with annealing time and temperature, crystals grew from randomly distributed nuclei in volume of the thin film → signs of homogeneous nucleation mechanism
- Non-steady state behavior described using Shneidman theory → values of I_{st}, t_{ind}, τ
- Test of CNT assumptions validity such as validity of the Stokes-Einstein relation for the description of molecular transport in nucleation process, capillarity approximation, and equality of thermodynamic properties of the critical cluster and the evolving macroscopic phase

- Incorporation of appropriate corrections of CNT into the model → satisfactory description of the found temperature dependence of steady-state nucleation rates, description of nucleation behavior in $Ge_{1.8}Sb_{36.8}S_{61.4}$ thin films in a wide temperature range
- Direct observations → nucleation in chalcogenide glasses occurs mostly at sample surface via heterogeneous mechanism → in most cases only qualitative data on nucleation
- Further investigations are necessary to achieve any general conclusion

Crystal Growth in chalcogenide glasses – the second aim of the doctoral thesis was to study crystal growth using mainly direct microscopy techniques in order to obtain further information about crystal morphologies, crystal growth behavior and kinetics for selected chalcogenide glasses.

Experiments and findings:

- Studies of chalcogenide glassy systems in the form of bulk glass or thin film: Se-Te, Ge-Sb-Se, As_2Se_3
- Mostly direct observations of crystal growth using microscopy technique – obtaining the information about crystal growth rates and morphology of formed crystals
- Joint objective of the presented papers – description of crystal growth behavior in a wide temperature range combining experimental results and growth models
- Discussion about the proportionality of crystal growth rate to viscosity, which was tested in various ways
- Verification of general validity of the Ediger's correlation between the kinetic exponent and fragility → relation does not hold for chalcogenide glasses
- Breakdown of Stokes-Einstein relation (mostly observed in thin films) → correction of standard growth models via incorporation of the kinetic exponent
- Activation energies of the overall crystallization process (from DSC) and activation energies of the crystal growth (from microscopic measurements) – only comparison in the same temperature range is meaningful
- Study of structure and melting parameters – obtaining the proper values
- Test of calculating ΔG using heat capacity data and using approximations → comparable results regarding the modeling of reduced crystal growth rate and operative crystal growth model (**Paper II**)

- Obvious necessity of combining direct and indirect techniques for crystallization studies in order to get reliable detailed results on the crystallization process

The presented thesis contains extended study of nucleation in chalcogenide glasses, providing not only the qualitative description of nucleation behavior in the studied system but also the quantitative results, which are quite unique. As far as we know, most studies of nucleation in chalcogenide glasses are only qualitative. With the knowledge of nucleation rate data, the test of suitability of famous classical nucleation theory (CNT) and its improvements was performed. It was found that CNT is sufficient for the description of nucleation behavior in a wide temperature range in the studied chalcogenide glass, nevertheless it has to be noted that more studies on nucleation kinetics in different chalcogenide glasses are necessary to be able to make a general conclusion.

Regarding the crystal growth, this systematic work yields further findings in the description of crystal growth behavior. The presented results extend the knowledge of the effect of $u - \eta$ relation on the description of crystal growth data using growth models. In the case of decoupling between u and η, the standard growth models can be modified by incorporation of the kinetic exponent ξ, which leads to a better description of experimental growth data. It was found that there is no simple general formula connecting the decoupling with fragility for chalcogenide glasses. Using the combination of results from classic microscopic studies with those of macroscopic ones, detailed and interesting information about crystallization process as a whole is obtained, and therefore more detailed understanding of crystallization process can be achieved.

REFERENCES

[1] N. Mehta, J. Sci. Ind. Res. **65**, 777-786 (2006).

[2] A. Feltz, *Amorphous inorganic materials and glasses*. (VCH, 1993).

[3] B. Bureau, X. H. Zhang, F. Smektala, J. L. Adam, J. Troles, H. L. Ma, C. Boussard-Pledel, J. Lucas, P. Lucas, D. Le Coq, M. R. Riley, and J. H. Simmons, J. Non-Cryst. Solids **345**, 276-283 (2004).

[4] X. Zhang, H. Ma, and J. Lucas, J. Optoelectron. Adv. Mater. **5**, 1327-1333 (2003).

[5] S. R. Ovshinsky, Phys. Rev. Lett. **21**, 1450-1453 (1968).

[6] S. Raoux, F. Xiong, M. Wuttig, and E. Pop, MRS Bull. **39**, 703-710 (2014).

[7] M. Terao, T. Morikawa, and T. Ohta, Jpn. J. Appl. Phys. **48**, 080001-1 - 080001-14 (2009).

[8] M. Wuttig and N. Yamada, Nat. Mater. **6**, 824-832 (2007).

[9] W. Holand, V. Rheinberger, and M. Schweiger, Philos. Trans. R. Soc. Lond. Ser. A-Math. Phys. Eng. Sci. **361**, 575-588 (2003).

[10] E. D. Zanotto, Am. Ceram. Soc. Bull. **89**, 19-27 (2010).

[11] E. D. Zanotto and J. C. Mauro, J. Non-Cryst. Solids **471**, 490-495 (2017).

[12] M. Frumar, *Chemie pevných látek: Určeno pro posl. VŠCHT Pardubice. Úvod*. (Vysoká škola chemicko-technologická, 1992).

[13] P. G. Debenedetti and F. H. Stillinger, Nature **410**, 259-267 (2001).

[14] M. D. Ediger, C. A. Angell, and S. R. Nagel, J. Phys. Chem. **100**, 13200-13212 (1996).

[15] A. Zakery and S. R. Elliott, J. Non-Cryst. Solids **330**, 1-12 (2003).

[16] K. F. Kelton and A. L. Greer, *Nucleation in Condensed Matter: Applications in Materials and Biology*. (Pergamon, 2010), pp.1-743.

[17] J. W. Gibbs, *The Collected Works of J. Willard Gibbs, Volume I: Thermodynamics*. (Yale University Press, 1928).

[18] I.V. Markov, *Crystal Growth for Beginners: Fundamentals of Nucleation, Crystal Growth and Epitaxy*. (World Scientific Publishing Company Incorporated, 2003).

[19] M. Volmer and A Weber, Z. Phys. Chem. **119U**, 277-301 (1926).

[20] Richard Becker and Werner Döring, Ann. Phys. **416**, 719-752 (1935).

[21] D. Turnbull and J. C. Fisher, J. Chem. Phys. **17**, 71-73 (1949).

[22] D. Turnbull, J. Appl. Phys. **21**, 1022-1028 (1950).

[23] K. F. Kelton, Solid State Phys. **45**, 75-177 (1991).

[24] V. M. Fokin, E. D. Zanotto, N. S. Yuritsyn, and J. W. P. Schmelzer, J. Non-Cryst. Solids **352**, 2681-2714 (2006).

[25] D. R. Uhlmann and B. Chalmers, Ind. Eng. Chem. **57**, 19-31 (1965).

[26] P. F. James, J. Non-Cryst. Solids **73**, 517-540 (1985).

[27] Jürn W. P. Schmelzer, J. Non-Cryst. Solids **354**, 269-278 (2008).

[28] Jürn W. P. Schmelzer, Mater. Phys. Mech. **6**, 21-33 (2003).

[29] C. V. Thompson and F. Spaepen, Acta Metall. **27**, 1855-1859 (1979).

[30] H. B. Singh and A. Holz, Solid State Commun. **45**, 985-988 (1983).

[31] J. D. Hoffman, J. Chem. Phys. **29**, 1192-1193 (1958).

[32] I.S. Gutzow and J.W.P. Schmelzer, *The Vitreous State: Thermodynamics, Structure, Rheology, and Crystallization*. (Springer, 2013).

[33] D. Turnbull, J. Chem. Phys. **20**, 411-424 (1952).

[34] Ya B. Zeldovich, Acta Physicochim., USSR **18**, 1-22 (1943).

[35] J. W. P. Schmelzer, A. S. Abyzov, and V. G. Baidakov, Int. J. Appl. Glass Sci. **8**, 48-60 (2017).

[36] F. C. Collins, Z. Elektrochem. **59**, 404-407 (1955).

[37] D. Kashchiev, Surf. Sci. **14**, 209-220 (1969).

[38] K. F. Kelton, A. L. Greer, and C. V. Thompson, J. Chem. Phys. **79**, 6261-6276 (1983).

[39] V. A. Shneidman, Zhurnal Tek. Fiz. **58**, 2202-2209 (1988).

[40] M. L. F. Nascimento and E. D. Zanotto, J. Chem. Phys. **133**, 174701-1 - 174701-10 (2010).

[41] R.J. Kirkpatrick, Am. Mineral. **60**, 798-814 (1975).

[42] D.R. Uhlmann, in *Advances in Nucleation and Crystallization in Glasses*, edited by L.L. Hench and S.W. Freiman (American Ceramics Society, Ohio, 1972), pp. 91-115.

[43] K. A. Jackson, D. R. Uhlmann, and J. D. Hunt, J. Cryst. Growth **1**, 1-36 (1967).

[44] A. S. Skapski, Acta Metall. **4**, 576-582 (1956).

[45] P. D. Calvert and D. R. Uhlmann, J. Cryst. Growth **12**, 291-296 (1972).

[46] Daniel Švadlák, Disertační práce, Univerzita Pardubice, 2008.

[47] K. L. Ngai, J. H. Magill, and D. J. Plazek, J. Chem. Phys. **112**, 1887-1892 (2000).

[48] M. D. Ediger, P. Harrowell, and L. Yu, J. Chem. Phys. **128**, 034709-1 - 034709-6 (2008).

[49] M. L. F. Nascimento, E. B. Ferreira, and E. D. Zanotto, J. Chem. Phys. **121**, 8924-8928 (2004).

[50] M. L. F. Nascimento and E. D. Zanotto, Phys. Rev. B **73**, 024209-1 - 024209-7 (2006).

[51] M. L. F. Nascimento, V. M. Fokin, E. D. Zanotto, and A. S. Abyzov, J. Chem. Phys. **135**, 194703-1 - 194703-17 (2011).

[52] J. W. P. Schmelzer, A. S. Abyzov, V. M. Fokin, C. Schick, and E. D. Zanotto, J. Non-Cryst. Solids **429**, 45-53 (2015).

[53] J. W. P. Schmelzer, A. S. Abyzov, V. M. Fokin, C. Schick, and E. D. Zanotto, J. Non-Cryst. Solids **428**, 68-74 (2015).

[54] S. Martinkova, J. Bartak, P. Kostal, J. Malek, and H. Segawa, J. Phys. Chem. B **121**, 7978-7986 (2017).

[55] J. Malek, J. Bartak, and J. Shanelova, Cryst. Growth Des. **16**, 5811-5821 (2016).

[56] S. Martinkova, J. Bartak, J. Malek, and H. Segawa, J. Appl. Phys. **120**, 145301-1 - 145301-7 (2016).

[57] S. C. Glotzer, J. Non-Cryst. Solids **274**, 342-355 (2000).

[58] E. D. Zanotto and P. F. James, J. Non-Cryst. Solids **74**, 373-394 (1985).

[59] J. Kalb, F. Spaepen, and M. Wuttig, Appl. Phys. Lett. **84**, 5240-5242 (2004).

[60] G. Ruitenberg, A. K. Petford-Long, and R. C. Doole, J. Appl. Phys. **92**, 3116-3123 (2002).

[61] S. K. Pillai and J. Malek, J. Mater. Sci. **50**, 3854-3859 (2015).

[62] S. K. Pillai, V. Podzemna, J. Bartak, and J. Malek, J. Cryst. Growth **382**, 87-93 (2013).

[63] J. A. Kalb, C. Y. Wen, F. Spaepen, H. Dieker, and M. Wuttig, J. Appl. Phys. **98**, 054902-1 - 054902-6 (2005).

[64] S. Privitera, C. Bongiorno, E. Rimini, and R. Zonca, Appl. Phys. Lett. **84**, 4448-4450 (2004).

[65] J. A. Kalb, F. Spaepen, and M. Wuttig, J. Appl. Phys. **98**, 054910-1 - 054910-7 (2005).

[66] J. Orava and A. L. Greer, Acta Mater. **139**, 226-235 (2017).

[67] S. Ziegler and M. Wuttig, J. Appl. Phys. **99**, 064907-1 - 064907-4 (2006).

[68] B. S. Lee, G. W. Burr, R. M. Shelby, S. Raoux, C. T. Rettner, S. N. Bogle, K. Darmawikarta, S. G. Bishop, and J. R. Abelson, Science **326**, 980-984 (2009).

[69] C. S. Ray and D. E. Day, J. Am. Ceram. Soc. **73**, 439-442 (1990).

[70] C. S. Ray, X. Y. Fang, and D. E. Day, J. Am. Ceram. Soc. **83**, 865-872 (2000).

[71] A. A. Cabral, V. M. Fokin, E. D. Zanotto, and C. R. Chinaglia, J. Non-Cryst. Solids **330**, 174-186 (2003).

[72] A. A. Cabral, V. M. Fokin, and E. D. Zanotto, J. Non-Cryst. Solids **343**, 85-90 (2004).

[73] G. Tammann, Z. Phys. Chem. **25**, 441-479 (1898).

[74] U. Köster, Mater. Sci. Eng. **97**, 233-239 (1988).

[75] R. Muller, E. D. Zanotto, and V. M. Fokin, J. Non-Cryst. Solids **274**, 208-231 (2000).

[76] E. D. Zanotto, Int. J. Appl. Glass Sci. **4**, 105-116 (2013).

[77] V. M. Fokin, N. S. Yuritsin, V. N. Filipovich, and A. M. Kalinina, J. Non-Cryst. Solids **219**, 37-41 (1997).

[78] V. M. Fokin and E. D. Zanotto, J. Non-Cryst. Solids **246**, 115-127 (1999).

[79] Ralf Müller, J. Non-Cryst. Solids **219**, 110-118 (1997).

[80] N. Diaz-Mora, E. D. Zanotto, R. Hergt, and R. Muller, J. Non-Cryst. Solids **273**, 81-93 (2000).

[81] E. D. Zanotto, J. Non-Cryst. Solids **130**, 217-219 (1991).

[82] E. D. Zanotto, J. Non-Cryst. Solids **129**, 183-190 (1991).

[83] E. Wittman and E. D. Zanotto, J. Non-Cryst. Solids **271**, 94-99 (2000).

[84] S. Kruger and J. Deubener, J. Non-Cryst. Solids **417**, 45-51 (2015).

[85] A. L. Greer, Mater. Sci. Eng. A-Struct. Mater. Prop. Microstruct. Process. **179**, 41-45 (1994).

[86] G. K. Johnson, G. N. Papatheodorou, and C. E. Johnson, J. Chem. Thermodyn. **13**, 745-754 (1981).

[87] Jana Shánělová, Petr Koštál, and Jiří Málek, J. Non-Cryst. Solids **352**, 3952-3955 (2006).

[88] J. Bartak, V. Podzemna, J. Malek, G. Eising, and B. J. Kooi, J. Non-Cryst. Solids **410**, 7-13 (2015).

[89] V. M. Fokin, A. S. Abyzov, E. D. Zanotto, D. R. Cassar, A. M. Rodrigues, and J. W. P. Schmelzer, J. Non-Cryst. Solids **447**, 35-44 (2016).

[90] J. W. P. Schmelzer and A. S. Abyzov, J. Non-Cryst. Solids **449**, 41-49 (2016).

[91] A. S. Abyzov, V. M. Fokin, A. M. Rodrigues, E. D. Zanotto, and J. W. P. Schmelzer, J. Non-Cryst. Solids **432**, 325-333 (2016).

[92] A. S. Abyzov, V. M. Fokin, N. S. Yuritsyn, A. M. Rodrigues, and J. W. P. Schmelzer, J. Non-Cryst. Solids **462**, 32-40 (2017).

[93] J. Holubova, Z. Cernosek, and E. Cernoskova, J. Therm. Anal. Calorim. **114**, 997-1002 (2013).

[94] R. Svoboda and J. Malek, J. Chem. Phys. **141**, 224507-1 - 224507-10 (2014).

[95] J. Barták, J. Málek, P. Koštál, H. Segawa, and Y. Yamabe-Mitarai, J. Appl. Phys. **115**, 123506-1 - 123506-7 (2014).

[96] W. A. Johnson and R. F. Mehl, Trans. Aime **135**, 416-458 (1939).

[97] M. Avrami, J. Chem. Phys. **9**, 177-184 (1941).

[98] M. Avrami, J. Chem. Phys. **7**, 1103-1112 (1939).

[99] M. Avrami, J. Chem. Phys. **8**, 212-224 (1940).

[100] J. Bartak, P. Kostal, V. Podzemna, J. Shanelova, and J. Malek, J. Phys. Chem. B **120**, 7998-8006 (2016).

[101] D. W. Henderson and D. G. Ast, J. Non-Cryst. Solids **64**, 43-70 (1984).

PAPER I

CRYSTAL GROWTH & DESIGN

Article

Cite This: Cryst. Growth Des. 2018, 18, 4562−4570

pubs.acs.org/crystal

Transient Nucleation in Ge−Sb−S Thin Films

Simona Martinková, Jana Shánělová,* Jaroslav Barták, and Jiří Málek

Department of Physical Chemistry, University of Pardubice, Studentská 573, Pardubice 532 10, Czech Republic

ABSTRACT: The crystal nucleation behavior and kinetics in $Ge_{1.8}Sb_{36.8}S_{61.4}$ thin films were studied using optical microscopy coupled with a computer-controlled heating stage. The single-stage in situ heat treatment method was chosen for the study of nucleation. In-situ experiments were performed in the temperature range of 236−295 °C. The time evolution of the number of nuclei at various temperatures revealed transient behavior at low nucleation times. The transient nucleation data were described using the Shneidman equation to get values of steady-state nucleation rate, induction period, and time-lag of nucleation for the studied temperatures. On the basis of nucleation experiments, the temperature dependence of crystal−liquid surface energy and decoupling of nucleation rate and viscosity was assessed. The nucleation rate data obtained from microscopy measurements were discussed in terms of classical nucleation theory. It was found that the nucleation curve with the maximum at 288 °C and previously published growth curve with maximum at 309 °C overlap significantly.

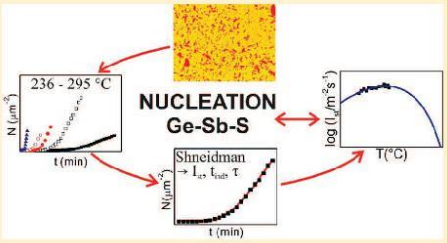

INTRODUCTION

The crystallization process involves the formation of stable nuclei which reach a critical size and their continuous growth.[1−3] The first step, nucleation, may occur by different mechanisms which are commonly divided into homogeneous and heterogeneous, where the former type occurs stochastically with the same probability in volume (surface) of sample, and the latter prefers places such as preexisting nuclei, impurities, and defects for the formation of new nuclei. Depending on the position where nucleation takes place, one can distinguish volume and surface crystallization. Regarding the glasses, controlled nucleation and crystal growth underlay the production of glass-ceramics,[4,5] and avoiding crystallization gives rise to optical fibers[6] and switching between the glassy and crystalline state is exploited in phase-change memories.[7] The nucleation stage determines the way of overall crystallization, and therefore its investigation is of great interest from a practical and theoretical point of view.

The study of nucleation kinetics is usually difficult and time-consuming. Several direct and indirect methods were developed for studying nucleation, such as microscopy,[8−10] differential scanning calorimetry (DSC)/differential thermal analysis (DTA),[11,12] and X-ray diffraction[13,14] measurements. The indirect non-isothermal DSC/DTA measurements can be fast and provide accurate quantitative data, but it is necessary to have some preliminary information about nucleation and crystal growth. This preliminary information is possible to get from microscopy measurements which are more laborious. The microscopy methods can be divided into two groups according to overlapping of the nucleation and growth rate curves. If the overlapping of the curves is weak, the double-stage Tammann method is used for the estimation of the crystal number and nucleation rates. The Tammann method consists of heat treatment at a low nucleation temperature, and then the crystals are grown up to microscopic sizes at a higher temperature. In the case of considerable overlapping, crystals are visible and can be counted after single-stage heat treatment.

The crystal nucleation in glasses is studied for several decades, and many papers have been published which significantly extended the understanding of the nucleation process and its description via classical nucleation theory (CNT) and resolved some problems occurring in the quantitative description of nucleation rates. It should be noted that the essential portion of the present knowledge on nucleation in glass forming systems is based on studies in oxide glasses, especially in lithium disilicate glass which has been used as a model system.[10,15−17] As far as we know, only a few studies of nucleation have been made in chalcogenide glasses, which were mostly qualitative without detailed information about nucleation kinetics and quantitative data on nucleation rates.[8,9,18−25] Therefore, the test of CNT, its improvements, and analysis of transient models for nucleation in chalcogenide glasses seem to be needed.

We chose the Ge−Sb−S system for the study of nucleation due to wide investigations especially on thermodynamic and viscosity data[26,27] which are necessary for calculations. Many studies on the crystallization process using DTA,[28,29] DSC,[30−36] and thermomechanical analysis[37,38] have been performed. There also have been direct investigations on crystal growth in the $(GeS_2)_x(Sb_2S_3)_{x-1}$ system using optical microscopy.[30,33,37,39−41] The study of nucleation kinetics was made in $(GeS_2)_{0.9}(Sb_2S_3)_{0.1}$ thin films using a double-stage

Received: April 13, 2018
Revised: June 7, 2018
Published: June 28, 2018

DOI: 10.1021/acs.cgd.8b00555
Cryst. Growth Des. 2018, 18, 4562−4570

heat treatment method and optical microscopy.[19] The Ge–Sb–S system is of interest to researchers for its applications in optoelectronics in the IR region, photocatalysis, and solar energy conversion.[42]

In this paper, we carefully examined the nucleation behavior and kinetics in $Ge_{1.8}Sb_{36.8}S_{61.4}$ thin films using optical microscopy coupled with a computer-controlled heating stage. The Shneidman expression[43] for the description of transient nucleation was used to obtain the information about the steady-state nucleation rate, induction period, and time-lag of nucleation. The experimental nucleation rate data were discussed in terms of CNT utilizing the constant or the temperature-dependent crystal–liquid surface energy. The crystal–liquid surface energy extracted from nucleation data is consistent with those reported for well-known phase-change materials.[23] The thermodynamic barrier calculated from experimental nucleation data is in good agreement with CNT prediction. It was found that nucleation and previously published growth curves overlap significantly.

■ EXPERIMENTAL SECTION

The $(GeS_2)_{0.1}(Sb_2S_3)_{0.9}$ (2.1 mol % Ge, 37.5 mol % Sb, 60.4 mol % S) bulk glass was prepared by a conventional melt-quench technique. An adequate amount of pure elements (5N purity, Sigma-Aldrich) was placed into a silica ampule. The ampule was evacuated to the pressure 10^{-3} Pa, sealed, and annealed in a rocking furnace at 950 °C for 24 h. After heat treatment and homogenization, the ampule was rapidly quenched in water with ice. The prepared bulk glass was used as a starting material for preparation of thin films. Thin films were prepared by thermal deposition on microscopy glass substrates. During preparation of thin films, the glass substrates were rotated by means of a planetary rotation system to ensure homogeneity in the film thickness. The deposition rate (1–2 nms^{-1}) was measured using the quartz microbalance technique. The final thickness of the thin films was 1 μm. Energy dispersive X-ray (EDX) microanalyzer coupled with a scanning electron microscope (LYRA 3, Tescan, Czech Republic; EDS analyzer Aztec X-Max 20, Oxford Instruments, 5 kV) was used to check the composition of the thin films. The composition of the prepared thin films was 1.8 mol % Ge, 36.8 mol % Sb, and 61.4 mol % S (±0.5 mol %). The amorphous nature of the prepared thin films was verified using X-ray diffraction analysis (XRD), which was performed using a Bruker D8 Advance AXS diffractometer (horizontal goniometer, scintillation counter, CuKα (40 kV, 30 mA).

The crystal nucleation in $Ge_{1.8}Sb_{36.8}S_{61.4}$ thin films was observed in situ using optical microscope Olympus BX51 coupled with a computer-controlled heating stage Linkam in the transmission mode. A one-step annealing process was applied on thin films which were cut into smaller pieces (1 × 1 cm^2). Every single sample was placed into the heating stage, heated up to the selected temperature with the rate of 50 °C min^{-1}, and annealed for a specific time. The micrographs/videos were taken during the isothermal step of the experiment. From micrographs, the number of formed crystals (nuclei) was determined by manual counting in the Olympus Stream Essentials program. The numbers of nuclei for each measured time were recalculated per noncrystallized area since significant overlap of nucleation and crystal growth occurred. The nucleation was followed in the temperature range of 236–295 °C. For each studied temperature, 3–8 experiments were performed.

■ RESULTS

The crystals in $Ge_{1.8}Sb_{36.8}S_{61.4}$ thin films grew from randomly distributed nuclei in the volume of thin film, and the crystallization is not initiated at the surface. Typical crystals, which are shown in Figure 1, are composed of an asymmetric radiating array of crystalline fibers which forms crystalline

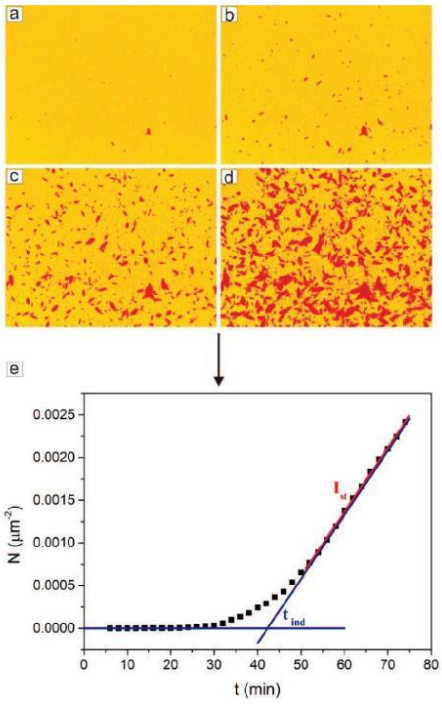

Figure 1. Time evolution of nuclei in $Ge_{1.8}Sb_{36.8}S_{61.4}$ thin films at temperature 236.1 °C: (a) t = 30 min, N = 31; (b) t = 42 min, N = 174; (c) t = 58 min, N = 694; (d) t = 74 min, N = 1302; (e) N–t curve with marked experimental evaluation of induction period t_{ind} and nucleation rate I_{st}.

aggregates. The same findings were reported in the paper on crystal growth in Ge–Sb–S thin films.[40,41] The XRD analysis of $(GeS_2)_x(Sb_2S_3)_{x-1}$ (x = 0.1, 0.2, 0.3) crystallized thin film performed by Barták et al.[41] revealed that crystalline phase corresponds to orthorhombic Sb_2S_3. The composition of thin films studied by Barták et al. is somewhat different ($Ge_{2.1}Sb_{37.5}S_{60.4}$) from ours; nevertheless, it will be shown (see the Discussion) that the composition does not significantly influence the crystal growth kinetics. Thus, we can compare the results from nucleation and previously published crystal growth.

The nucleation rate I is one of the most important characteristics in nucleation kinetics and is generally expressed with the formula $I = dN/dt$, where N is number of formed nuclei and t is the time of nucleation. Therefore, to estimate the nucleation rate at any given temperature, it is necessary to know the number of nuclei as a function of nucleation time. The single-stage method was chosen as the appropriate way to study nucleation in $Ge_{1.8}Sb_{36.8}S_{61.4}$ thin films on the basis of our previous published results on crystal growth in the Ge–Sb–S system.[41] A broad distribution of crystal sizes was observed, which indicates the significant overlapping of nucleation and crystal growth curves. The isothermal nucleation was studied in the temperature range 236–295

DOI: 10.1021/acs.cgd.8b00555
Cryst. Growth Des. 2018, 18, 4562–4570

°C using optical microscope coupled with a heating stage. The numbers of grown nuclei, which increase during the heat treatment of sample, were estimated by manual counting from micrographs and then recalculated per noncrystallized unit area. Digital image analysis was not able to be used because of overlapping of growing crystals and insufficient contrast between the crystalline and glassy matrix. The time evolution of number of nuclei N at temperature 236.1 °C is shown in Figure 1 together with the $N-t$ curve.

It should be considered that in the case of single-stage heat treatment the $N-t$ curves are shifted to higher times by a time t_0, which is more pronounced for low nucleation temperatures.[10] This time is needed for growing crystals up to the microscope resolution limit ($\varepsilon = 2r_{res} = 0.9$ μm for our measurements) and can be calculated using the equation:

$$t_0 = \frac{r_{res} - r^*}{u(T_N)} \cong \frac{r_{res}}{u(T_N)} \quad (1)$$

where r^* is the critical size of the nucleus, which was very small in comparison with r_{res} of the optical microscope and was omitted in calculations of t_0, and $u(T_N)$ is the crystal growth rate at the nucleation temperature, which was obtained from the work of Barták et al.[41] The critical size of nucleus r^* for mean undercooling 280 °C was estimated[10] to be approximately 7.7 Å. The calculated values of t_0 are in the range from 22 to 0.08 s for the lowest and highest measured temperature, respectively. These values are in comparison with the time range of the whole $N-t$ curve, and the values of t_{ind}, τ (see next paragraph for more details) very low and therefore can be neglected. The effect of the shift of the $N-t$ curve is important for glasses with a weak overlap of nucleation and growth rate curves.[44]

One can see typical non-steady-state (transient) nucleation behavior at low times in the $N-t$ curves (Figure 2). Some

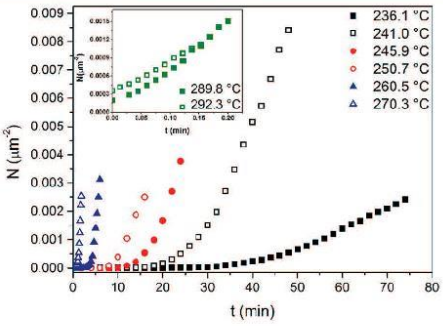

Figure 2. Representative dependences of number of nuclei N on time t for various temperatures. The inset shows $N-t$ curves for temperatures near T_{max}.

transient period is needed to build up the initial nuclei distribution toward the time independent distribution corresponding to the nucleation temperature T. After this period the steady-state nucleation regime, which is characterized by a constant nucleation rate, is established. Steady-state nucleation regime is represented with a linear part in the $N-t$ curves. The slope of this straight line corresponds to the steady-state nucleation rate I_{st} at temperature T (Figure 1).

The time required to establish a steady-state nucleation rate I_{st} is denoted as the time-lag in nucleation τ and can be determined with the knowledge of values of the induction period t_{ind} in a way depending on the chosen theory for transient nucleation. The induction period t_{ind} can be found from the experimental data as the intercept of the extrapolated linear part of the $N-t$ curve with the time axis as illustrated in Figure 1. It is obvious that the induction period decreases with increasing nucleation temperature (Figure 2). The experimental way of determination the values of I_{st} and t_{ind} is easy and not laborious; on the other hand, the selection of the linear part of the $N-t$ curve is a subjective procedure, considering that curve asymptotically approaches a linear dependence. The phase transformation can be terminated prior to the establishment of the steady-state nucleation rate in the case of significant overlapping of nucleation and growth temperature dependencies. Then a more accurate way for finding the values of nucleation rate, induction period, and time-lag is by fitting the whole $N-t$ curve (see the Discussion).

Figure 2 represents selected $N-t$ curves with the non-steady-state part, which can be seen especially at low nucleation temperatures during the initial stage of heat treatment. $N-t$ curves at nucleation temperatures near and above T_{max} (temperature at maximum nucleation rate) had frequently the form of straight lines with negligible or no induction period (inset of Figure 2). The shift of these dependences along N-axis was observed, which was caused by formation and growing crystals before the appropriate nucleation temperature was reached ($T_N > T_{max}$).

DISCUSSION

Treatment of the $N(t, T)$ Curves. Transient nucleation in glasses is usually described in terms of the classical kinetic model of crystal nucleation proposed by Turnbull and Fisher,[45] who applied the Becker–Döring theory[46] of vapor condensation to nucleation in condensed systems. The first expression for transient nucleation proposed by Zeldovich[47] allows one to describe the time dependent nucleation rate and find the time-lag in nucleation. The Zeldovich equation fails mainly at large times of the time dependence of nuclei number,[48] so many other analytical and numerical solutions for transient nucleation were proposed.[16] Here we introduce two successful analytical solutions for the description of transient nucleation.

One of the most famous solutions for transient nucleation was proposed by Collins and Kashchiev.[49,50] Collins–Kashchiev equation is commonly used for the treatment of experimental data ($N-t$) to obtain the steady-state nucleation rate I_{st} and time-lag τ in silicate glasses. Moreover, the Collins–Kashchiev equation provides the values of I_{st} and τ, which are in a good agreement with those from numerical solutions.[51] The authors expressed the non-steady-state nucleation rate $I(t)$ as

$$I(t) = I_{st}\left[1 + 2\sum_{m=1}^{\infty}(-1)^m \exp\left(-m^2\frac{t}{\tau}\right)\right] \quad (2)$$

which results in the following equation for the time dependence of number of nuclei N:

$$N(t) = I_{st}\tau\left[\frac{t}{\tau} - \frac{\pi^2}{6} - 2\sum_{m=1}^{\infty}\frac{(-1)^m}{m^2}\exp\left(-m^2\frac{t}{\tau}\right)\right] \quad (3)$$

DOI: 10.1021/acs.cgd.8b00555
Cryst. Growth Des. 2018, 18, 4562–4570

The test of the fitting of our experimental $N-t$ data for 241 °C using the Collins−Kashchiev equation is depicted in Figure 3.

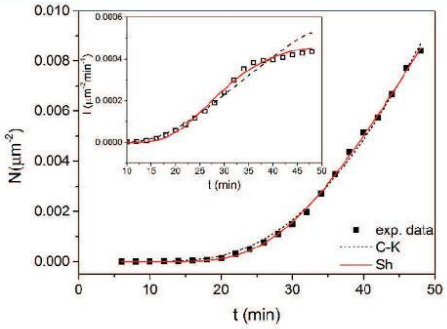

Figure 3. Experimental $N-t$ curve for 241 °C along with calculated curves using Collins−Kashchiev[49,50] (C−K; dashed line) and Shneidman[43] (Sh; solid line) theories for transient nucleation; the inset shows the time dependence of the nucleation rate.

Another analytical solution was suggested by Shneidman[43] for the time dependent nucleation rate for nuclei of sizes sufficiently larger than the critical size. According to Shneidman a double-exponential time-dependent nucleation rate $I(r, t)$ is given by the expression:

$$I(r, t) = I_{st} \exp\left[-\exp\left\{-\frac{t - t_i(r)}{\tau}\right\}\right] \quad (4)$$

with

$$t_i(r) = t_{ind}(r) - \gamma\tau$$

where γ is Euler's constant ($\gamma = 0.57721...$). In order to find the expression for the time dependence of number of nuclei N eq 4 can be integrated:

$$N(r, t) = \tau I_{st} E_1[\exp(-z)] \quad (5)$$

with

$$z = [(t - t_{ind}(r))/\tau] + \gamma$$

where E_1 is the exponential integral. The fitting of our experimental $N-t$ data using the Shneidman equation was tested, and Figure 3 shows the results for the temperature 241 °C.

Figure 3 depicting the experimental results and theoretical interpretation of the time dependence of number of nuclei using Collins−Kashchiev[49,50] and Shneidman[43] theories for the temperature 241 °C reveals discrepancies between the calculated curves. Although both theories for transient nucleation describe the $N-t$ curve sufficiently, one can see in the inset of Figure 3, which shows time development of non-steady-state nucleation rate toward its steady-state value, that a better description of experimental data is provide by the Shneidman theory. The found values of I_{st}, t_{ind}, and τ obtained by fitting experimental data for 241 °C using Collins−Kashchiev equation were $I_{st} = 0.0011\ \mu m^{-2}\ min^{-1}$, $t_{ind} = 58.2$ min, and $\tau = 35.4$ min. Employing the Shneidman theory for description of experimental data for 241 °C, we got more realistic values: $I_{st} = 0.00049\ \mu m^{-2}\ min^{-1}$, $t_{ind} = 30.9$ min, and $\tau = 7.6$ min. The value of I_{st} is consistent with the value obtained from the linear part of the $N-t$ curve: $I_{st} = 0.00041\ \mu m^{-2}\ min^{-1}$. The Collins−Kashchiev equation overestimates the steady-state nucleation rate, induction time, and time-lag and is not the proper theory for the description of transient nucleation in $Ge_{1.8}Sb_{36.8}S_{61.4}$ thin films. Therefore, we employed the Shneidman equation for the description of $N-t$ curves.

The experimental data for the number of nuclei N for a given nucleation temperature T vs nucleation time t were described by the Shneidman theory[43] to obtain the value of steady-state nucleation rate I_{st}, induction period t_{ind} and time-lag τ. The parameters I_{st}, t_{ind}, and τ were determined from nonlinear fitting of the $N-t$ curves using eq 5. The steady-state nucleation rates I_{st} at various temperatures along with the appropriate induction periods t_{ind} and time-lags τ for $Ge_{1.8}Sb_{36.8}S_{61.4}$ thin films are summarized in Table 1. The

Table 1. Steady-State Nucleation Rates I_{st}, Induction Periods t_{ind}, and Time-Lags τ in $Ge_{1.8}Sb_{36.8}S_{61.4}$ Thin Films[a]

T (°C)	$I_{st} \times 10^3$ ($min^{-1}\ \mu m^{-2}$)	t_{ind} (min)	τ (min)
236.1	0.088	46.7	11.5
241	0.41 ± 0.07	30.7 ± 1.6	7.7 ± 0.8
245.9	1.3 ± 0.9	21.8 ± 4.1	5.5 ± 1.4
250.7	0.41 ± 0.07	7.9 ± 0.9	1.3 ± 0.2
255.6	3.2 ± 3.2	9.4 ± 2.5	1.5 ± 1.4
260.5	1.9 ± 0.8	5.3 ± 1.3	1.2 ± 0.6
265.4	2.3 ± 1.5	2.2 ± 0.7	0.39 ± 0.08
270.3	2.1 ± 1.4	1.2 ± 0.4	0.3 ± 0.2
275.2	5.2 ± 2.5	1.3 ± 0.1	0.4 ± 0.2
280.1	6.6 ± 1.5	0.6 ± 0.1	0.21 ± 0.10
284.9	23.1 ± 5.5	0.4 ± 0.1	0.12 ± 0.03
287.4	4.7 ± 3.1	0.09 ± 0.09	0.05 ± 0.04
289.8	7.7 ± 5.2	0.07 ± 0.02	0.058 ± 0.003
292.3	13.1 ± 7.7	0.07 ± 0.08	0.05 ± 0.04
294.7	3.0 ± 2.8	0.04 ± 0.07	0.02 ± 0.04

[a]Temperature was constant within ±0.5 °C.

results of t_{ind} and τ are graphically presented by plotting log t_{ind} vs $1/T$ and log τ vs $1/T$ in Figure 4. One can see that the ratio between t_{ind} and τ is not constant in temperature, which is contrary to the prediction of the Collins−Kashchiev solution for transient nucleation.[49,50]

Temperature Dependence of Steady-State Nucleation Rates. According to CNT, commonly used for the analysis of crystal nucleation in glass-forming liquids, the steady-state homogeneous nucleation rate at temperature T can be written as[10]

$$I_{st} = A_N \exp\left(-\frac{W^* + \Delta G_D}{k_B T}\right) \quad (6)$$

where W^* and ΔG_D are respectively the thermodynamic and kinetic barriers of nucleation, k_B is the Boltzmann constant, and A_N is pre-exponential term which is only weakly temperature dependent. In the temperature range used for nucleation measurements A_N can be approximated by $A_N = n_S k_B T/h$, where $n_S \approx 1/\lambda^2$ is the number of structural units, with a size λ, per unit area and h is the Planck constant. For a spherical nucleus, the thermodynamic barrier of nucleation is given by

DOI: 10.1021/acs.cgd.8b00555
Cryst. Growth Des. 2018, 18, 4562−4570

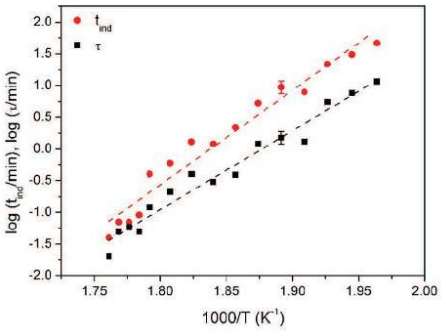

Figure 4. Logarithm of the induction period t_{ind} and τ vs $1/T$. The characteristic standard deviations of log t_{ind} and log τ are shown. The straight lines are least-squares fits.

$$W^* = \frac{16\pi\sigma^3 V_m^2}{3\Delta G^2} \tag{7}$$

where σ is the crystal−liquid surface energy, V_m is the molar volume of the crystalline phase, and ΔG is the thermodynamic driving force for crystallization, i.e., the free energy difference between crystalline phase and undercooled melt. Due to the absence of the experimental data on heat capacities of crystalline phase and undercooled melt, ΔG is frequently approximated using the Turnbull expression $\Delta G = \Delta H_m \Delta T / T_m = \Delta S_m \Delta T$ with ΔT being undercooling ($\Delta T = T_m - T$) and ΔH_m and T_m being melting enthalpy and melting temperature. DTA of Ge−Sb−S thin films performed by Barták et al.[52] showed a large distortion in the measured data, which prevent finding the appropriate melting parameters. Moreover, the crystalline phase is formed by pure Sb_2S_3. Therefore, we use melting parameters of pure Sb_2S_3 published by Johnson et al.[26] for calculations (T_m = 550 °C, $\Delta S_m/R$ = 5.94). The kinetic barrier of nucleation ΔG_D is usually related to the experimental available parameter, viscosity η. It is assumed that the molecular transport for nucleation process is controlled by diffusion and can be described in terms of an effective diffusion coefficient D:

$$D = \frac{k_B T \lambda^2}{h} \exp\left(-\frac{\Delta G_D}{k_B T}\right) \tag{8}$$

where λ is the diameter of the diffusing molecules or the jump distance. The measurement of diffusion is complicated, and the temperature dependence of diffusion coefficient is mostly not available, so D is usually related to the viscosity via the Stokes−Einstein relation:

$$D = \frac{k_B T}{3\pi\lambda\eta} \tag{9}$$

Viscosity of the Ge−Sb−S system was published in the work of Shánělová et al.[27] Temperature dependence of viscosity was studied in the bulk glass; nevertheless, it is assumed that the viscosity behavior in bulk glass and thin films is similar.[53]

Combining eqs 6, 7, 8, and 9 and relations for A_N and ΔG, we obtained the expression for the steady-state homogeneous nucleation rate in the following form:

$$I_{st} = \frac{n_S k_B T}{3\pi\lambda^3\eta} \exp\left(-\frac{16\pi\sigma^3 V_m^2}{3k_B T \Delta S_m^2 \Delta T^2}\right) \tag{10}$$

The logarithm of eq 10 can be rewritten in the simple parametric form as

$$\ln\left(\frac{I_{st}\eta}{T}\right) = \ln A - \frac{B}{T\Delta T^2} \tag{11}$$

The plot of $\ln(I_{st}\eta/T)$ vs $1/T\Delta T^2$ depicted in Figure 5 gave a good straight line in the studied temperature range, which is in

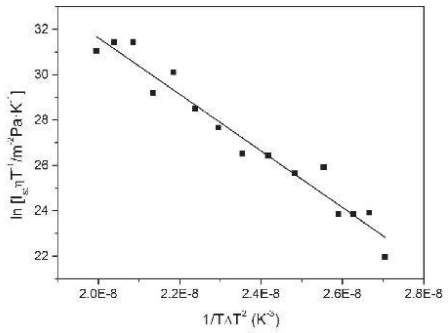

Figure 5. Dependence of $\ln(I_{st}\eta/T)$ vs $1/T\Delta T^2$ for $Ge_{0.8}Sb_{39.1}S_{60.1}$ thin films.

accordance with CNT. The parameters A and B determined from the plot were found to be 3.66×10^{24} Pa m^{-2} K^{-1} and 1.25×10^9 K^3, respectively.

The CNT is based on the assumption that the Stokes−Einstein relation $D \approx \eta^{-1}$ (eq 9) for the description of molecular transport in nucleation process is valid. The standard growth models are also based on this assumption, and it was shown that below 1.2 T_g the crystal growth rate and viscosity can decouple.[54] In this case the correction of growth models in the form of $D \approx \eta^{-\xi}$, where exponent ξ expresses the extent of decoupling, is necessary.[55] Nascimento et al.[44] investigated the effects of decoupling of dynamics of crystal nucleation and growth from those of viscous flow and found that decoupling between nucleation rate and viscous flow occurs at a lower temperature near T_g and is not so significant as that of the growth rate and viscous flow. Taking into account these findings, the extent of decoupling between the nucleation rate and viscous flow was tested. Assuming the classical nucleation model for the homogeneous steady-state nucleation and introducing the exponent ξ, $\ln(I_{st}/T)$ is a linear combination of $\ln\eta$ and $1/(T\Delta T^2)$:

$$\ln\left(\frac{I_{st}}{T}\right) = \ln A - \xi \ln\eta - B\left(\frac{1}{T\Delta T^2}\right) \tag{12}$$

The parameters A, B, and ξ were obtained by least-squares fit in three dimensional space. The exponent ξ is equal to 1, and parameters A and B are the same as that estimated using eq 11. The Stokes−Einstein relation is fulfilled near the melting point T_m as well as in highly supercooled liquid down to T_g. No other correction of classical nucleation model by exponent ξ is necessary.

DOI: 10.1021/acs.cgd.8b00555
Cryst. Growth Des. 2018, 18, 4562−4570

According to the basic assumption of CNT, the crystal−liquid interface energy is treated as a macroscopic property with a value equal to that of a planar interface, which is known as capillarity approximation. The semiempirical Skapski−Turnbull equation[56,57] can be used for the estimation of the crystal−liquid surface energy σ:

$$\sigma_{ST} = \alpha \Delta H_m V_m^{-2/3} N_A^{-1/3} \quad (13)$$

where N_A is Avogadro's number and α is coefficient obtained from nucleation experiments. The value of α was found to be on average 0.3 for a nonmetallic material,[15] and this value was used for calculation of σ_{ST}. The necessary crystallographic data of Sb_2S_3 (V_m, λ) were published by Bayliss and Nowacki:[58] $V_m = 7.35 \times 10^{-5}$ m^3 mol^{-1}. Combining these data and using the eq 13, the surface energy of crystal−liquid interface was determined to be $\sigma_{ST} = 0.082$ J m^{-2}. Another way for estimation of the crystal−liquid surface energy with the same assumption of constant σ is from the plot of $\ln(I_s\eta/T)$ vs $1/T\Delta T^2$.[15] The slope yielded crystal−liquid surface energy (σ_{CNT}) of 0.077 J m^{-2}.

It is well-known that usually CNT fails in calculation of $I-T$ curve if a constant crystal−liquid surface energy σ is used so the temperature-dependent interfacial energies should be employed. Only a few methods exist for the determination of $\sigma(T)$, which are based on the transient nucleation data.[15,59,60] With the knowledge of theoretical pre-exponential term of the nucleation rate equation (see eqs 10 and 11) A_{theo} the crystal−liquid surface energy can be calculated from CNT.[15,17,61] In this case, calculations lead to the temperature-dependent surface energy. The theoretical pre-exponential term A_{theo} was expressed in the following form utilizing λ as the diameter of the Sb_2S_3 molecule ($\lambda = 6.15 \times 10^{-10}$ m):[58]

$$A_{theo} = \frac{n_S k_B}{3\pi\lambda^3}$$

$$n_S = \frac{1}{\lambda^2} \quad (14)$$

The value of A_{theo} was found to be 1.7×10^{22} J m^{-5} K^{-1}. Experimental value of pre-exponential term A_{exp} was found as the intercept of $\ln(I\eta/T)$ vs $1/T\Delta T^2$ plot: $A_{exp} = 3.7 \times 10^{24}$ J m^{-5} K^{-1}. Usually there is a strong disagreement (up to many orders of magnitude) between the value of theoretical and experimental pre-exponential term.[15,17,61] For that reason, it was proposed that the crystal−liquid surface energy is calculated from eq 10, employing the theoretical value A_{theo} and the experimental values of nucleation rates.[15] The discrepancy between A_{theo} and A_{exp} was explained by postulating a temperature-dependent surface energy.[15,17] In our case, the discrepancy is not so significant; nevertheless, the temperature dependence of surface energy was determined even for our experimental data. Using the above-described method, the values of σ at measured nucleation temperatures were calculated, and following dependence was found:

$$\sigma = 1.597 \times 10^{-7} T(K)^2 - 1.439 \times 10^{-4} T(K) + 0.1033 \quad (15)$$

The dependence $\sigma(T)$ is depicted in Figure 6 showing a slight increase of σ with increasing temperature. This increase observed also for silicate glasses[10] was widely discussed, attributed, and can be partly removed by the size dependence of the surface energy.[62,63] On the other hand, the results of $\sigma(r, T)$ are strongly affected by the choice of Tolman's parameter

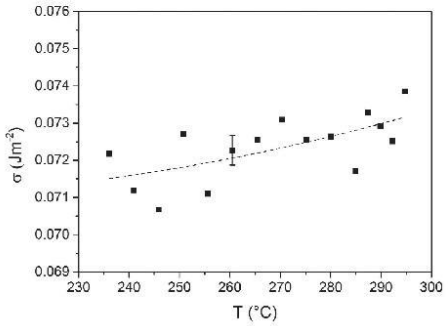

Figure 6. Temperature dependence of crystal−liquid surface energy calculated using eq 10 with the theoretical pre-exponential term and experimental nucleation rates. The characteristic standard deviation is shown.

(the width of the interfacial region between phases), which is included in equations for the curvature dependence of the surface energy.[63,64] Another interpretation of the increase of σ with increasing temperature discussed by Spaepen[65] is based on increased ordering of the liquid near the crystal, resulting in an entropy decrease and thus the increase of surface energy.

Comparing our results with the most famous phase-change materials GST and AIST, the crystal−liquid surface energy of studied $Ge_{0.8}Sb_{39.1}S_{60.1}$ is nearly the same as that of GST (σ = 0.075 J m^{-2})[23] and somewhat lower as that of AIST (σ = 0.11 J m^{-2}).[23] The crystal−liquid surface energy can be also estimated from crystal growth data, which are described using a 2D surface-nucleated growth model. This calculation was performed by Barták et al.[41] The found $\sigma = 0.389$ J m^{-2} from the growth data is substantially larger than the others derived from nucleation data. Such a discrepancy was also found in the study of $(GeS_2)_{0.9}(Sb_2S_3)_{0.1}$ thin films.[19] This discrepancy can be explained as a possible consequence of the stress induced changes in thin films due to growth of complex crystallites or by compositional shifts due to crystallization.[19]

In accordance with CNT the thermodynamic barrier for nucleation W^* defined via eq 7 is given by the crystal−liquid surface energy σ and the thermodynamic driving force for crystallization ΔG. CNT assumes that the thermodynamic properties of the critical cluster and the evolving macroscopic phase are equivalent. Following that and the validity of the capillarity approximation, the thermodynamic driving force for crystallization ΔG increases with decreasing temperature, the crystal−liquid surface energy σ is constant, and hence monotonic decrease of the thermodynamic barrier for nucleation W^* with decreasing temperature is expected. An anomalous behavior of W^*, i.e., decrease of W^* with decreasing T and then increase of W^* with any further decrease of T below the temperature of nucleation rate maximum T_{max}, was observed in silicate glasses. Therefore, some additional assumptions and corrections were introduced, and different hypothesis for the explanation of unexpected behavior of W^* were tested (outlined in refs 66−69). Figure 7 shows the temperature dependence of reduced thermodynamic barrier W^*/kT calculated from experimental nucleation rate data along with the reduced thermodynamic barrier calculated via eq 7 employing $\sigma(T)$ for $Ge_{1.8}Sb_{36.8}S_{61.4}$ thin films. The

DOI: 10.1021/acs.cgd.8b00555
Cryst. Growth Des. 2018, 18, 4562−4570

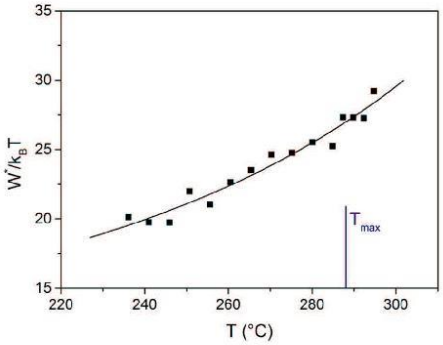

Figure 7. Dependence of the reduced thermodynamic barrier for nucleation on temperature. The points refer to values calculated from the experimental nucleation rates on the basis of eq 10; solid line was calculated using eq 7 employing $\sigma(T)$. T_{max} corresponds to the temperature of the maximum nucleation rate.

deviation from the theoretic course of W^*/kT vs T is not apparent in the studied temperature range. It seems, therefore, that CNT approximation is fulfilled, and therefore no correction of thermodynamic barrier for nucleation is needed for the studied Ge–Sb–S thin films.

Figure 8 shows the experimental nucleation data along with the calculated classical nucleation model using eq 10 and

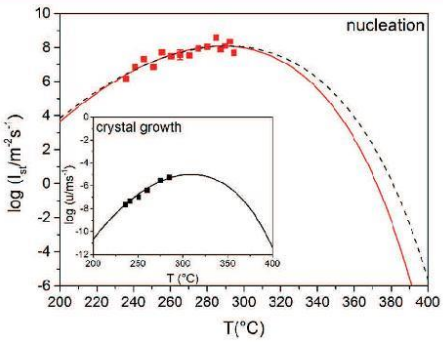

Figure 8. Experimental steady-state nucleation data (points) along with the calculated classical nucleation model utilizing constant σ (dashed line) and with the calculated classical nucleation model utilizing $\sigma(T)$ (solid line) of $Ge_{1.8}Sb_{36.8}S_{61.4}$ thin films (the characteristic standard deviation of experimental data is shown). The inset shows the experimental crystal growth data of $Ge_{0.8}Sb_{39.1}S_{60.1}$ thin films (points) described with the calculated 2D surface nucleated growth model (solid line) published by Barták et al.[41]

utilizing the constant or the temperature-dependent crystal–liquid surface energy (eq 15). The classical nucleation model for homogeneous steady-state nucleation provided satisfactory agreement with the experimental nucleation rates in both cases. However, the inclusion of the temperature-dependent crystal–liquid surface energy in model took better the experimental observations into consideration. According to observations the steady-state nucleation rate above T_{max} should decrease faster with increasing temperature than is the prediction of the model utilizing constant σ. The classical nucleation model utilizing the temperature-dependent crystal–liquid surface energy was used for the construction of Figure 9.

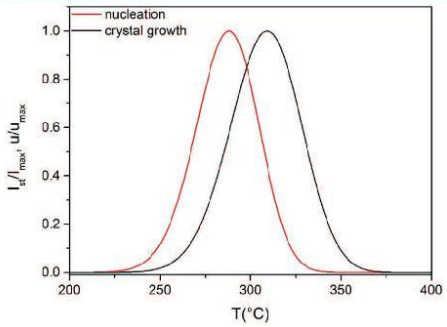

Figure 9. Calculated nucleation and crystal growth curve normalized to the maximum rate (I_{max} = 1.2 × 10^8 m^{-2} s^{-1}; u_{max} = 9.9 × 10^{-6} ms^{-1}).

A slight discrepancy between the model and experimental data observed at temperatures above T_{max} (around 288 °C) can be caused by the simplifying assumptions of CNT, such as identifying the properties of the critical clusters with those of the evolving macroscopic phase, or by the significant influence of crystal growth on nucleation and thus reducing the nucleation rates. The calculated 2D surface nucleated growth model (depicted in the inset of Figure 8 and Figure 9) was taken from the work of Barták et al.[41] It was mentioned earlier that the composition of thin films is slightly different from that of studied in this paper, so we verified the crystal growth in our thin films. The experimental results on crystal growth in $Ge_{1.8}Sb_{36.8}S_{61.4}$ thin films shown in the inset of Figure 8 are in agreement with the calculated growth model. Thus, we can compare the presented nucleation data and previously published growth data. The normalized nucleation and crystal growth curve (Figure 9) show the strong overlap with the maxima at 288 °C for nucleation and 309 °C for crystal growth. In comparison with the results of nucleation and crystal growth in $(GeS_2)_{0.9}(Sb_2S_3)_{0.1}$[19] (in fact opposite composition of the $(GeS_2)_x(Sb_2S_3)_{1-x}$ row), where the nucleation and growth curve are weakly intersecting, the maximum of the nucleation rate and crystal growth rate is shifted to the lower temperatures.

■ CONCLUSION

The nucleation behavior and kinetics in the $Ge_{1.8}Sb_{36.8}S_{61.4}$ thin films were studied in situ using optical microscopy coupled with a computer-controlled heating stage in the temperature range 236–295 °C. The single stage annealing method was chosen for the study of nucleation due to the previously published results on crystal growth in Ge–Sb–S thin films which showed broad size distribution of formed crystals. The Sb_2S_3 crystals grow in the volume of thin films from randomly distributed nuclei, and the crystallization is not initiated at the surface. Number of grown nuclei increases as the heat treatment of the sample continues. The time evolution of

DOI: 10.1021/acs.cgd.8b00555
Cryst. Growth Des. 2018, 18, 4562–4570

number of nuclei at various temperatures revealed transient behavior at low nucleation times. For the description of the obtained transient nucleation data and finding the values of steady-state nucleation rate, induction period, and time-lag of nucleation, the Shneidman equation was used.

The nucleation rate data obtained from microscopy measurements were discussed in terms of CNT. The semiempirical Skapski−Turnbull equation was used for the estimation of the crystal−liquid surface energy (σ_{ST} = 0.082 J m^{-2}). The value of crystal−liquid surface energy was also evaluated from the linearized CNT model for homogeneous steady-state nucleation (σ_{CNT} = 0.077 J m^{-2}). For a better description of experimental nucleation data by the classical nucleation model, the temperature-dependent crystal−liquid surface energy was assessed. With the knowledge of theoretical pre-exponential term of classical nucleation model for homogeneous steady-state nucleation and experimental nucleation rates for various temperatures, the dependence of crystal−liquid surface energy on temperature was found.

The extent of decoupling between the nucleation rate and viscous flow was tested. The exponent ξ was found to be 1, which means that the Stokes−Einstein relation describing the process of molecular transport in nucleation is valid, and no correction of nucleation model by exponent ξ is necessary.

It was confirmed that the thermodynamic barrier calculated from experimental nucleation data is in good agreement with CNT prediction. It seems, therefore, that no additional correction or adjustment of the thermodynamic barrier for nucleation is needed in this case.

The calculated classical nucleation model utilizing the temperature-dependent crystal−liquid surface energy describes the experimental steady-state nucleation data sufficiently. The nucleation and crystal growth curves show the strong overlap with the maxima of curve at 288 °C for nucleation and 309 °C for crystal growth.

AUTHOR INFORMATION

Corresponding Author

*E-mail: jana.shanelova@upce.cz.

ORCID

Jana Sháněllová: 0000-0001-5517-7434

Notes

The authors declare no competing financial interest.

ACKNOWLEDGMENTS

The authors would like to express their gratitude for financial support from the Czech Science Foundation under Grant No. 16-10562S and from Project SGS_2018_007. The authors appreciate financial support from Grants LM2015082 and ED4.100/11.0251 from the Ministry of Education, Youth and Sports of the Czech Republic from which the EDS analysis was performed.

REFERENCES

(1) Uhlmann, D. R.; Chalmers, B. Energetics of nucleation. *Ind. Eng. Chem.* **1965**, *57*, 19−31.

(2) Kirkpatrick, R. J. Crystal Growth from the Melt: A Review. *Am. Mineral.* **1975**, *60*, 798−814.

(3) Kelton, K. F.; Greer, A. L. *Nucleation in Condensed Matter: Applications in Materials and Biology*; Pergamon: 2010; Vol. *15*, pp 1−743.

(4) Holand, W.; Rheinberger, V.; Schweiger, M. Control of nucleation in glass ceramics. *Philos. Trans. R. Soc., A* **2003**, *361*, 575−588.

(5) Zanotto, E. D. A bright future for glass-ceramics. *Am. Ceram. Soc. Bull.* **2010**, *89*, 19−27.

(6) Zakery, A.; Elliott, S. R. Optical properties and applications of chalcogenide glasses: a review. *J. Non-Cryst. Solids* **2003**, *330*, 1−12.

(7) Raoux, S.; Xiong, F.; Wuttig, M.; Pop, E. Phase change materials and phase change memory. *MRS Bull.* **2014**, *39*, 703−710.

(8) Kalb, J.; Spaepen, F.; Wuttig, M. Atomic force microscopy measurements of crystal nucleation and growth rates in thin films of amorphous Te alloys. *Appl. Phys. Lett.* **2004**, *84*, 5240−5242.

(9) Ruitenberg, G.; Petford-Long, A. K.; Doole, R. C. Determination of the isothermal nucleation and growth parameters for the crystallization of thin Ge2Sb2Te5 films. *J. Appl. Phys.* **2002**, *92*, 3116−3123.

(10) Fokin, V. M.; Zanotto, E. D.; Yuritsyn, N. S.; Schmelzer, J. W. P. Homogeneous crystal nucleation in silicate glasses: A 40 years perspective. *J. Non-Cryst. Solids* **2006**, *352*, 2681−2714.

(11) Ray, C. S.; Day, D. E. Determining the nucleation rate curve for lithium disilicate glass by differential thermal analysis. *J. Am. Ceram. Soc.* **1990**, *73*, 439−442.

(12) Ray, C. S.; Fang, X. Y.; Day, D. E. New method for determining the nucleation and crystal-growth rates in classes. *J. Am. Ceram. Soc.* **2000**, *83*, 865−872.

(13) Cabral, A. A.; Fokin, V. M.; Zanotto, E. D. Nanocrystallization of fresnoite glass. II. Analysis of homogeneous nucleation kinetics. *J. Non-Cryst. Solids* **2004**, *343*, 85−90.

(14) Cabral, A. A.; Fokin, V. M.; Zanotto, E. D.; Chinaglia, C. R. Nanocrystallization of fresnoite glass. I. Nucleation and growth kinetics. *J. Non-Cryst. Solids* **2003**, *330*, 174−186.

(15) James, P. F. Kinetics of crystal nucleation in silicate-glasses. *J. Non-Cryst. Solids* **1985**, *73*, 517−540.

(16) Kelton, K. F. Crystal nucleation in liquids and glasses. *Solid State Phys.* **1991**, *45*, 75−177.

(17) Zanotto, E. D.; James, P. F. Experimental tests of the classical nucleation theory for glasses. *J. Non-Cryst. Solids* **1985**, *74*, 373−394.

(18) Pillai, S. K.; Malek, J. Study of nucleation in a Se90Te10 chalcogenide glass by microscopy and differential scanning calorimetry. *J. Mater. Sci.* **2015**, *50*, 3854−3859.

(19) Pillai, S. K.; Podzemna, V.; Bartak, J.; Malek, J. Nucleation and growth in amorphous (GeS2)(0.9)(Sb2S3)(0.1) thin films. *J. Cryst. Growth* **2013**, *382*, 87−93.

(20) Kalb, J. A.; Wen, C. Y.; Spaepen, F.; Dieker, H.; Wuttig, M. Crystal morphology and nucleation in thin films of amorphous Te alloys used for phase change recording. *J. Appl. Phys.* **2005**, *98*, 054902−1−054902−6.

(21) Privitera, S.; Bongiorno, C.; Rimini, E.; Zonca, R. Crystal nucleation and growth processes in Ge2Sb2Te5. *Appl. Phys. Lett.* **2004**, *84*, 4448−4450.

(22) Kalb, J. A.; Spaepen, F.; Wuttig, M. Kinetics of crystal nucleation in undercooled droplets of Sb- and Te-based alloys used for phase change recording. *J. Appl. Phys.* **2005**, *98*, 054910−1−054910−7.

(23) Orava, J.; Greer, A. L. Classical-nucleation-theory analysis of priming in chalcogenide phase-change memory. *Acta Mater.* **2017**, *139*, 226−235.

(24) Ziegler, S.; Wuttig, M. Nucleation of AgInSbTe films employed in phase-change media. *J. Appl. Phys.* **2006**, *99*, 064907−1−064907−4.

(25) Lee, B. S.; Burr, G. W.; Shelby, R. M.; Raoux, S.; Rettner, C. T.; Bogle, S. N.; Darmawikarta, K.; Bishop, S. G.; Abelson, J. R. Observation of the Role of Subcritical Nuclei in Crystallization of a Glassy Solid. *Science* **2009**, *326*, 980−984.

(26) Johnson, G. K.; Papatheodorou, G. N.; Johnson, C. E. The enthalpies of formation of SbF5(l) and Sb2S3(c) and the high-temperature thermodynamic functions of Sb2S3(c) and Sb2S3(l). *J. Chem. Thermodyn.* **1981**, *13*, 745−754.

DOI: 10.1021/acs.cgd.8b00555
Cryst. Growth Des. 2018, 18, 4562−4570

(27) Shánělová, J.; Koštál, P.; Málek, J. Viscosity of (GeS2)x-(Sb2S3)1−x supercooled melts. *J. Non-Cryst. Solids* **2006**, *352*, 3952−3955.
(28) Rysava, N.; Barta, C.; Tichy, L. On the crystallization of Sb_2S_3 in glassy $(GeS_2)_{0.3}(Sb_2S_3)_{0.7}$. *J. Mater. Sci. Lett.* **1989**, *8*, 91−93.
(29) Malek, J.; Smrcka, V. The kinetic-analysis of the crystallization processes in glasses. *Thermochim. Acta* **1991**, *186*, 153−169.
(30) Málek, J.; Švadlák, D.; Mitsuhashi, T.; Haneda, H. Kinetics of crystal growth of Sb2S3 in (GeS2)0.3(Sb2S3)0.7 glass. *J. Non-Cryst. Solids* **2006**, *352*, 2243−2253.
(31) Pustková, P.; Švadlák, D.; Shánělová, J.; Málek, J. The non-isothermal crystallization kinetics of Sb2S3 in the (GeS2)0.2(Sb2S3)-0.8 glass. *Thermochim. Acta* **2006**, *445*, 116−120.
(32) Pustková, P.; Zmrhalová, Z.; Málek, J. The particle size influence on crystallization kinetics of (GeS2)0.1(Sb2S3)0.9 glass. *Thermochim. Acta* **2007**, *466*, 13−21.
(33) Švadlák, D.; Zmrhalová, Z.; Pustková, P.; Málek, J.; Pérez-Maqueda, L. A.; Criado, J. M. Crystallization behavior of (GeS2)0.1-(Sb2S3)0.9 glass. *J. Non-Cryst. Solids* **2008**, *354*, 3354−3361.
(34) Baro, M. D.; Clavaguera, N.; Surinach, S.; Barta, C.; Rysava, N.; Triska, A. DSC Study of Some Ge-Sb-S Glasses. *J. Mater. Sci.* **1991**, *26*, 3680−3684.
(35) Baro, M. D.; Surinach, S.; Clavagueramora, M. T.; Clavaguera, N.; Barta, C.; Rysava, N.; Triska, A. A crystallization study of the Ge25Sb20S55 glassy alloy. *J. Mater. Sci.* **1991**, *26*, 678−682.
(36) Málek, J.; Černošková, E.; Švejka, R.; Šesták, J.; Van der Plaats, G. Crystallization kinetics of $Ge_{0.3}Sb_{1.4}S_{2.7}$ glass. *Thermochim. Acta* **1996**, *280−281*, 353−361.
(37) Zmrhalova, Z.; Malek, J.; Svadlak, D.; Bartak, J. The crystallization kinetics of Sb_2S_3 in (GeS2)(0.4)(Sb2S3)(0.6) glass. *Phys. Status Solidi C* **2011**, *8*, 3127−3130.
(38) Málek, J.; Zmrhalová, Z.; Barták, J.; Honcová, P. A novel method to study crystallization of glasses. *Thermochim. Acta* **2010**, *511*, 67−73.
(39) Švadlák, D.; Pustková, P.; Koštál, P.; Málek, J. Crystal growth kinetics in $(GeS_2)_{0.2}(Sb_2S_3)_{0.8}$ glass. *Thermochim. Acta* **2006**, *446*, 121−127.
(40) Bartak, J.; Malek, J. Crystal growth kinetics of Sb2S3 in Ge-Sb-S amorphous thin films. *J. Therm. Anal. Calorim.* **2012**, *110*, 275−280.
(41) Bartak, J.; Podzemna, V.; Malek, J.; Eising, G.; Kooi, B. J. Crystal growth in $(GeS_2)(x)(Sb_2S_3)(1-x)$ thin films. *J. Non-Cryst. Solids* **2015**, *410*, 7−13.
(42) Mane, R. S.; Lokhande, C. D. Photoelectrochemical cells based on nanocrystalline Sb_2S_3 thin films. *Mater. Chem. Phys.* **2003**, *78*, 385−392.
(43) Shneidman, V. A. Determination of stationary regime of nucleation - theory and its comparison with experimental data for glasses. *Z. Tek. Fiz.* **1988**, *58*, 2202−2209.
(44) Nascimento, M. L. F.; Fokin, V. M.; Zanotto, E. D.; Abyzov, A. S. Dynamic processes in a silicate liquid from above melting to below the glass transition. *J. Chem. Phys.* **2011**, *135*, 194703−1−194703−17.
(45) Turnbull, D.; Fisher, J. C. Rate of nucleation in condensed systems. *J. Chem. Phys.* **1949**, *17*, 71−73.
(46) Becker, R.; Döring, W. Kinetische behandlung der keimbildung in übersättigten dämpfen. *Ann. Phys.* **1935**, *416*, 719−752.
(47) Zeldovich, Y. B. On the Theory of New Phase Formation. *Cavitation. Acta Physicochim. USSR* **1943**, *18*, 1−22.
(48) Schmelzer, J. W. P.; Abyzov, A. S.; Baidakov, V. G. Time of Formation of the First Supercritical Nucleus, Time-lag, and the Steady-State Nucleation Rate. *Int. J. Appl. Glass Sci.* **2017**, *8*, 48−60.
(49) Collins, F. C. Time lag in spontaneous nucleation due to non-steady state effects. *Z. Elektrochem.* **1955**, *59*, 404−407.
(50) Kashchiev, D. Solution of non-steady state problem in nucleation kinetics. *Surf. Sci.* **1969**, *14*, 209−220.
(51) Kelton, K. F.; Greer, A. L.; Thompson, C. V. Transient nucleation in condensed systems. *J. Chem. Phys.* **1983**, *79*, 6261−6276.
(52) Barták, J. *Crystallization Kinetics in Undercooled Chalcogenide Systems*; University of Pardubice: Pardubice, 2014.
(53) Stephens, R. B. Viscosity and structural relaxation rate of evaporated amorphous selenium. *J. Appl. Phys.* **1978**, *49*, 5855−5864.
(54) Ediger, M. D.; Harrowell, P.; Yu, L. Crystal growth kinetics exhibit a fragility-dependent decoupling from viscosity. *J. Chem. Phys.* **2008**, *128*, 034709−1−034709−6.
(55) Martinkova, S.; Bartak, J.; Kostal, P.; Malek, J.; Segawa, H. Extended Study on Crystal Growth and Viscosity in Ge-Sb-Se Bulk Glasses and Thin Films. *J. Phys. Chem. B* **2017**, *121*, 7978−7986.
(56) Turnbull, D. Formation of crystal nuclei in liquid metals. *J. Appl. Phys.* **1950**, *21*, 1022−1028.
(57) Skapski, A. S. A theory of surface tension of solids. 1.Application to metals. *Acta Metall.* **1956**, *4*, 576−582.
(58) Bayliss, P.; Nowacki, W. Refinement of crystal-structure of stibnite, Sb2S3. *Z. Kristallogr. Krist.* **1972**, *135*, 308−315.
(59) Deubener, J.; Weinberg, M. C. Crystal-liquid surface energies from transient nucleation. *J. Non-Cryst. Solids* **1998**, *231*, 143−151.
(60) Fokin, V. M.; Zanotto, E. D.; Schmelzer, J. W. P. Method to estimate crystal/liquid surface energy by dissolution of subcritical nuclei. *J. Non-Cryst. Solids* **2000**, *278*, 24−34.
(61) Grujić, S. R.; Blagojević, N. S.; Tošić, M. B.; Živanović, V. D.; Nikolić, J. D. The nucleation behavior of $K_2O{\cdot}TiO_2{\cdot}3GeO_2$ undercooled melt. *Ceram.-Silik.* **2009**, *53*, 128−136.
(62) Weinberg, M. C.; Zanotto, E. D.; Manrich, S. Classical nucleation theory with a size dependent interfacial-tension - $Li_2O{\cdot}2SiO_2$ crystal nucleation. *Phys. Chem. Glasses* **1992**, *33*, 99−102.
(63) Fokin, V. M.; Zanotto, E. D. Crystal nucleation in silicate glasses: the temperature and size dependence of crystal/liquid surface energy. *J. Non-Cryst. Solids* **2000**, *265*, 105−112.
(64) Tolman, R. C. The effect of droplet size on surface tension. *J. Chem. Phys.* **1949**, *17*, 333−337.
(65) Spaepen, F., Homogeneous nucleation and the temperature dependence of the crystal-melt interfacial tension. In *Solid State Physics - Advances in Research and Applications, Vol 47*, Ehrenreich, H.; Turnbull, D., Eds.; Elsevier Academic Press Inc: San Diego, 1994; Vol. *47*, pp 1−32.
(66) Abyzov, A. S.; Fokin, V. M.; Rodrigues, A. M.; Zanotto, E. D.; Schmelzer, J. W. P. The effect of elastic stresses on the thermodynamic barrier for crystal nucleation. *J. Non-Cryst. Solids* **2016**, *432*, 325−333.
(67) Fokin, V. M.; Abyzov, A. S.; Zanotto, E. D.; Cassar, D. R.; Rodrigues, A. M.; Schmelzer, J. W. P. Crystal nucleation in glass-forming liquids: Variation of the size of the "structural units" with temperature. *J. Non-Cryst. Solids* **2016**, *447*, 35−44.
(68) Schmelzer, J. W. P.; Abyzov, A. S. Crystallization of glass-forming liquids: Thermodynamic driving force. *J. Non-Cryst. Solids* **2016**, *449*, 41−49.
(69) Abyzov, A. S.; Fokin, V. M.; Yuritsyn, N. S.; Rodrigues, A. M.; Schmelzer, J. W. P. The effect of heterogeneous structure of glass-forming liquids on crystal nucleation. *J. Non-Cryst. Solids* **2017**, *462*, 32−40.

DOI: 10.1021/acs.cgd.8b00555
Cryst. Growth Des. 2018, 18, 4562−4570

PAPER II

CRYSTAL GROWTH & DESIGN

Article

pubs.acs.org/crystal

Crystal Growth Kinetics in Se–Te Bulk Glasses

Jaroslav Barták,* Simona Martinková, and Jiří Málek

Department of Physical Chemistry, University of Pardubice, Studentská 573, Pardubice 532 10, Czech Republic

ABSTRACT: The isothermal crystal growth in $Se_{100-x}Te_x$ bulk glasses (x = 10, 20, and 30) was studied directly using infrared microscopy. The crystals grew spherulitically and linearly in the course of time, which is typical for crystal growth controlled by liquid-crystal interface kinetics. An operative growth model was found using a combination of growth and viscosity data, and using two different approaches for calculations of the Gibbs free energy change between the undercooled melt and crystalline phase. The study shows that the exact knowledge of the Gibbs free energy change calculated from both, heat capacities, and the simple approximation proposed by Turnbull, can provide comparable results regarding determination of an operative crystal growth model. A detailed discussion about the relationship between the kinetic coefficient of crystal growth rate and viscosity ($u_{kin} \propto \eta^{-s}$) is presented. Moreover, the activation energies of crystal growth were found to be higher than the activation energies of the overall crystallization process obtained by differential scanning calorimetry. The relation between these two quantities is considered under the experimental conditions.

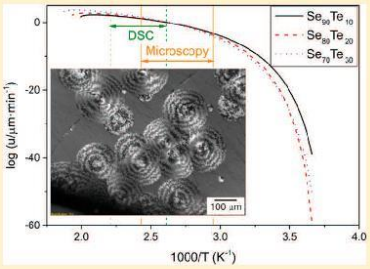

■ INTRODUCTION

Chalcogenide glasses and thin films are very interesting materials that exhibit unique physical properties. Because of their diverse active properties, chalcogenide materials can be used in various optical and optoelectronical devices or in various electronic thresholds and switches.[1−3] Interesting applications of chalcogenide materials also are found in modern high-tech memory devices.[4−6]

Thermal stability and crystallization play a key role in processing and usage of the materials. In particular, the crystallization process needs to be considered from two points of view—in order to obtain an ideal glass the crystallization has to be prevented, and, on the other hand, the controlled amorphous-to-crystalline transformation is a fundamental process of considered technology (modern phase change materials, PCM). Thus, knowledge and understanding of crystal growth kinetics and nucleation in such materials are essential for their future applications. The crystallization studies[7−11] focus on evaluation of mechanism of crystal growth and nucleation, and on prediction of crystallization behavior in a wide temperature range. Such a description can be useful for tailoring and optimization of new high-tech materials as they provide a possibility to predict the crystallization behavior in similar materials by revealing the basic mechanisms and properties of the material.

Selenium-based materials have been commercially applied in photoreceptors, photovoltaic materials, etc.[12] The properties of pure selenium can be significantly improved by alloying with other elements such as tellurium, germanium, antimony, arsenic, etc. Se–Te glasses and thin films are very attractive materials that exhibit an intermediate behavior between pure selenium and tellurium. The Se–Te mixtures exhibit numerous advantages in comparison with pure Se, for example, greater hardness, higher electrical conductivity, and photosensitivity.[12,13] The Se–Te alloys form a completely miscible isomorphous system in both liquid and solid states.[14] The Se–Te mixtures consist of mixed chains in which atoms of Se and Te are randomly distributed, and the crystalline phase is composed of a hexagonal lattice similar to those of pure Se and Te.[14,15] Owing to properties of the Se–Te system mentioned earlier, Se–Te glasses and thin films have been intensively studied recently. Structural relaxation in Se-rich bulk glasses was studied using differential scanning calorimetry (DSC).[16,17] Different experimental techniques (DSC, microscopy, electrical measurements, in situ X-ray diffraction) were used to study crystallization behavior in bulk glasses[18−26] and thin films[27−29] of the Se–Te system.

In this article, the crystal growth in $Se_{100-x}Te_x$ (x = 10, 20, and 30) bulk glasses was studied directly by infrared microscopy. The crystal growth data are combined with viscosity and heat capacity data to obtain an appropriate crystal growth model and to predict the crystal growth behavior in a wide temperature range.

■ MATERIALS AND METHODS

Chalcogenide glasses of compositions $Se_{100-x}Te_x$, where x = 10, 20 and 30, were prepared from pure elements (5N, Sigma-Aldrich) by the conventional melt-quenching method. Appropriate amounts of these elements were placed into quartz ampule. The ampule was then evacuated to a pressure 10^{-3} Pa and sealed. The sealed ampule was annealed in a rocking furnace at 600 °C for 20 h. The glasses were then prepared by quenching the melt in ampule in cold water. The

Received: April 30, 2015
Revised: July 9, 2015
Published: July 29, 2015

DOI: 10.1021/acs.cgd.5b00598
Cryst. Growth Des. 2015, 15, 4287−4295

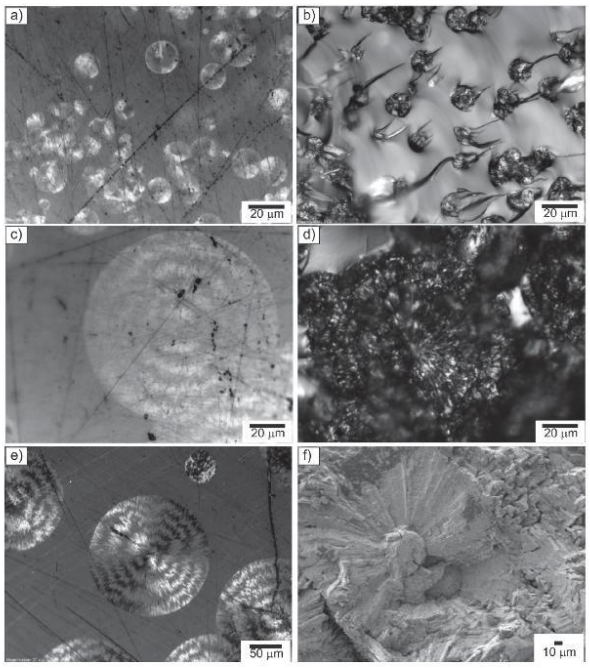

Figure 1. Morphology of formed spherulitical crystals in Se−Te system observed by IR microscopy and SEM (a) $Se_{90}Te_{10}$, polarized light, T = 101.5 °C, t = 45 min; (b) $Se_{90}Te_{10}$, T = 101.3 °C, t = 40 min; (c) $Se_{80}Te_{20}$, T = 118.3 °C, t = 30 min; (d) $Se_{80}Te_{20}$, T = 118.3 °C; t = 30 min; (e) $Se_{70}Te_{30}$, polarized light, T = 132.6 °C, t = 7 min; (f) $Se_{70}Te_{30}$, SEM micrograph, fully crystallized sample.

amorphous nature of prepared glasses was checked by X-ray diffraction analysis.

In order to examine the crystal growth process, microscope Olympus BX51 equipped with an infrared XM10 camera was used in the reflection mode. The bulk samples were previously heat treated at selected temperatures in a computer-controlled furnace (central hot zone was constant within ±0.5 °C). The heated samples were in the form of small cylinders with a size of ca. 4.3 mm in diameter and ca. 1.5 mm in height. Because of quite fast surface crystallization, the samples were polished or broken to remove the surface crystalline layer to observe bulk crystallization.

Differential scanning calorimetry (DSC) was used to study the melting of fully crystallized samples of $Se_{90}Te_{10}$, $Se_{80}Te_{20}$, and $Se_{70}Te_{30}$ compositions. The measurements were performed using a conventional DSC 822e (Mettler, Toledo) equipped with a cooling accessory. Dry nitrogen was used as the purge gas at a rate of 20 $cm^3 \cdot min^{-1}$. The calorimeter calibration was performed based on the melting temperatures and heats of melting of pure In, Zn, and Ga. The samples with an average mass of approximately 10 mg were measured in the form of very fine powder (d < 125 μm) in standard aluminum pans. The samples were heated from room temperature (RT) to 300 °C at a heating rate of 5 $°C \cdot min^{-1}$. From the endothermic peak, the temperature of melting was determined, and the enthalpy of melting was evaluated.

■ RESULTS AND DISCUSSION

The crystal growth in $Se_{100-x}Te_x$ (x = 10, 20, and 30) was observed directly using infrared microscopy in the temperature range of 70−135 °C. Regarding the bulk crystallization, crystals grew spherulitically and from randomly distributed nuclei as shown in Figure 1.

Figure 1 shows that for the compositions of $Se_{80}Te_{20}$ and $Se_{70}Te_{30}$, the cross-section of formed 3D spherical aggregates reveals concentric equidistant rings. A similar structure was observed by Ryschenkow and Bisault[7,8] in crystal growth of pure selenium. These so-called "Mode B" crystals have been observed in the crystallization of pure selenium at temperatures below 130 °C, which corresponds to the temperature range where the crystal growth in Se−Te bulk glasses was studied (70−135 °C). According to Bisault,[8] the Mode B crystals are subdivided into microlamellae parallel to the basal plane and ending in the liquid by two prismatic facets forming an hexagonal vertex. In the case of the $Se_{90}Te_{10}$ composition, the concentric rings were not found. This phenomenon can be explained that the described concentric rings are only visible in crystals with a size larger than cca 15 μm. This behavior can be explained on the basis of photography from SEM measurements (Figure 1f), where a small, compact core can be seen, and the as-described facets are growing from this core or nuclei. Nevertheless, for the $Se_{90}Te_{10}$ composition it was not possible to grow crystals with a larger diameter than ~20 μm because of significant overlapping of nucleation and crystal growth regions.[30]

A size of well-developed crystals was measured as a diameter (D) of formed spherulites. Figure 2 shows the time dependence of crystal sizes at selected temperatures. Every point in Figure 2

DOI: 10.1021/acs.cgd.5b00598
Cryst. Growth Des. 2015, 15, 4287−4295

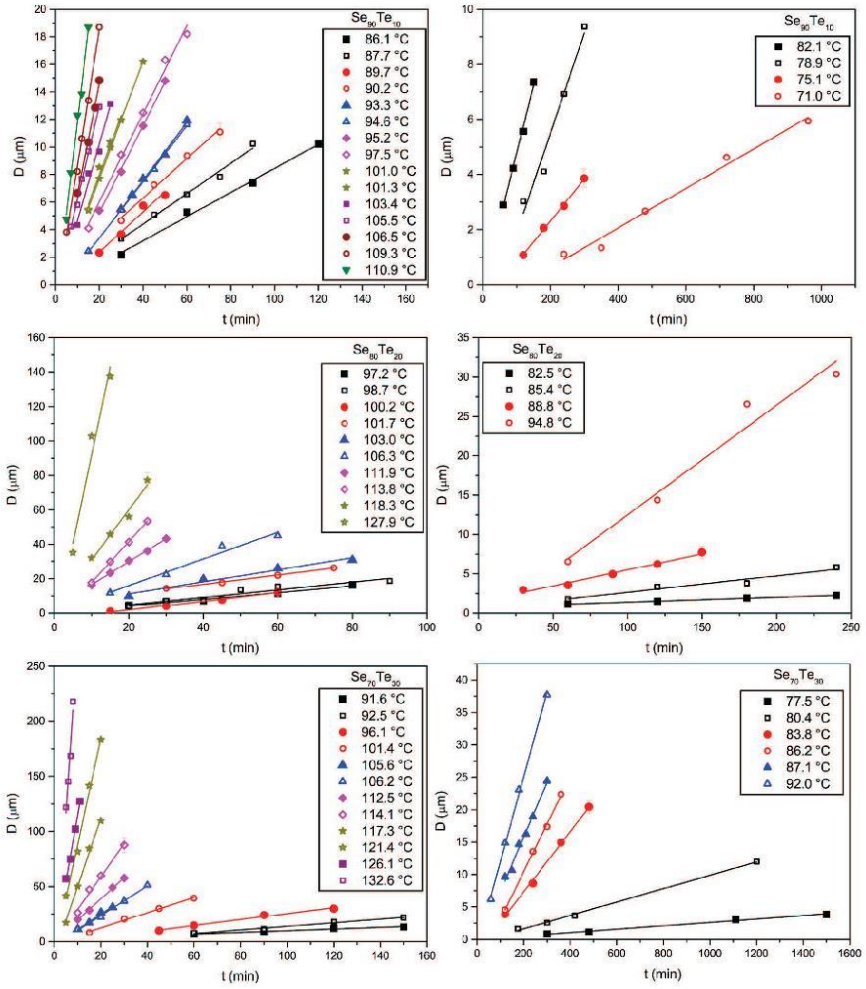

Figure 2. Linear time dependence of diameters of grown crystals in $Se_{100-x}Te_x$ bulk samples annealed at different temperatures.

corresponds to a mean value of independent measurements of 30−100 separated crystals. For better clarity of Figure 2, typical standard deviation is shown only for one point. Note that standard deviation was found to be in the range of 5−12% of the crystal size. The data shown in Figure 2 demonstrate a linear increase of crystal size in time during the isothermal crystallization. Crystal growth rates (u) were determined as slopes of the linear fits of these dependences and are listed in Table 1 for the three studied compositions.

As was anticipated and shown in Figure 2, the size of spherulitical crystals changed linearly with time during the isothermal heating. This type of behavior is typical for crystal growth controlled by liquid-crystal interface kinetics. There are three basic phenomenological[31,32] growth models that can be used to describe crystal growth controlled by liquid-crystal interface kinetics: normal, screw dislocation, and 2D surface nucleated growth model. According to Jackson,[33] the appropriate growth mechanism can be assessed from dependence of reduced crystal growth rate (U_R) on undercooling ($\Delta T = T_m - T$, where T_m is temperature of melting of the studied system):

$$U_R = \frac{u \cdot \eta}{1 - \exp\left(-\frac{\Delta G}{RT}\right)} \quad (1)$$

where u is crystal growth rate, η is viscosity, R is universal gas constant, and ΔG is change of Gibbs free energy between the undercooled melt and crystalline phase. The appropriate crystal

DOI: 10.1021/acs.cgd.5b00598
Cryst. Growth Des. 2015, 15, 4287−4295

Table 1. Crystal Growth Rates in the $Se_{100-x}Te_x$ System

$Se_{90}Te_{10}$		$Se_{80}Te_{20}$		$Se_{70}Te_{30}$	
T (°C)	u (μm·min^{-1})	T (°C)	u (μm·min^{-1})	T (°C)	u (μm·min^{-1})
71	0.0072 ± 0.0005	78.3	0.0024 ± 0.0004	77.5	0.0026 ± 0.0002
75.1	0.0153 ± 0.0005	82.5	0.0063 ± 0.0002	80.4	0.0103 ± 0.0003
78.9	0.032 ± 0.008	85.4	0.021 ± 0.004	83.8	0.047 ± 0.002
82.1	0.049 ± 0.003	88.8	0.037 ± 0.004	86.2	0.074 ± 0.002
86.1	0.088 ± 0.004	94.8	0.139 ± 0.018	87.1	0.084 ± 0.005
87.7	0.110 ± 0.007	97.2	0.195 ± 0.017	91.6	0.076 ± 0.010
89.7	0.15 ± 0.02	98.7	0.22 ± 0.03	92	0.131 ± 0.004
90.2	0.143 ± 0.009	100.2	0.273 ± 0.014	92.5	0.165 ± 0.010
93.3	0.210 ± 0.007	101.7	0.268 ± 0.011	96.1	0.269 ± 0.022
94.6	0.204 ± 0.003	103	0.35 ± 0.04	101.4	0.68 ± 0.03
95.2	0.316 ± 0.008	106.3	0.77 ± 0.09	105.6	1.4 ± 0.2
97.5	0.32 ± 0.02	111.9	1.33 ± 0.03	106.2	1.34 ± 0.06
101	0.43 ± 0.05	113.8	2.37 ± 0.02	112.5	1.9 ± 0.2
101.3	0.428 ± 0.005	118.3	2.9 ± 0.3	114.1	3.0 ± 0.2
103.4	0.56 ± 0.06	127.9	10.2 ± 1.9	117.3	6.2 ± 0.3
105.5	0.68 ± 0.03			121.4	9.7 ± 0.5
106.5	0.81 ± 0.04			126.1	11.9 ± 0.7
109.3	1.00 ± 0.03			132.6	23.36 ± 0.00
110.9	1.35 ± 0.07			132.6	31 ± 4

growth model can be then assessed from a plot of U_R vs ΔT, where ΔT is undercooling of the system with respect to the melting point T_m ($\Delta T = T_m - T$). The U_R vs ΔT plot then results in a shape of horizontal line for the normal growth model, or a straight line with a positive slope for the screw dislocation growth model, and for the 2D surface nucleated model the U_R versus ΔT plot is expected to be in the form of a curve of increasing positive slope.[33]

To estimate the reduced crystal growth rates from the growth data, temperature dependences of η and ΔG are needed.

Temperature dependence of viscosity in the Se−Te system was described in the work of Koštál,[34] and is redrawn in Figure 3. Combining the viscosity data with viscosities of corresponding melts, reported by Perron,[35] the temperature dependence of viscosity could be described by Vogel−Fulcher−Tammann equation in the temperature range of 35−530 °C, which corresponds to the viscosity region of 10^{-2}−10^{12} Pa·s.

The change in Gibbs free energy can be calculated directly from a difference of heat capacity (ΔC_p) between crystalline phase (C_p^{cr}) and undercooled melt (C_p^{m}):

$$\Delta G = \Delta H_m \frac{\Delta T}{T_m} - \int_T^{T_m} \Delta C_p \, dT + T \int_T^{T_m} \Delta C_p \frac{dT}{T} \quad (2)$$

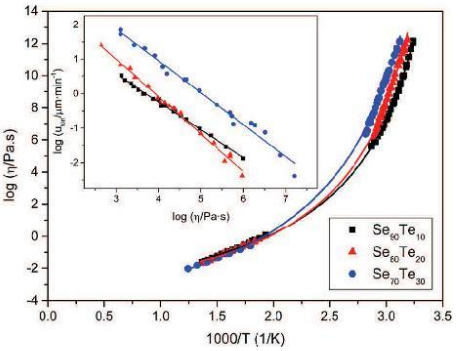

Figure 3. Temperature dependence of viscosity in $Se_{100-x}Te_x$ system, the data were taken from the article of Koštál.[34] The inset shows dependence of kinetic coefficient u_{kin} (see the text below) on viscosity for the studied compositions.

where ΔH_m is enthalpy of melting. Nevertheless, measurements of specific heat capacities in highly undercooled liquids are difficult, and for chalcogenide glasses and undercooled melts they are often missing. Owing to this, the ΔG can be approximated by simpler expressions.[36−39] The most convenient and widely used approximation of ΔG is the relation proposed by Turnbull:[36]

$$\Delta G = \Delta H_m \frac{\Delta T}{T_m} \quad (3)$$

The temperature dependence of ΔG in the studied $Se_{100-x}Te_x$ system was calculated using both expressions described by eqs 2 and 3. The melting parameters (ΔH_m and T_m) were measured by DSC and are listed in Table 2. The

Table 2. Temperatures and Enthalpies of Melting in the $Se_{100-x}Te_x$ System

	T_m (°C)	ΔH_m (kJ·mol^{-1})
$Se_{90}Te_{10}$	231.4 ± 0.3	6.18 ± 0.02
$Se_{80}Te_{20}$	246.3 ± 0.5	6.64 ± 0.06
$Se_{70}Te_{30}$	264.6 ± 1.0	7.28 ± 0.25

change of Gibbs free energy between the undercooled melt and crystalline phase (ΔG) was directly calculated using the heat capacity data for the Se−Te system published by Svoboda.[24] Temperature dependences of ΔG are shown in Figure 4 for all studied compositions. It can be seen from Figure 4 that with increasing undercooling the difference in ΔG that was calculated according eqs 2 and 3 is higher. In the growth region the difference is in the range of 100−500 J·mol^{-1} (8−15% relatively). Nevertheless, in the following text we will show that for the modeling of reduced crystal growth rate U_R eq 1) and further for calculation of the crystal growth model and its parameters, it is possible to use both expressions (eq 2 and 3 of ΔG obtaining comparable results.

With knowledge of ΔG and viscosity (η), the reduced crystal growth rate can be calculated according to eq 1 using the growth data in Table 1. Figure 5 shows the dependence of reduced crystal growth rate (U_R) on undercooling (ΔT) of the studied compositions. Standard deviations of the U_R were

DOI: 10.1021/acs.cgd.5b00598
Cryst. Growth Des. 2015, 15, 4287−4295

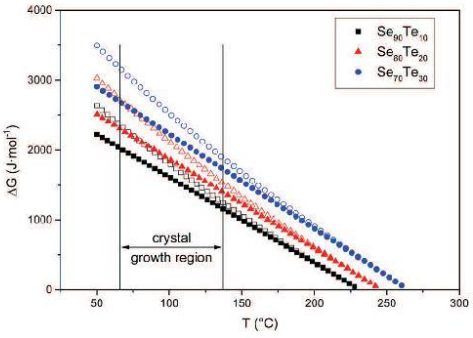

Figure 4. Temperature dependence of ΔG calculated directly from heat capacity data (empty symbols) and by the Turnbull approximation (full symbols).

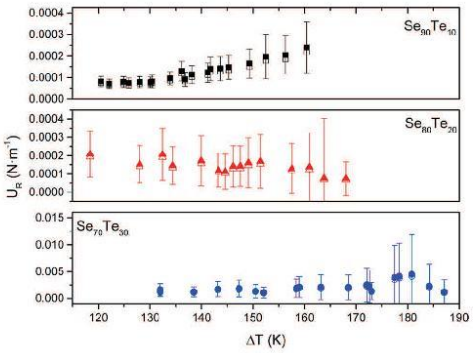

Figure 5. Dependence of reduced crystal growth rate (U_R) on undercooling (ΔT) in the $Se_{100-x}Te_x$ system. Empty symbols correspond to calculations of U_R using heat capacity data, full symbols correspond to calculations of U_R using the Turnbull approximation.

calculated using the error propagation model in QCExpert software (TriloByte Statistical Software, Ltd.). Considering the U_R errors, the U_R vs ΔT dependence appears to be constant which suggests a normal crystal growth model[33] for the $Se_{80}Te_{20}$ and $Se_{70}Te_{30}$ compositions. In the case of $Se_{90}Te_{10}$ the plot of U_R versus ΔT appears to be constant for lower undercooling (ΔT < ~135 °C). With increasing undercooling it appears that the U_R increases slightly, linearly with ΔT, which can suggest the screw dislocation growth model. Similar behavior was also observed in crystal growth in pure selenium, which was measured in a wide temperature range from the glass forming temperature (T_g) to the melting temperature (T_m).[40] This type of behavior can be ascribed to the change of crystal growth mechanism. The screw dislocation growth model was also used for description of crystal growth in thin films of $Se_{90}Te_{10}$ and $Se_{80}Te_{20}$.[28] Nevertheless, owing to the calculating errors of U_R and to the narrow temperature range, the crystal growth rate may not be able to clearly distinguish which growth model is appropriate for the description of $Se_{90}Te_{10}$ experimental data. Taking into account the constant dependence of U_R vs ΔT within the calculated errors for the compositions $Se_{80}Te_{20}$ and $Se_{70}Te_{30}$, and similar temperature and viscosity regions, it is reasonable to assume similar crystal growth behavior for the $Se_{90}Te_{10}$ composition. Taking into account what have been mentioned earlier, the normal crystal growth model was used to describe growth behavior in the three studied compositions.

The normal crystal growth model can be expressed as follows:[31]

$$u = \frac{k_B T}{3\pi a_0^2 \eta}\left[1 - \exp\left(-\frac{\Delta G}{RT}\right)\right] \quad (4)$$

where k_B is the Boltzmann constant and a_0 is the mean interatomic distance in the interface layer. The normal crystal growth model was calculated for all studied compositions of the $Se_{100-x}Te_x$ system using nonlinear regression. The calculated growth model is shown in Figure 6 along with corresponding crystal growth rates from Table 1. Insets of Figure 6 show a reasonable agreement between the experimental data and the calculated curves for the normal crystal growth model for compositions $Se_{80}Te_{20}$ and $Se_{70}Te_{30}$. Regarding the composition $Se_{90}Te_{10}$, the inset of Figure 6a shows deviation of the experimental data from the calculated normal growth model at lower temperatures. That is probably caused by change in a growth mechanism, which can be described by the screw dislocation growth model at lower temperatures. At higher temperatures the growth can be described by the normal growth model, as was predicted by the dependence of reduced crystal growth rate on undercooling of the system. A similar crystal growth behavior was observed also in pure selenium.[40] The change in crystal growth mechanism can be associated with the change of structure of the formed spherulites (change from mode B to mode A), as was mentioned at the beginning of this section. In consideration of the mentioned phenomenon, the growth data of $Se_{90}Te_{10}$ composition were also fitted by the screw dislocation growth model. The inset of Figure 6a shows that the crystal growth data for the composition $Se_{90}Te_{10}$ can be described by screw dislocation model at lower temperatures (T < ~100 °C). At higher temperatures the growth mechanism is changing, and the data can be described by the normal growth model. The screw dislocation growth model can be expressed as follows:[31]

$$u = \frac{\Delta T}{2\pi T_m}\frac{k_B T}{3\pi a_0^2 \eta}\left[1 - \exp\left(-\frac{\Delta G}{RT}\right)\right] \quad (5)$$

Parameters of eq 5 have the same meaning as in eq 4.

The fitting parameter a_0 was calculated using nonlinear regression for all compositions and the values are listed in Table 3 along with parameters calculated for crystal growth in pure selenium.[40] It is obvious that with increasing tellurium content in pure selenium, the parameter a_0 decreases. As anticipated earlier, two expressions of ΔG eqs 2 and 3 were used for calculation of the parameter a_0 of the normal crystal growth model. Table 3 provides a comparison of parameters a_0 calculated using different expressions of ΔG. The values of parameter a_0 listed in Table 3 are comparable within the experimental errors for both used expressions of ΔG. These calculations showed that the growth models can be estimated without proper knowledge of heat capacity data to calculate changes of Gibbs free energy between the undercooled melt and crystalline phase. Even a simple approximation of ΔG, proposed by Turnbull,[36] can provide comparable results.

DOI: 10.1021/acs.cgd.5b00598
Cryst. Growth Des. 2015, 15, 4287−4295

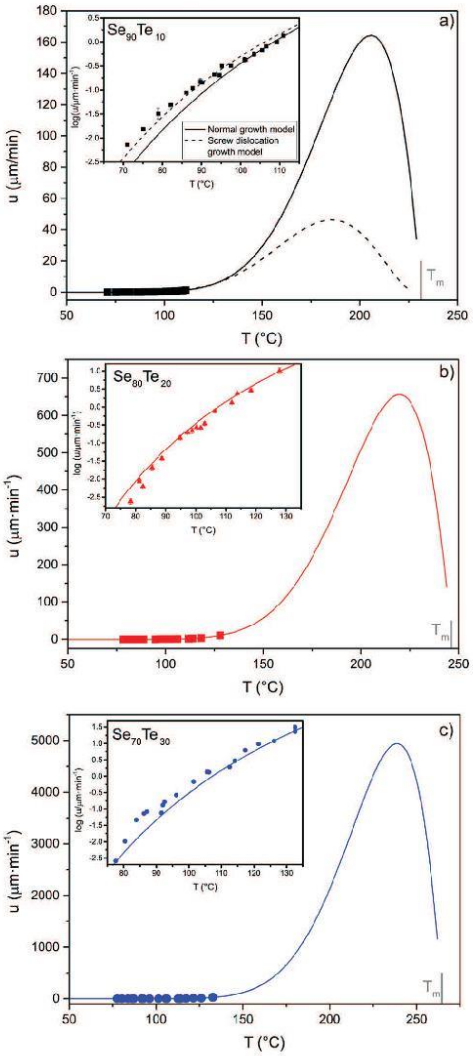

Figure 6. (a−c) Temperature dependence of crystal growth rates in the $Se_{100-x}Te_x$ system fitted by the normal crystal growth model.

As is shown in Table 3, there is a significant change in the parameter a_0 for the studied $Se_{100-x}Te_x$ system. For the $Se_{90}Te_{10}$ composition this parameter is comparable with the one found for pure selenium.[40] However, the a_0 parameter further decreases with tellurium content as evident from Table 3. The reason for such a decrease is unknown. Nevertheless, we would like to point out, that the a_0 parameter is quite sensitive to the applied kinetic model. The difference can be seen in case of the $Se_{90}Te_{10}$ composition, where the growth data were fitted by normal and screw dislocation growth model, and the

Table 3. Mean Interatomic Distance a_0 in Interface Layer Calculated from the Normal Crystal Growth Model in the $Se_{100-x}Te_x$ System and for Pure Selenium[40] Using Heat Capacity Data and Turnbull Approximation of ΔG

	heat capacity	Turnbull
	a_0 (Å)	a_0 (Å)
Se	27.9 ± 0.5	
$Se_{90}Te_{10}$	27.8 ± 0.3	26.7 ± 0.3
$Se_{80}Te_{20}$	17.8 ± 0.2	17.1 ± 0.2
$Se_{70}Te_{30}$	7.10 ± 0.11	6.50 ± 0.11

parameters a_0 were determined to be 27.8 ± 0.3 Å and 5.48 ± 0.06 Å, respectively.

The standard crystal growth models assume a simple inverse proportionality of crystal growth rate to viscosity ($u \propto \eta^{-1}$). This assumption is valid at small undercooling of the studied system. Nevertheless, with increasing undercooling the crystal growth rate and viscosity can decouple, as was shown by several authors.[41−44] The decoupling can be caused by breake-down of the Stokes−Einstein relationship between diffusivity and viscosity. Ediger[41] proposed a power law dependence of kinetic coefficient u_{kin} on viscosity:

$$u_{kin} \propto \eta^{-\xi} \tag{6}$$

The u_{kin} represents crystal growth rate corrected for the thermodynamic factor:

$$u_{kin} = \frac{u}{1 - \exp\left(-\frac{\Delta G}{RT}\right)} \tag{7}$$

The exponent $\xi \leq 1$ represents extent of decoupling of crystal growth rate and viscous flow. Ediger[41] demonstrated for several inorganic and organic glasses, that the exponent ξ depends linearly on fragility (m) of the system ($\xi = 1.1-0.005m$).

Fragility of the studied compositions of the Se−Te system can be taken from the work of Koštál[34] and their values are shown in Table 4. According to Ediger's assumption, the

Table 4. Kinetic Fragility (m) Values[34] and Values of Exponent ξ for the $Se_{100-x}Te_x$ System

	m	ξ
$Se_{90}Te_{10}$	87.2	0.80 ± 0.02
$Se_{80}Te_{20}$	87.6	1.05 ± 0.16
$Se_{70}Te_{30}$	76.8	0.89 ± 0.01

exponent ξ should be in the range 0.66−0.72 for the studied samples. However, the linear logarithmic dependence of u_{kin} on η (inset of Figure 3) provides the values of exponent ξ in the range of 0.80−1.05 (Table 4). The difference between the predicted ξ using the relation proposed by Ediger, and the calculated values suggest that the proposed relation might not be generally valid. The values of the exponent ξ are close to the value of 1;, thus it can be assumed that the Stokes−Einstein relationship is nearly fulfilled in the studied system even at higher undercooling.

The finding of the crystal growth model and its parameters is one part of the primary kinetic analysis of crystal growth process.

An alternative way to study crystallization process is based on calorimetric measurements. The heat released during the crystal growth can be measured nonisothermally by differential

DOI: 10.1021/acs.cgd.5b00598
Cryst. Growth Des. 2015, 15, 4287−4295

scanning calorimetry (DSC). In this case, however, both nucleation and growth processes are involved. The crystal growth proceeds until the whole or substantial part of the sample has been transformed. The fraction crystallized (α) can then easily be obtained by partial integration of DSC curve. It is assumed that the measured heat flow (Φ) is proportional to the rate of crystal growth, provided that the entire nucleation process takes place during the early stages of transformation and it becomes negligible afterward. Then the Johnson−Mehl−Avrami (JMA) kinetic model can be applied and the heat flow corresponding to crystallization process can be written as[45]

$$\Phi = \Delta HA \exp\left(\frac{-E_{DSC}}{RT}\right) n(1-\alpha)[-\ln(1-\alpha)]^{1-1/n} \quad (8)$$

where ΔH corresponds to the total enthalpy change associated with the crystallization process, A is the preexponential factor, n is the JMA exponent, and E_{DSC} is the apparent activation energy describing the overall crystallization process assuming the Arrhenian type temperature dependence.

The crystallization behavior in Se−Te powders, bulk and thin films has recently been studied quite extensively by DSC.[23,46,47] The values of apparent activation energy obtained from these calorimetric experiments are summarized in Table 5. It is quite

Table 5. Activation Energies of Crystal Growth in Bulk Samples (E_G) and Activation Energy of Crystallization Evaluated from DSC Experiments (E_{DSC})[23] in the $Se_{100-x}Te_x$ System

	E_G (kJ·mol^{-1})	E_{DSC} (kJ·mol^{-1})
$Se_{90}Te_{10}$	135 ± 10	86 ± 3
$Se_{80}Te_{20}$	193 ± 8	99 ± 6
$Se_{70}Te_{30}$	176 ± 8	114 ± 3

interesting to compare these values with direct microscopic measurements of crystal growth kinetics. In a narrow temperature range we can expect a simple exponential dependence of crystal growth rate on temperature as shown in Figure 7. From the slope of these dependences, we can estimate the apparent activation energy of crystal growth E_G for all three studied compositions of the Se−Te system (Table 5).

The activation energy for the $Se_{90}Te_{10}$ is comparable with the activation energy of crystal growth found by Calventus[19] (E_G = 146 ± 16 kJ/mol). The E_G values are also comparable with data reported in previous studies on crystal growth in Se−Te thin films.[28] However, there are significant differences compared to the values of activation energy obtained from DSC experiments. This can be explained assuming the calculated crystal growth rates for the normal crystal growth model. The temperature dependence of log u versus $1/T$ is in fact highly nonlinear as shown in Figure 8. The slope corresponding to "activation energy" is in fact meaningful only in a relatively narrow interval corresponding to temperature range of the measurement. Assuming this, the activation energies of crystal growth were calculated from the model growth data in the temperature region corresponding to DSC measurements, as shown in the inset of Figure 8 for the $Se_{90}Te_{10}$ composition. The activation energies of crystal growth were then found to be 88 ± 2 kJ/mol, 102 ± 2 kJ/mol, and 127 ± 2 kJ/mol for $Se_{90}Te_{10}$, $Se_{80}Te_{20}$, and $Se_{70}Te_{30}$ composition, respectively. These values are in good agreement with the apparent activation energy of the overall crystallization process found from the DSC

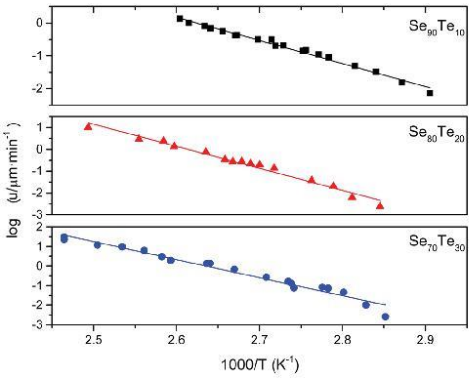

Figure 7. Plot of log u vs $1000/T$ for evaluation of activation energy of crystal growth in the $Se_{100-x}Te_x$ system.

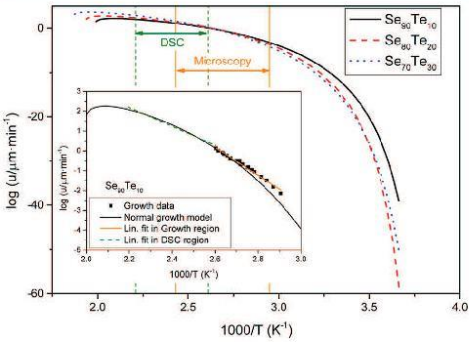

Figure 8. Temperature dependence of logarithm of crystal growth rate in $Se_{100-x}Te_x$ bulk glasses.

measurements[23] (Table 5). A similar change of activation energy of crystallization was observed in pure selenium in a wide temperature region for both microscopy[7,40] and DSC[48,49] measurements.

■ CONCLUSIONS

Crystal growth kinetics was studied in $Se_{100-x}Te_x$ bulk glasses, where x = 10, 20, and 30. The isothermal crystal growth was observed directly using infrared microscopy. The diameter of the growing spherulitical crystals depended linearly on time, which is typical for crystal growth controlled by liquid-crystal interface kinetics.

Using the crystal growth rates combined with viscosity data, reduced crystal growth rates were calculated. The specific dependence of reduced crystal growth on undercooling suggested normal crystal growth model for the compositions of $Se_{80}Te_{20}$ and $Se_{70}Te_{30}$. In the case of $Se_{90}Te_{10}$ composition, the growth data show a change of a crystal growth mechanism, which can be described by the normal crystal growth model at smaller undercooling, and by the screw dislocation growth model at higher undercooling. The change in crystal growth mechanism can be associated with the change of structure of

DOI: 10.1021/acs.cgd.5b00598
Cryst. Growth Des. 2015, 15, 4287−4295

the formed spherulites. Parameters of the growth models were found and the models appear to be operative for description of the found growth data in bulk glasses of all studied compositions. For the calculations of reduced crystal growth rates and the normal crystal growth model, the knowledge of temperature dependence of Gibbs free energy change (ΔG) between the undercooled melt and crystalline phase was needed. Two different expressions of ΔG were used: direct calculation from heat capacity data and simple approximation using enthalpy of melting and temperature of melting. It was shown that in case of missing heat capacity data the ΔG can be substituted by a simple expression proposed by Turnbull to provide results with reliable accuracy.

The relationship between crystal growth rate and viscosity was tested using a relationship proposed by Ediger. The predicted dependence $u_{kin} \propto \eta^{-\frac{\xi}{s}}$ showed, that even for highly fragile $Se_{100-x}Te_x$ system ($m \approx 76-88$), the exponent ξ is close to 1. Thus, we can assume that the Stokes−Einstein relationship between crystal growth rate and viscosity holds in this particular case even for relatively high undercooling of the system.

Activation energies of crystal growth were calculated from the simple exponential behavior of crystal growth rate on temperature and were compared with activation energies of the overall crystallization process evaluated from DSC data.

AUTHOR INFORMATION

Corresponding Author

*Tel: 00420466037346. E-mail: j-bartak@seznam.cz.

Notes

The authors declare no competing financial interest.

ACKNOWLEDGMENTS

The authors would like to express their gratitude for financial support from the Czech Science Foundation under Grant No. P106/11/1152.

REFERENCES

(1) Elliott, S. R. Chalcogenide Glasses. In *Materal Science Technology*; Wiley-VCH Verlag GmbH & Co. KGaA: Weinheim, 2006.

(2) Mehta, N. Applications of chalcogenide glasses in electronics and optoelectronics: A review. *J. Sci. Ind. Res. India* **2006**, *65*, 777−786.

(3) Lyubin, V. Chalcogenide glassy photoresists: History of development, properties, and applications. *Phys. Status Solidi B* **2009**, *246*, 1758−1767.

(4) Lacaita, A. L. Phase change memories: State-of-the-art, challenges and perspectives. *Solid-State Electron.* **2006**, *50*, 24−31.

(5) Wuttig, M.; Yamada, N. Phase-change materials for rewriteable data storage. *Nat. Mater.* **2007**, *6*, 1004−1004.

(6) Raoux, S.; Welnic, W.; Ielmini, D. Phase Change Materials and Their Application to Nonvolatile Memories. *Chem. Rev.* **2010**, *110*, 240−267.

(7) Ryschenkow, G.; Faivre, G. Bulk crystallization of liquid selenium - primary nucleation, growth kinetics and modes of crystallization. *J. Cryst. Growth* **1988**, *87*, 221−235.

(8) Bisault, J.; Ryschenkow, G.; Faivre, G. Spherulitic branching in the crystallization of liquid selenium. *J. Cryst. Growth* **1991**, *110*, 889−909.

(9) Chovanec, J.; Chromčíková, M.; Pilný, P.; Shánělová, J.; Málek, J.; Liška, M. As2Se3 melt crystallization studied by quadratic approximation of nucleation and growth rate temperature dependence. *J. Therm. Anal. Calorim.* **2013**, *114*, 971−977.

(10) Pillai, S. K.; Podzemná, V.; Barták, J.; Málek, J. Nucleation and growth in amorphous thin films of $(GeS_2)_{0.9}(Sb_2S_3)_{0.1}$. *J. Cryst. Growth* **2013**, *382*, 87−93.

(11) Reinsch, S.; Nascimento, M. L. F.; Müller, R.; Zanotto, E. D. Crystal growth kinetics in cordierite and diopside glasses in wide temperature ranges. *J. Non-Cryst. Solids* **2008**, *354*, 5386−5394.

(12) Bureau, B.; Boussard-Pledel, C.; Lucas, P.; Zhang, X.; Lucas, J. Forming Glasses from Se and Te. *Molecules* **2009**, *14*, 4337−4350.

(13) Bureau, B.; Danto, S.; Ma, H. L.; Boussard-Pledel, C.; Zhang, X. H.; Lucas, J. Tellurium based glasses: A ruthless glass to crystal competition. *Solid State Sci.* **2008**, *10*, 427−433.

(14) Ghosh, G.; Sharma, R. C.; Li, D. T.; Chang, Y. A. The Se-Te (Selenium-Tellurium) system. *J. Phase Equilib.* **1994**, *15*, 213−224.

(15) Lanyon, H. P. D.; Hockings, E. F. The Selenium-Tellurium System. *Phys. Status Solidi B* **1966**, *17*, K185−K186.

(16) Svoboda, R.; Honcová, P.; Málek, J. Enthalpic structural relaxation in Te-Se glassy system. *J. Non-Cryst. Solids* **2011**, *357*, 2163−2169.

(17) Svoboda, R.; Honcová, P.; Málek, J. Apparent activation energy of structural relaxation for $Se_{70}Te_{30}$ glass. *J. Non-Cryst. Solids* **2010**, *356*, 165−168.

(18) Calventus, Y.; Surinach, S.; Baro, M. D. Crystallization mechanisms of a $Se_{85}Te_{15}$ glassy alloy. *J. Phys.: Condens. Matter* **1996**, *8*, 927−940.

(19) Calventus, Y.; Surinach, S.; Baro, M. D. Crystallization mechanisms of some $Se_{100-x}Te_x$ glassy alloys. *J. Mater. Res.* **1997**, *12*, 1069−1075.

(20) Svoboda, R.; Krbal, M.; Málek, J. Crystallization kinetics in Se-Te glassy system. *J. Non-Cryst. Solids* **2011**, *357*, 3123−3129.

(21) Svoboda, R.; Málek, J. Interpretation of crystallization kinetics results provided by DSC. *Thermochim. Acta* **2011**, *526*, 237−251.

(22) Barták, J.; Svoboda, R.; Málek, J. Electrical conductivity and crystallization kinetics in Te-Se glassy system. *J. Appl. Phys.* **2012**, *111*, 094908.

(23) Svoboda, R.; Málek, J. Extended study of crystallization kinetics for Se-Te glasses. *J. Therm. Anal. Calorim.* **2013**, *111*, 161−171.

(24) Svoboda, R.; Málek, J. Thermal behavior in Se-Te chalcogenide system: Interplay of thermodynamics and kinetics. *J. Chem. Phys.* **2014**, *141*, 224507.

(25) Vermeulen, P. A.; Momand, J.; Kooi, B. J. Reversible amorphous-crystalline phase changes in a wide range of Se1−xTex alloys studied using ultrafast differential scanning calorimetry. *J. Chem. Phys.* **2014**, *141*, 024502.

(26) Svoboda, R.; Málek, J. Crystallization mechanisms occurring in the Se−Te glassy system. *J. Therm. Anal. Calorim.* **2015**, *119*, 155−166.

(27) Moharram, A. H. Electrical conductivity and crystallization kinetics of $Se_{70}Te_{30}$ films. *Thin Solid Films* **2001**, *392*, 34−39.

(28) Barták, J.; Málek, J.; Koštál, P.; Segawa, H.; Yamabe-Mitarai, Y. Crystallization behavior in Se90Te10 and Se80Te20 thin films. *J. Appl. Phys.* **2014**, *115*, 123506.

(29) Svoboda, R.; Gutwirth, J.; Málek, J.; Wágner, T. Crystallization kinetics of Se−Te thin films. *Thin Solid Films* **2014**, *571*, 121−126.

(30) Pillai, S.; Málek, J. Study of nucleation in a Se90Te10 chalcogenide glass by microscopy and differential scanning calorimetry. *J. Mater. Sci.* **2015**, *50*, 3854−3859.

(31) Uhlmann, D. R. Crystal growth in glass-forming systems - A review. *Advances in Nuclection and Crystalline in Glasses* **1972**, 91−115.

(32) Kirkpatrick, R. J. Crystal Growth from the Melt: A Review. *Am. Mineral.* **1975**, *60*, 798−814.

(33) Jackson, K. A.; Uhlmann, D. R.; Hunt, J. D. On the nature of crystal growth from the melt. *J. Cryst. Growth* **1967**, *1*, 1−36.

(34) Koštál, P.; Málek, J. Viscosity of Se−Te glass-forming system. *Pure Appl. Chem.* **2015**, *87*, 239−247.

(35) Perron, J. C.; Rabit, J.; Rialland, J. F. Impurity dependence of the viscosity of liquid selenium. *Philos. Mag. B* **1982**, *46*, 321−330.

(36) Turnbull, D. Formation of crystal nuclei in liquid metals. *J. Appl. Phys.* **1950**, *21*, 1022−1028.

(37) Hoffman, J. D. Thermodynamic driving force in nucleation and growth processes. *J. Chem. Phys.* **1958**, *29*, 1192−1193.

(38) Thompson, C. V.; Spaepen, F. Approximation of the free-energy change on crystallization. *Acta Metall.* **1979**, *27*, 1855−1859.

DOI: 10.1021/acs.cgd.5b00598
Cryst. Growth Des. 2015, 15, 4287−4295

(39) Singh, H. B.; Holz, A. Stability limit of supercooled liquids. *Solid State Commun.* **1983**, *45*, 985−988.
(40) Barták, J. Crystallization kinetics in undercooled chalcogenide systems. Ph.D. Dissertation, University of Pardubice: Pardubice, 2014.
(41) Ediger, M. D.; Harrowell, P.; Yu, L. Crystal growth kinetics exhibit a fragility-dependent decoupling from viscosity. *J. Chem. Phys.* **2008**, *128*, 034709.
(42) Nascimento, M. L. F.; Zanotto, E. D. Does viscosity describe the kinetic barrier for crystal growth from the liquidus to the glass transition? *J. Chem. Phys.* **2010**, *133*, 174701.
(43) Orava, J.; Greer, A. L. Fast and slow crystal growth kinetics in glass-forming melts. *J. Chem. Phys.* **2014**, *140*, 214504.
(44) Barták, J.; Podzemná, V.; Málek, J.; Eising, G.; Kooi, B. J. Crystal growth in (GeS2)x(Sb2S3)1 - X thin films. *J. Non-Cryst. Solids* **2015**, *410*, 7−13.
(45) Málek, J.; Shánělová, J., Crystallization kinetics in amorphous and glassy materials. In *Thermal Analysis of Micro, Nano- and Non-Crystalline Materials*; Šesták, J.; Šimon, P., Eds.; Springer: Berlin, 2013; pp 291−324.
(46) Svoboda, R.; Malek, J. Applicability of Fraser-Suzuki function in kinetic analysis of complex crystallization processes. *J. Therm. Anal. Calorim.* **2013**, *111*, 1045−1056.
(47) Svoboda, R.; Kincl, M.; Málek, J. Thermal characterization of Se-Te thin films. *J. Alloys Compd.* **2015**, *644*, 40−46.
(48) Svoboda, R.; Málek, J. Crystallization kinetics of amorphous Se - Part 1. Interpretation of kinetic functions. *J. Therm. Anal. Calorim.* **2013**, *114*, 1−10.
(49) Svoboda, R.; Málek, J. Crystallization kinetics of a-Se - Part 2. Deconvolution of a complex process: the final answer. *J. Therm. Anal. Calorim.* **2014**, *115*, 1−11.

DOI: 10.1021/acs.cgd.5b00598
Cryst. Growth Des. 2015, 15, 4287−4295

PAPER III

JOURNAL OF APPLIED PHYSICS **120**, 145301 (2016)

Crystal growth in $Se_{70}Te_{30}$ thin films followed by SEM and *in situ* XRD

Simona Martinková,[1,a)] Jaroslav Barták,[1] Jiri Málek,[1] and Hiroyo Segawa[2]
[1]*Department of Physical Chemistry, Faculty of Chemical Technology, University of Pardubice, Studentská 573, 532 10 Pardubice, Czech Republic*
[2]*National Institute for Material Science, 1-1 Namiki, Tsukuba, Ibaraki 305-0044, Japan*

(Received 27 June 2016; accepted 25 September 2016; published online 10 October 2016)

The isothermal crystal growth kinetics in $Se_{70}Te_{30}$ thin films was investigated using the microscopy and *in situ* X-ray diffraction (XRD) measurements. Plate-like crystals grew linearly with time which is the sign of liquid-crystal interface kinetics. In the studied temperature range, from 68 °C to 88 °C, crystal growth rates exhibit simple exponential behavior with an activation energy of crystal growth $E_G = 168 \pm 12$ kJ mol^{-1}. The growth data obtained from the microscopy measurements were combined with viscosity data, melting parameters and the appropriate crystal growth model was assessed. The relation between the kinetic coefficient of crystal growth and viscosity ($u \propto \eta^{-\xi}$) is described in detail, and a correction of the standard growth model is suggested. The crystal growth data obtained from the *in situ* XRD measurements were described using the Johnson-Mehl-Avrami nucleation-growth model with the Avrami exponent $m = 2.2 \pm 0.2$. The activation energy of the overall crystallization process E_A was estimated and its value is 171 ± 11 kJ mol^{-1}. *Published by AIP Publishing.* [http://dx.doi.org/10.1063/1.4964425]

INTRODUCTION

Chalcogenide glasses are interesting materials because of their unique structural, electronic, optical and thermal properties. They can be used as photo-resistant, microelectronic, optoelectronic and holographic media.[1–3] Tellurium-based glasses are also used as phase change materials in rewritable optical and non-volatile electronic memories due to their sensitivity to laser beam and easy amorphization process.[4–7] Storage mechanism is based on the change of optical or electrical properties due to a reversible switching from an amorphous to a crystalline phase.[6,7] Switching speed and data retention of memories are related to crystallization kinetics.[8] This is the reason why it is important to study and understand nucleation and crystal growth kinetics and mechanisms in these materials.

Se-Te glasses exhibit intermediate behavior between pure selenium and tellurium. They have higher hardness, photosensitivity, electrical conductivity and smaller aging effect than pure selenium.[4,9] Various studies have already been reported for Se-Te bulk glasses and thin films.[10–14] Crystallization kinetics has been investigated by differential scanning calorimetry (DSC)[15–25] and by the measurements of dc conductivity.[26] There are some investigations on direct observation of crystal growth using microscopy techniques,[22,23,27–30] on electric and optical properties[31–33] and on thermodynamic properties of the Se-Te system.[34–37]

In this work, the crystal growth kinetics in $Se_{70}Te_{30}$ thin films was studied using scanning electron microscopy (SEM), infrared microscopy (IR) and *in situ* X-ray diffraction measurements (XRD). The results found for the studied $Se_{70}Te_{30}$ composition (activation energies of crystal growth and the overall crystallization process, and growth model) are compared with the previously found results for the $Se_{90}Te_{10}$ and $Se_{80}Te_{20}$ thin films.[29]

EXPERIMENTAL

$Se_{70}Te_{30}$ bulk glass was prepared by the conventional melt-quench technique. The adequate amounts of pure elements (5N purity, Sigma Aldrich) were inserted into a quartz ampule. The ampule was evacuated to a pressure of 10^{-3} Pa, sealed and placed into a rocking furnace afterwards. The sealed ampule was annealed at 650 °C for 20 h. After heat treatment and homogenization, the ampule was quenched in cold water. The prepared bulk glass was used as a starting material for the preparation of thin films. The thin films were prepared by thermal deposition on clean microscopy glass substrates. The glass substrates were rotated by means of a planetary rotation system during deposition to ensure high homogeneity in the film thickness. Deposition rate was measured using a quartz microbalance technique. Two different sets of samples were prepared with the film thicknesses of 1 μm and 520 nm. Energy dispersive X-ray (EDX) microanalyzer Bruker coupled with a scanning electron microscope (Low Voltage Hitachi FE-SEM SU 8000) was used to measure the Se:Te ratio. The composition of thin films corresponds well with the stoichiometric composition of the prepared bulk glass.

Amorphous nature of the prepared thin films was verified by an X-ray diffraction analysis (XRD). The XRD analysis of amorphous and fully crystallized samples was performed using Rigaku XRD SmartLab with parallel beam, utilizing CuK_α radiation (40 kV, 30 mA). The scans were taken over scattering angles, 2θ, from 10° to 80° at the scanning speed of 1°/min.

The crystal growth in $Se_{70}Te_{30}$ thin films of the thickness of 1 μm was observed using a scanning electron microscope (Low Voltage Hitachi FE-SEM SU 8000). The samples were cut into smaller pieces (0.5×0.5 mm^2) and heat-treated in a

a)Author to whom correspondence should be addressed. Electronic mail: simona.martinkova@student.upce.cz

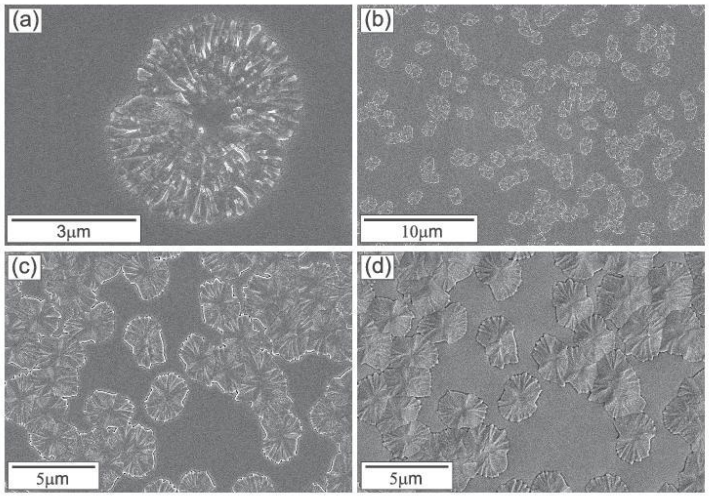

FIG. 1. Crystals growing in $Se_{70}Te_{30}$ thin films of 1 μm thickness (SEM photographs): (a) sample was annealed at 81 °C for 45 min; (b) sample was annealed at 73 °C for 75 min; (c) sample was annealed at 73 °C for 120 min, and upper detector was used for detection of secondary electrons; and (d) sample was annealed at 73 °C for 120 min, and lower detector was used for detection of secondary electrons.

computer-controlled furnace at selected temperatures for a specific amount of time. The micrographs were taken by the SEM. The sizes of well-developed crystals grown in thin films were measured. The crystal growth in $Se_{70}Te_{30}$ thin films of lower thickness (520 nm) was observed using an optical microscope Olympus BX51 with an infrared XM10 camera in the reflection mode and using SEM JEOL JSM-7500 F; 1 kV, gentle beam mode. Samples were prepared and sizes of crystals were evaluated like in the case of thin films with 1 μm thickness.

In situ XRD Rigaku TTR-III (CuK_α radiation −50 kV, 300 mA, parallel plate method) with Pt heater was used to study isothermal crystal growth kinetics of thin films with 520 nm thickness. The samples were heat-treated in the temperature range from 68 °C to 88 °C. The XRD scans were taken during isothermal treatment over scattering angles, 2θ, from 15° to 45° at the scanning speed of 15°/min.

RESULTS

Crystal growth followed by microscopy

The crystal growth in $Se_{70}Te_{30}$ thin films was studied using microscopy. The plate-like crystals grew in the vicinity of the surface of thin film; therefore, it can be assumed that the roughness of the substrate did not affect the crystal growth.

Crystal growth in $Se_{70}Te_{30}$ thin films of 1 μm thickness was studied in the temperature range from 68 °C to 88 °C using SEM. The samples were heat-treated for various times at temperatures where optimum crystal growth rates were observed. Figure 1 shows a typical morphology of growing crystals. Crystals grew from randomly distributed nuclei (Figure 1(b)). Crystal size was measured as the length of crystal's long axis. The mean crystal size was calculated as the average size of 10–30 crystals found in the thin films. The crystals grew linearly with time which is typical for crystal growth controlled by liquid-crystal interface kinetics. Time dependences of crystal sizes at different temperatures are shown in Figure 2. Slopes of these dependences correspond with the crystal growth rates summarized in Table I.

Crystal growth in $Se_{70}Te_{30}$ thin films of 520 nm thickness was studied using an infrared microscope. Three temperatures were chosen to verify that no change in crystal growth rate and morphology occurs as the film thickness is reduced. It can be seen in Figure 3 that the morphology of the formed crystals is the same as in 1 μm thin films. The crystals grew linearly with time, and the dependences of crystal sizes on time at different temperatures are shown in Figure 2. Crystal growth rate was evaluated in the same way as in the case of the thin films of 1 μm thickness.

Crystal growth followed by *in situ* XRD measurements

The study of crystal growth kinetics in $Se_{70}Te_{30}$ thin films of 520 nm thickness was performed in the same temperature

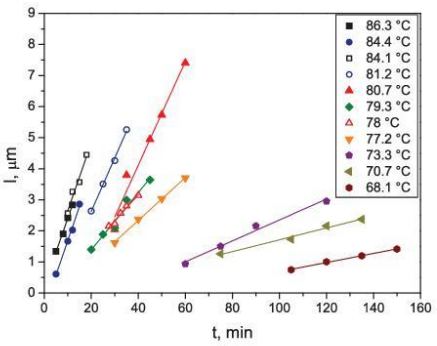

FIG. 2. Dependences of crystal sizes on time at various temperatures; the point size corresponds with the experimental error of the crystal size, and the empty and full symbols are used for thin films of 520 nm and 1 μm thick, respectively.

TABLE I. Crystal growth rates. The stability of the temperature was ±0.5 °C.

T (°C)	$Se_{70}Te_{30}$ (1 μm) u (μm min^{-1})	$Se_{70}Te_{30}$ (520 nm) u (μm min^{-1})
68.1	0.015 ± 0.001	
70.7	0.019 ± 0.002	
73.3	0.034 ± 0.003	
77.2	0.069 ± 0.002	
78		0.084 ± 0.007
79.3	0.092 ± 0.009	
80.7	0.17 ± 0.02	
81.2		0.17 ± 0.01
84.1		0.22 ± 0.03
84.4	0.22 ± 0.01	
86.3	0.22 ± 0.01	

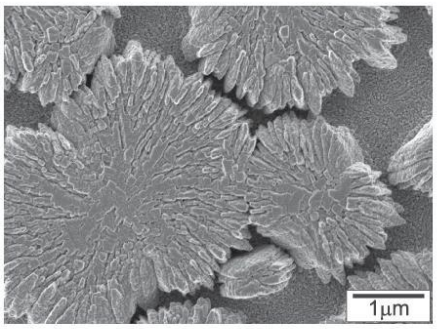

FIG. 3. Crystals growing in $Se_{70}Te_{30}$ thin films of 520 nm thickness.

range as in the microscopy measurements using the *in situ* XRD measurements. Figure 4 shows an XRD pattern of fully crystallized thin film in the range of $2\theta = 10°–80°$. The diffraction lines occur between the diffraction lines of pure selenium and tellurium. This could be expected because of the complete miscible system, where the atoms in Se-chains are randomly substituted by Te-atoms.[38] The crystallized fraction is formed by hexagonal crystals with lattice parameters a = 4.402 Å, c = 5.273 Å. The most intensive peaks are situated in the range of diffraction angles, 2θ, from 15° to 45°. This region was, therefore, chosen to follow the changes in diffraction peaks during isothermal annealing. The XRD profiles were used for determining the amount of phase transformed. The crystallized fraction, α, was calculated using the following formula[39]

$$\alpha = \frac{I - I_a}{I_{cr} - I_a}, \tag{1}$$

where I is the integrated intensity of diffraction peak at different time, I_{cr} is the integrated intensity of diffraction peak of fully crystallized sample, and I_a is background correction to the diffraction pattern measured for amorphous samples at room temperature (RT). The evolution of the crystallized fractions as a function of time at different measured temperatures is shown in Figure 5.

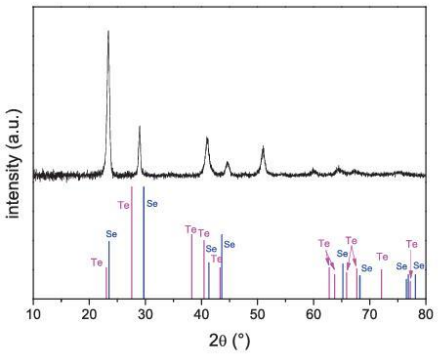

FIG. 4. XRD patterns of fully crystallized $Se_{70}Te_{30}$ thin films.

DISCUSSION

Crystal growth kinetics from microscopy measurements

Crystal growth was also observed in $Se_{70}Te_{30}$ thin films of 520 nm thickness. Raoux *et al.* found[40] that crystallization temperature can increase as film thickness is reduced, especially in case of thickness lower than about 20 nm. In our case, no change in crystal growth kinetics in 520 nm and 1 μm thin films was noted.

A simple exponential dependence of crystal growth rate on temperature can be assumed in narrow temperature range. The activation energy of crystal growth can be estimated from the slope of linearized dependence of log u on $1/T$, which is shown in Figure 6. The value of activation energy of crystal growth was found to be $E_G = 168 \pm 12$ kJ mol^{-1}. This value is in good agreement with the value of activation energy of crystal growth in $Se_{70}Te_{30}$ bulk glass.[28] The values of activation energies of crystal growth in the $Se_{90}Te_{10}$ and $Se_{80}Te_{20}$ thin films[29] are slightly higher ($E_G = 193 \pm 4$ kJ mol^{-1} for $Se_{90}Te_{10}$ composition and $E_G = 195 \pm 4$ kJ mol^{-1} for $Se_{80}Te_{20}$ composition) than the value found in $Se_{70}Te_{30}$ thin films.

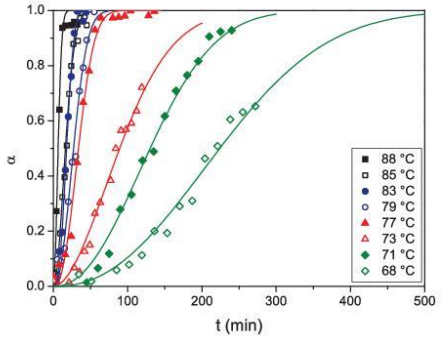

FIG. 5. Time evolution of crystallized fraction at different temperatures. Lines correspond with the JMA plot (see the following text in the Discussion part).

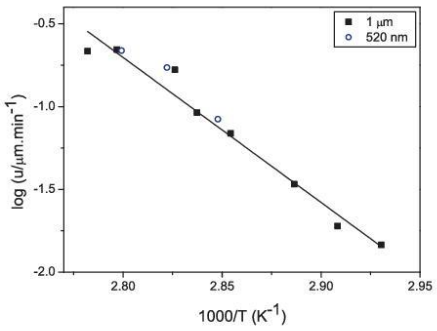

FIG. 6. Dependence of log u vs. 1000/T. Activation energy of crystal growth in $Se_{70}Te_{30}$ thin films was estimated from the slope of this dependence.

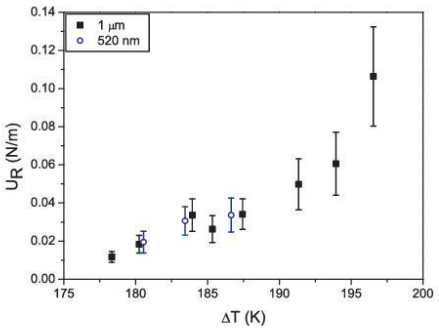

FIG. 7. Dependence of reduced crystal growth rate on undercooling.

As shown in Figure 2, the time evolution of crystal sizes was linear. This is a sign of crystal growth controlled by liquid-crystal interface kinetics. Three phenomenological growth models[41] are usually used for describing the crystal growth controlled by liquid-crystal interface kinetics: normal growth model, screw dislocation growth model and 2D surface nucleated growth model. According to Jackson,[42] the appropriate growth model can be assessed from the dependence of reduced crystal growth rate U_R on undercooling ΔT. Reduced crystal growth rate U_R is given by following equation:

$$U_R = \frac{u\eta}{1 - \exp\left(-\frac{\Delta G}{RT}\right)}, \tag{2}$$

where u is crystal growth rate measured at temperature T, η is viscosity, ΔT is undercooling ($\Delta T = T_m - T$; T_m is melting point) and ΔG is change of Gibbs free energy between undercooled melt and crystalline phase. ΔG can be easily expressed by Turnbull's approximation[43] ($\Delta G = \Delta H_m \Delta T / T_m$), which is the most widely used approximation and is sufficient for calculating U_R and crystal growth models in this system.[28]

The crystal growth rates u at different temperatures T (Table I), temperature dependence of viscosity η, enthalpy of fusion ΔH_f and temperature of melting T_m of the crystalline phase are needed for calculating the reduced crystal growth rate. Melting parameters were measured by DSC; $\Delta H_f = 7.28$ kJ mol^{-1}, $T_m = 264.6$ °C.[28] Temperature dependence of viscosity of Se-Te system was studied in bulk glasses.[44] It is assumed that the viscosity of thin films is not different that of bulk glasses.[45]

The plot of U_R on ΔT of the studied $Se_{70}Te_{30}$ thin films is shown in Figure 7. The standard deviations of the U_R were calculated using the error propagation model in the QCExpert software (TriloByte Statistical Software, Ltd.). The dependence of U_R on ΔT appears to be a straight line with a positive slope, which suggests a screw dislocation growth model. Nevertheless, more data on crystal growth rates in wider temperature region are needed for clearly distinguishing the appropriate growth model from the dependence of reduced crystal growth rate on undercooling. This is out of possibility for the used techniques. With increasing temperature, the crystal growth rate increases and even for short annealing times (5 min) the crystals became partially overlapped. The overlapping crystals make difficult the measurement and evaluation of the crystal growth rate at higher temperature. Sometimes, the signs of spirals are observed in materials, where the growth can be described by the screw dislocation model.[46,47] This was observed in the $Se_{90}Te_{10}$ and $Se_{80}Te_{20}$ thin films.[29] Nevertheless, the micrographs of the crystals formed in the studied $Se_{70}Te_{30}$ thin films do not clearly show such curvature or spiral-like structure (Figures 1 and 3). Previous studies on crystal growth in the $Se_{90}Te_{10}$ and $Se_{80}Te_{20}$ thin films[29] showed that the screw dislocation growth model is operative for the description of the crystal growth in this system. Therefore, the screw dislocation growth model was considered for the description of the crystal growth behavior in $Se_{70}Te_{30}$ thin films.

Screw dislocation growth model can be expressed by following equation:[41]

$$u = \frac{\Delta T}{2\pi T_m} \frac{k_B T}{3\pi a_0^2 \eta} \left[1 - \exp\left(-\frac{\Delta G}{RT}\right)\right], \tag{3}$$

where k_B is Boltzmann constant and a_0 is the mean interatomic distance in the interface layer. Figure 8 shows experimental crystal growth data along with calculated crystal growth model (dashed line). It is clearly shown that the simple screw dislocation growth model does not fit the experimental data well. The value of the only parameter of the growth model a_0 was found to be 0.358 ± 0.013 Å, which corresponds with the cca 1/10 of elementary cell. The reason that the screw dislocation growth model does not correspond with the experimental growth data might be caused by the deviation from the Stokes-Einstein (SE) relation, which assumes that the temperature dependence of diffusion coefficient can be described by inverse shear viscosity.[48] This assumption is valid at small undercoolings, just below the melting point. Below 1.2 T_g, the change in the diffusion mechanism can occur and the crystal growth rate and viscosity can decouple.[49–51] Ediger[50] proposed a power law dependence of u_{kin} on the liquid viscosity

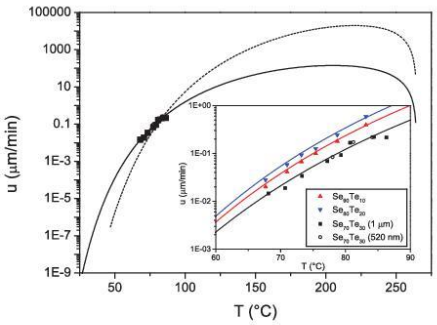

FIG. 8. Temperature dependence of crystal growth rates in $Se_{70}Te_{30}$ thin films fitted by standard (dashed line) and corrected (solid line) screw dislocation growth model (see the following text in the Discussion part). The inset shows the crystal growth rates in $Se_{70}Te_{30}$ (this work), and $Se_{80}Te_{20}$ and $Se_{90}Te_{10}$ (Barták[29]) thin films fitted by the corrected screw dislocation growth model.

$$u_{kin} \propto \eta^{-\xi}, \tag{4}$$

where u_{kin} is a kinetic part of the crystal growth rate ($u_{kin} = u/[1\text{-}\exp(-\Delta G/RT)]$). The values of the exponent $\xi < 1$ express the decoupling of viscosity and crystal growth rate. Plot u_{kin} versus η in the log-log scale yields straight line with a slope ξ. This plot is depicted in Figure 9. Exponent ξ was found to be 0.64 ± 0.04 which is the sign of breakdown of the Stokes-Einstein relationship between viscosity and diffusivity. The same analysis was also performed for the data published earlier by Barták.[29] In the case of $Se_{90}Te_{10}$ and $Se_{80}Te_{20}$, the values of the exponent ξ were found to be 0.88 ± 0.01 and 0.75 ± 0.02, respectively. Taking into account this decoupling of viscosity from the growth rate, the Eq. (3) can be combined with Eq. (4)

$$u = \frac{\Delta T}{2\pi T_m} \frac{k_B T}{3\pi a_0^2 \eta^{\xi}} \left[1 - \exp\left(-\frac{\Delta G}{RT}\right)\right]. \tag{5}$$

Using the corrected growth model for the exponent $\xi = 0.64$, the calculated fit agrees well with the experimental data (Figure 8, solid line). The corrected parameter a_0 was found to be 5.47 ± 0.10 Å that corresponds with the size of elementary cell. The improvement of the growth model was also performed to the previously published data for the $Se_{90}Te_{10}$ and $Se_{80}Te_{20}$ thin films[29] (Figure 8, inset) to find the corrected values of the parameter a_0, with the values estimated to be 2.96 ± 0.03 Å and 3.47 ± 0.06 Å for the $Se_{90}Te_{10}$ and $Se_{80}Te_{20}$ thin films, respectively. These values are more plausible for the meaning of the parameter a_0, which supposed to mean an interatomic distance in the interface layer.

Crystal growth followed by *in situ* XRD measurements

Isothermal crystal growth kinetics was also studied using the *in situ* X-ray diffraction measurements. These measurements were performed in the same temperature range as the growth measurements followed by microscopy. Experimental data (Figure 5) can be fitted by the Johnson-Mehl-Avrami (JMA) nucleation-growth model,[52–54] which can be expressed by following equation:

$$\alpha = 1 - \exp\left[-(Kt)^m\right], \tag{6}$$

where α is the crystallized fraction at time t, K is the rate constant that reflects the rates of both nucleation and growth process and m is Avrami exponent reflecting the characteristics of nucleation and growth process. The values of Avrami exponent m were obtained from the linearized JMA plot

$$\ln[-\ln(1-\alpha)] = m \cdot \ln t + m \cdot \ln K. \tag{7}$$

Taking into account the experimental errors, Avrami exponent m was estimated from α values in the interval of 0.3–0.7. The dependence of $\ln(-\ln(1-\alpha))$ vs. $\ln t$ is shown in Figure 10. The average value of Avrami exponent m was found to be 2.2 ± 0.2, which indicates two-dimensional crystal growth. This value was expected because the direct observations using microscopy show that nucleation occurs at the beginning of the crystallization process and the growth of crystals is two-dimensional. In comparison with the values of Avrami exponent m found in the $Se_{90}Te_{10}$ and $Se_{80}Te_{20}$ thin films,[29] the value of Avrami exponent m found in $Se_{70}Te_{30}$ thin films is slightly higher. As was reported by Svoboda[24] the m for $Se_{70}Te_{30}$ thin films from DSC data is

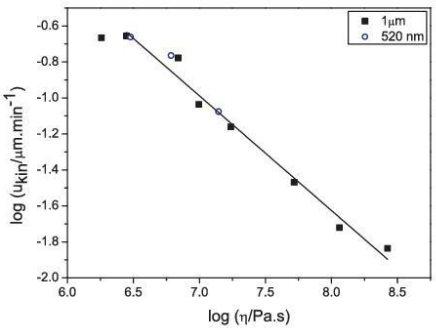

FIG. 9. Dependence of kinetic coefficient u_{kin} on viscosity η.

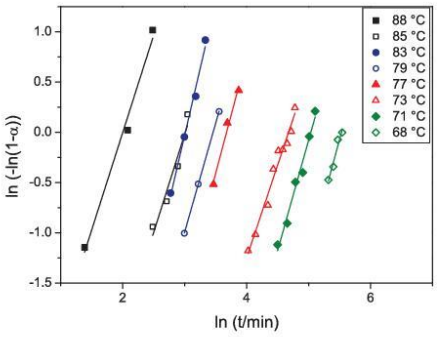

FIG. 10. JMA linearized plots for different temperatures. The values of Avrami exponent m were obtained from the slope of the linear dependences.

2.2 ± 0.3, it could be caused by the tendency to change the mechanism toward three-dimensional growth with an addition of tellurium.

The values of Avrami exponent m found from a linearized JMA plot were used to calculate the theoretical fits of JMA plot. The rate constant K was then determined as the fitting parameter. Figure 5 shows experimental data of the evolution of crystallized fraction with time along with the calculated theoretical JMA plots.

Temperature dependence of the rate constant K can be described using the Arrhenius equation[55]

$$K = K_0 \exp\left(-\frac{E_A}{RT}\right), \tag{8}$$

where K_0 is pre-exponential factor and E_A is the activation energy of the overall crystallization process. Linearized dependence of the rate constant K on temperature T is shown in Figure 11. Activation energy of nucleation-growth process E_A was found to be 171 ± 11 kJ mol^{-1}.

This value is the same within the experimental error as the value of the activation energy of crystal growth determined using the microscopy measurements ($E_G = 168 \pm 12$ kJ mol^{-1}). The fact that the activation energy of the overall nucleation-growth process is similar to the growth one can be explained in two possible ways. According to microscopy, there was no difference in crystal density, so it can be assumed that the nucleation process has been finished before the measurements in this particular temperature region started. Moreover, the XRD technique is quite insensitive in detecting nuclei, and only the crystal growth is followed.

In comparison with the activation energies of overall crystallization process and of crystal growth in the $Se_{90}Te_{10}$ and $Se_{80}Te_{20}$ thin films,[29] the activation energies found in $Se_{70}Te_{30}$ thin films are lower. Crystallization kinetics in Se-Te thin films using DSC measurements was studied by Svoboda.[24] The value of activation energy of overall crystallization process in $Se_{70}Te_{30}$ thin films obtained from DSC measurements was found to be $E_A = 147$ kJ mol^{-1}. The difference in values of the activation energies of overall crystallization process obtained from DSC and *in situ* XRD measurements can be explained by different temperature range where the activation energies were evaluated (DSC measurements: 90–135 °C;[24] *in situ* XRD: 68–88 °C). The temperature dependence of log u versus $1/T$ is in fact highly nonlinear and the activation energy is changing with temperature as was shown in the article of Barták.[28]

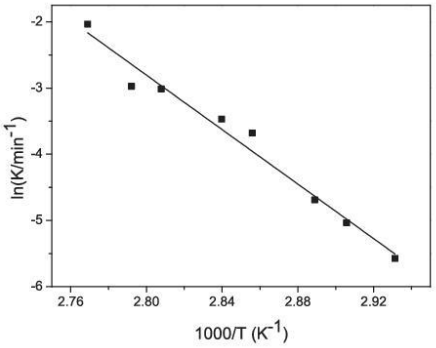

FIG. 11. Temperature dependence of the rate constant K.

CONCLUSIONS

The isothermal crystal growth kinetics in $Se_{70}Te_{30}$ thin films was studied using the microscopy and *in situ* X-ray diffraction (XRD) measurements. Two-dimensional crystal growth was observed in the temperature range 68–88 °C. The plate-like crystals grew from randomly distributed nuclei and their length increased linearly with time so the interface controlled crystal growth kinetics. The activation energy of crystal growth was found to be 168 ± 12 kJ mol^{-1}.

The dependence of reduced crystal growth rate on undercooling suggested screw dislocation growth model as the most probable. Simple screw dislocation model does not fit the experimental data well which is probably caused by the breakdown of the Stokes-Einstein relationship between viscosity and diffusivity. Taking into account the decoupling of viscosity from growth rate, the corrected screw dislocation growth model was used for the description of crystal growth data in $Se_{70}Te_{30}$ thin films. The improvement was also performed to the previously studied data found in the $Se_{90}Te_{10}$ and $Se_{80}Te_{20}$ thin films. Parameter of the growth model was found and discussed with the parameters of the growth models describing crystal growth in the $Se_{90}Te_{10}$ and $Se_{80}Te_{20}$ thin films.

The crystal growth was also studied by *in situ* XRD. The measured crystallization data were interpreted using the Johnson-Mehl-Avrami (JMA) model with Avrami exponent 2.2 ± 0.2. This value indicated that crystal growth showed two-dimensional growth. The activation energy of nucleation-growth process was estimated from the linearized dependence of rate constant on temperature ($E_A = 171 \pm 11$ kJ mol^{-1}). The activation energy of overall crystallization process is comparable with that of crystal growth estimated from the microscopy measurements.

ACKNOWLEDGMENTS

The authors would like to express their gratitude for the financial support from the Czech Science Foundation under Grant No. 16-10562S and the International Cooperative Graduate Program between the University of Pardubice and NIMS. The authors would like to thank Dr. Veronika Podzemná for being part of the SEM measurements and Dr. Yoko Yamabe-Mitarai and Ms. Tatiana Bolotova for helping with the *in situ* XRD measurements.

[1]N. Mehta, J. Sci. Ind. Res. **65**, 777 (2006).
[2]A. Feltz, *Amorphous Inorganic Materials and Glasses* (VCH, 1993).
[3]A. Zakery and S. R. Elliott, J. Non-Cryst. Solids **330**, 1 (2003).
[4]B. Bureau, S. Danto, H. L. Ma, C. Boussard-Plédel, X. H. Zhang, and J. Lucas, Solid State Sci. **10**, 427 (2008).
[5]G. F. Zhou, Mater. Sci. Eng.-Struct. Mater. Prop. Microstruct. Process. **304**, 73 (2001).
[6]M. Wuttig and N. Yamada, Nat. Mater. **6**, 824 (2007).
[7]S. Raoux, W. Welnic, and D. Ielmini, Chem. Rev. **110**, 240 (2010).

[8]M. Salinga, E. Carria, A. Kaldenbach, M. Bornhofft, J. Benke, J. Mayer, and M. Wuttig, Nat. Commun. **4**, 2371 (2013).
[9]B. Bureau, C. Boussard-Pledel, P. Lucas, X. H. Zhang, and J. Lucas, Molecules **14**, 4337 (2009).
[10]C. Bichara, Comput. Mater. Sci. **8**, 208 (1997).
[11]N. V. Quang, I. Shih, and C. H. Champness, J. Cryst. Growth **70**, 529 (1984).
[12]R. C. Keezer, C. H. Griffiths, and J. P. Vernon, J. Cryst. Growth **3–4**, 755 (1968).
[13]S. A. Kozyukhin, Inorg. Mater. **42**, 210 (2006).
[14]R. Bellissent and G. Tourand, J. Non-Cryst. Solids **35–36**(Part 2), 1221 (1980).
[15]R. Svoboda, M. Krbal, and J. Málek, J. Non-Cryst. Solids **357**, 3123 (2011).
[16]R. Svoboda and J. Malek, J. Therm. Anal. Calorim. **111**, 161 (2013).
[17]N. Afify, J. Non-Cryst. Solids **142**, 247 (1992).
[18]N. Afify, J. Non-Cryst. Solids **136**, 67 (1991).
[19]N. Afify, J. Non-Cryst. Solids **128**, 279 (1991).
[20]N. Afify, A. Gaber, I. Abdalla, and H. Talaat, Physica B **229**, 167 (1997).
[21]N. Afify, M. A. Hussein, N. El-Kabany, and N. Fathy, J. Non-Cryst. Solids **354**, 3260 (2008).
[22]Y. Calventus, S. Surinach, and M. D. Baro, J. Mater. Res. **12**, 1069 (1997).
[23]Y. Calventus, S. Surinach, and M. D. Baro, J. Phys.-Condens. Matter **8**, 927 (1996).
[24]R. Svoboda, J. Gutwirth, J. Malek, and T. Wagner, Thin Solid Films **571**, 121 (2014).
[25]R. Svoboda and J. Malek, J. Chem. Phys. **141**, 224507 (2014).
[26]J. Barták, R. Svoboda, and J. Malek, J. Appl. Phys. **111**, 094908 (2012).
[27]J. S. Vermaak and D. Raubenheimer, J. Cryst. Growth **86**, 183 (1988).
[28]J. Bartak, S. Martinkova, and J. Malek, Cryst. Growth Des. **15**, 4287 (2015).
[29]J. Barták, J. Málek, P. Koštál, H. Segawa, and Y. Yamabe-Mitarai, J. Appl. Phys. **115**, 123506 (2014).
[30]J. S. Vermaak and D. Raubenheimer, J. Cryst. Growth **85**, 521 (1987).
[31]J. C. Perron, J. Non-Cryst. Solids **8–10**, 272 (1972).
[32]Z. H. Khan, N. Salah, S. Habib, A. A. Al-Ghamdi, and S. A. Khan, Opt. Laser Technol. **44**, 6 (2012).
[33]S. K. Bahl and J. H. Chen, Mater. Res. Bull. **10**, 1121 (1975).
[34]G. C. Das and M. B. Bever, Metall. Trans. **4**, 1457 (1973).
[35]G. Ghosh, H. L. Lukas, and L. Delaey, Calphad **12**, 295 (1988).
[36]A. Amzil, M. Gilbert, C. Bichara, and J. C. Mathieu, J. Phys.-Condens. Matter **8**, 5281 (1996).
[37]W. Gierlotka and W. H. Wu, Int. J. Mater. Res. **103**, 698 (2012).
[38]G. Ghosh, R. C. Sharma, D. T. Li, and Y. A. Chang, J. Phase Equilib. **15**, 213 (1994).
[39]L. Zhang, C. Y. Xie, and J. S. Wu, Scr. Mater. **55**, 609 (2006).
[40]S. Raoux, G. W. Burr, M. J. Breitwisch, C. T. Rettner, Y. C. Chen, R. M. Shelby, M. Salinga, D. Krebs, S. H. Chen, H. L. Lung, and C. H. Lam, Ibm J. Res. Dev. **52**, 465 (2008).
[41]D. R. Uhlmann, in *Advances in Nucleation and Crystallization in Glasses*, edited by L. L. Hench and S. W. Freiman (American Ceramics Society, Ohio, 1972), p. 91.
[42]K. A. Jackson, D. R. Uhlmann, and J. D. Hunt, J. Cryst. Growth **1**, 1 (1967).
[43]D. Turnbull, J. Appl. Phys. **21**, 1022 (1950).
[44]P. Kostal and J. Malek, Pure Appl. Chem. **87**, 239 (2015).
[45]R. B. Stephens, J. Appl. Phys. **49**, 5855 (1978).
[46]A. Zhuang, J. J. Li, Y. C. Wang, X. Wen, Y. Lin, B. Xiang, X. P. Wang, and J. Zeng, Angew. Chem.-Int. Ed. **53**, 6425 (2014).
[47]G. L. Hao, X. Qi, Y. P. Fan, L. Xue, X. Y. Peng, X. L. Wei, and J. X. Zhong, Appl. Phys. Lett. **102**, 013105 (2013).
[48]I. S. Gutzow and J. W. P. Schmelzer, *The Vitreous State: Thermodynamics, Structure, Rheology, and Crystallization* (Springer, Berlin, Heidelberg, 2013).
[49]M. L. F. Nascimento and E. D. Zanotto, J. Chem. Phys. **133**, 174701 (2010).
[50]M. D. Ediger, P. Harrowell, and L. Yu, J. Chem. Phys. **128**, 034709 (2008).
[51]K. L. Ngai, J. H. Magill, and D. J. Plazek, J. Chem. Phys. **112**, 1887 (2000).
[52]M. Avrami, J. Chem. Phys. **9**, 177 (1941).
[53]M. Avrami, J. Chem. Phys. **7**, 1103 (1939).
[54]M. Avrami, J. Chem. Phys. **8**, 212 (1940).
[55]J. Šesták, *Thermophysical Properties of Solids: Their Measurements and Theoretical Thermal Analysis* (Elsevier, 1984).

PAPER IV

THE JOURNAL OF PHYSICAL CHEMISTRY B

Article

pubs.acs.org/JPCB

Extended Study on Crystal Growth and Viscosity in Ge–Sb–Se Bulk Glasses and Thin Films

Simona Martinková,[†] Jaroslav Barták,*[,†] Petr Koštál,[‡] Jiri Málek,[†] and Hiroyo Segawa[§]

[†]Department of Physical Chemistry, University of Pardubice, Studentská 573, Pardubice 532 10, Czech Republic

[‡]Department of Inorganic Technology, University of Pardubice, Doubravice 41, Pardubice 532 10, Czech Republic

[§]National Institute for Material Science, 1-1 Namiki, Tsukuba, Ibaraki 305-0044, Japan

ABSTRACT: Crystal growth rates in $Ge_{18}Sb_{28}Se_{54}$ bulk glass and thin film were measured using optical and scanning electron microscopy under isothermal conditions. The studied temperature region was 255–346 °C and 254–286 °C for bulk glass and thin film, respectively. The compact crystalline layer growing from the surface into the amorphous core was formed in bulk glasses and no bulk crystallization was observed. In the case of thin films, needle-shape crystals were formed. The crystalline layer and needle-shape crystals grew linearly with time that corresponds to a crystal growth controlled by the crystal–liquid interface kinetics. In the narrow temperature range, crystal growth rates exhibit simple exponential behavior, so the activation energies of crystal growth for the studied temperature regions were estimated (E_G = 294 ± 6 kJ/mol for bulk glass and E_G = 224 ± 12 kJ/mol for thin film). Viscosity of $Ge_{18}Sb_{28}Se_{54}$ material was measured in the region of the undercooled melt and glass. The extrapolation of viscosity data into the immeasurable, but important, temperature range is discussed. The experimental growth data were combined with melting and viscosity data and the appropriate growth models were proposed to describe crystal growth in a wide temperature region. The standard crystal growth models are based on a simple proportionality of the crystal growth rate to the viscosity ($u \propto \eta^{-1}$). This simple proportionality holds for the bulk material. Nevertheless, in the thin films the decoupling of the crystal growth rate from the inverse viscosity occurs, and the standard kinetic growth models need to be corrected. Such corrections provide better description of experimental data and more realistic value of the parameter describing the mean interatomic distance in the crystal–liquid interface layer, where the crystal growth takes place.

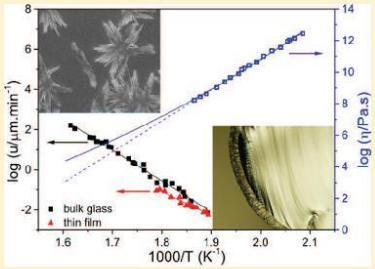

■ INTRODUCTION

Many researchers have taken an interest in glassy alloys of chalcogen elements for several decades because of their unique structural, electronic, optical, and thermal properties. Thermal stability and crystallization play a key role in processing and applicability of these chalcogenide materials. The thermal stability of amorphous state is important also for optical applications. Ge–Sb–Se glasses are attractive candidates for infrared applications, such as optical components used in thermal imaging systems, or integrated optical waveguides devices. They are good transmitters in the infrared region (2–16 μm) and more environmentally favorable compared to the Ge–As–Se glasses.[1,2] Various studies related to the optical, electric, thermodynamic, and structural properties[1,3−7] have already been reported for Ge–Sb–Se system. Crystallization kinetics and thermal stability of this system has been investigated using differential scanning calorimetry (DSC).[8−14] Direct microscopy measurements have been used to study morphology and crystal growth in $Ge_2Sb_2Se_5$ bulk glass.[15]

Knowledge of viscosity and crystallization behavior plays a key role in preparation, processing, and possible application of glasses. Understanding the crystallization process is a fundamental phenomenon, either to prevent, or control the amorphous-to-crystalline transformation. The crystallization takes place in undercooled melt, in this region the viscosity influences the transport of structural units from the undercooled melt to the growing crystal surface. The relation between viscosity and crystal growth rate is then very important for description and prediction of the crystallization process in a wide temperature region. Standard crystal growth models assume a simple proportionality of crystal growth rate to inverse viscosity ($u \propto \eta^{-1}$),[16,17] according to the standard Stokes–Einstein equation, which is frequently used to replace the effective diffusion coefficient by the viscosity. Nevertheless, during the past two decades the relation between viscosity and crystal growth rate was investigated and tested in different types of glasses.[15,18−25] This analysis was found to be important because some fragile glasses show a decoupling of the crystal growth rate from the inverse viscosity, and the relation between them is corrected for the parameter ξ ($u \propto \eta^{-\xi}$). The growth

Received: May 9, 2017
Revised: July 19, 2017
Published: July 24, 2017

DOI: 10.1021/acs.jpcb.7b04429
J. Phys. Chem. B 2017, 121, 7978−7986

models can be then corrected to describe the growth data in the measured temperature range.[24,25]

The aim of this work is direct investigation of the crystal growth kinetics in $Ge_{18}Sb_{28}Se_{54}$ bulk glasses and thin films using optical and scanning electron microscopy. The extended study of $Ge_{18}Sb_{28}Se_{54}$ system is performed including the study of melting parameters and temperature dependence of viscosity for the bulk material. It is shown that the viscosity of the undercooled liquid is closely coupled with crystal growth velocity in bulk glasses. A weaker viscosity dependence of crystal growth kinetics is found for thin films of the same composition. Consequence of these dependences for phenomenological kinetic models of crystal growth is analyzed and discussed.

■ EXPERIMENTAL SECTION

Thin films were prepared by flash evaporation on the microscopy glass substrates. Bulk glass of the $Ge_{22}Sb_{22}Se_{56}$ composition which was prepared by conventional melt-quench technique was totally crystallized in a computer-controlled furnace at 350 °C for 30 min, ground, and used as a starting material for preparation of the thin films. The glass substrates were rotated by means of a planetary rotation system during deposition to ensure high homogeneity in the film thickness. The deposition rate (1−2 nm/s) was measured using the quartz microbalance technique. Final thickness of the thin films was 520 nm. The composition and the homogeneity of the thin films were confirmed by energy dispersive X-ray (EDX) microanalyzer Bruker coupled with scanning electron microscope (low voltage Hitachi FE-SEM SU 8000). The composition of the prepared thin film was shifted from the starting material to the composition $Ge_{18}Sb_{28}Se_{54}$. For comparison of crystal growth in thin film and bulk material, the bulk glass of the $Ge_{18}Sb_{28}Se_{54}$ composition was prepared by conventional melt-quench method. The adequate amounts of pure elements were weighed into a quartz ampule. The ampule was evacuated to a pressure of 10^{-3} Pa, sealed, and placed into a rocking furnace afterward. The sealed ampule was annealed at 800 °C for 20 h. After the heat treatment and homogenization, the ampule was immersed in cold water to avoid crystallization. EDX microanalyzer coupled with SEM was also used to measure the composition and homogeneity of prepared $Ge_{18}Sb_{28}Se_{54}$ bulk glass.

Amorphous nature of the prepared bulk glasses and thin films was verified by X-ray diffraction analysis (XRD). The XRD analysis of amorphous and crystallized bulk samples was performed using Bruker AXS X-ray diffractometer D8 Advance equipped with a scintillation counter, utilizing CuK_α radiation (40 kV, 30 mA). The scans were taken over scattering angles, 2θ from 5° to 70° at the scanning speed 0.03°/min. In the case of thin films, Rigaku XRD SmartLab with parallel beam, utilizing CuK_α radiation (40 kV, 30 mA), was used to analyze amorphous and crystallized samples. The scans were taken over scattering angles, 2θ from 5° to 70° at the scanning speed 1°/min.

Crystallization and melting of the amorphous bulk samples were measured using differential scanning calorimeter (DSC) SensysEvo DSC (Setaram co.). Samples with a mass of 30−50 mg were placed into open silica ampules and heated to 650 °C at a heating rate 10 °C/min. Heat flow was calibrated using the Joule effect method. Calibration of heat flow and real temperature was verified using melting of pure Zn.

Viscous behavior of the prepared material was studied by thermomechanical analyzer, TMA CX 03 (R.M.I., Czech Republic). Penetration method using two different shapes of indenters was performed. Penetration method is based on a measuring of penetration rate of an indenter, which is isothermally pushed into a sample applying a constant force.[26] A stainless steel cylindrical indenter (1 mm in diameter) and a corundum hemispherical indenter (3.98 mm in diameter) were used for measurements of $Ge_{18}Sb_{28}Se_{54}$ viscosity. Bulk samples approximately 6 × 6 × 2.5 mm^3 in size were cut from the glassy samples, ground by corundum abrasive powder and used for these measurements. More details about the instrument and experimental arrangement can be found elsewhere.[27,28] The temperature was calibrated on melting of pure metals (Ga, In, Sn, Pb, Zn, Al).

Crystal growth was directly studied in bulk glasses and in the thin films of the $Ge_{18}Sb_{28}Se_{54}$ system using microscopy techniques. In the case of the $Ge_{18}Sb_{28}Se_{54}$ bulk glasses, crystal growth was observed using optical microscope Olympus BX51 equipped with camera DP72 and using optical microscope Olympus BX51 equipped with infrared camera XM10, both in the reflection mode. Due to the presence of the surface crystallization, samples were sectioned to follow crystal growth. The presence of the bulk crystallization was not observed. The samples were previously heat treated in a computer-controlled furnace at selected temperatures for different times. The surface crystalline layer thickness was measured by optical microscopy. The crystal growth in thin films of the same composition was observed using scanning electron microscope low voltage Hitachi FE-SEM SU 8000. The samples were also heat treated in a computer-controlled furnace at selected temperatures for specific time. Samples were etched using 0.5 M NaOH solution afterward to improve visibility of grown crystals by SEM. The sizes of well-developed crystals grown in thin films were measured in SEM micrographs.

■ RESULTS

Crystal Growth in Bulk Glasses and Thin Films. The crystal growth in the $Ge_{18}Sb_{28}Se_{54}$ bulk glasses was studied in the temperature range from 255 to 346 °C using optical and infrared microscopy in the reflection mode. This temperature interval was optimal for observation of the crystal growth in the bulk glasses by microscopy. At higher temperatures the crystal growth was too fast, and at lower temperatures too slow to follow. The samples were heat-treated at different temperatures for various times. Figure 1a−c shows typical morphology of the formed crystals in the bulk glasses. Figure 1a represents a micrograph of the surface of previously heat-treated sample. It is obvious that the crystals grew from the randomly distributed nuclei formed on the surface (Figure 1a) and there was no visible bulk crystallization. Regarding the surface crystallization, the crystals grew as hemispherical particles (Figure 1b) and as the crystal growth proceeded, surface was covered by a compact crystalline layer growing from the surface to the amorphous core (Figure 1c). The crystalline layer was uniform around the whole sample. Figure 1a shows that crystals started growing from one point. The same morphology and type of crystal growth were observed in the $Ge_2Sb_2Se_5$ bulk glasses.[15]

The crystal growth in the $Ge_{18}Sb_{28}Se_{54}$ thin films was studied in the temperature range from 254 to 286 °C. Scanning electron microscopy (SEM) was used to observe crystal growth. The samples were previously heat-treated at different temperatures for various times. The needle-shape crystals grew from

DOI: 10.1021/acs.jpcb.7b04429
J. Phys. Chem. B 2017, 121, 7978−7986

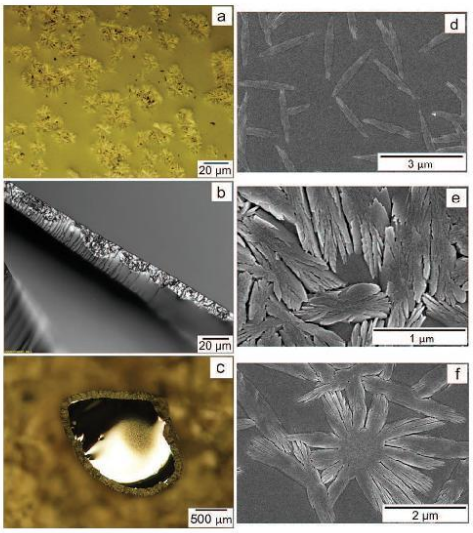

Figure 1. Crystals formed in the $Ge_{18}Sb_{28}Se_{54}$ bulk glasses and thin films: (a) surface of a bulk sample, T = 280.2 °C, t = 120 min, optical microscopy; (b) fracture of a bulk sample, T = 280.3 °C, t = 120 min, infrared microscopy; (c) fracture of a bulk sample, T = 326 °C, t = 5 min, optical microscopy; (d) thin film, T = 276.5 °C, t = 10 min, SEM; (e,f) thin film, T = 281.5 °C, t = 15 min, SEM.

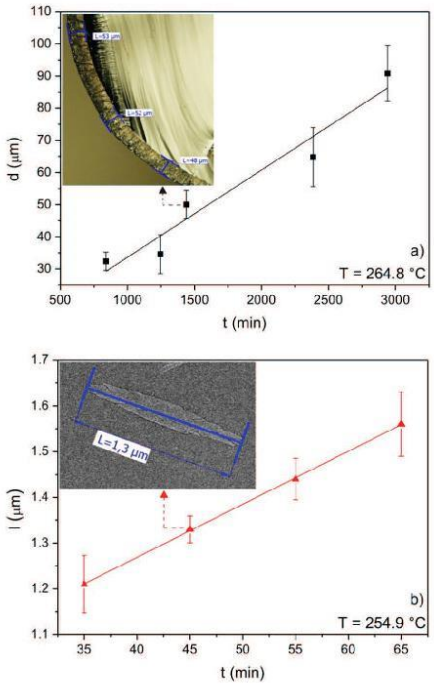

Figure 2. Dependences of crystal sizes on time at T = 264.8 °C for the $Ge_{18}Sb_{28}Se_{54}$ bulk glass (a) and at T = 254.9 °C for $Ge_{18}Sb_{28}Se_{54}$ thin film (b) along with typical crystals growing in the bulk glasses and thin films, and with the way of the determination of crystal sizes.

randomly distributed nuclei (Figure 1d,e). As can be seen in Figure 1e,f, the crystals formed aggregates as the growth continues. The etching of samples using NaOH solution was necessary because crystals were covered by an amorphous layer.

The thickness of the crystalline layer for the bulk glasses and the length of crystal's long axis for the thin films were measured to find out crystal size and determined crystal growth rates afterward. The way of determination crystal sizes and crystal growth rates in bulk glasses and thin films is shown in Figure 2. In both cases, crystals grew linearly with heat-treatment time (Figure 2) and the slopes of the time dependences of crystal sizes at different temperatures correspond with the crystal growth rates summarized in Table 1. In the case of the thin films, crystals can grow in two directions, on the other hand, in the bulk glasses the crystal growth can occur only in one direction according to the surface crystallization. The crystal growth rates found in the thin films were divided by two so the comparison with the crystal growth rates found in the bulk glasses was possible. In a narrow temperature range, Arrhenius behavior is observed, and a simple exponential dependence of crystal growth rate on temperature can be assumed. The activation energy can be evaluated from the linear dependence of log u on $1/T$, which is depicted in Figure 3. The value of the activation energy of the crystal growth was found to be E_G = 294 ± 6 kJ/mol and E_G = 224 ± 12 kJ/mol for the bulk glasses and thin films, respectively.

Viscosity. The viscosities of the $Ge_{18}Sb_{28}Se_{54}$ bulk samples were measured in the region of the undercooled melt and glass using the penetration method. The experimental data are summarized in Table 1. The dependence of viscosity logarithm on reciprocal temperature is plotted in Figure 3. This dependence shows a straight line behavior. Hence simple Arrhenius type equation can be used for fitting of experimental data. This equation contains two empirical parameters. One of them is apparent activation energy of viscous flow E_η which is equal to 410 ± 4 kJ/mol for $Ge_{18}Sb_{28}Se_{54}$. Arrhenius type equation can be rewritten to the form:[28]

$$\log \eta = 12 - m + \frac{m \cdot T_{12}}{T} \quad (1)$$

where T_{12} is viscosity glass transition temperature and m is kinetic fragility parameter. This form of the eq 1is usually more suitable in glass science because both parameters are often used for description of glass-formers viscosity behavior. Viscosity glass transition temperature is a temperature at which viscosity value corresponds to 10^{12} Pa·s. This point was determined by definition but it is generally accepted. The value of T_{12} for studied $Ge_{18}Sb_{28}Se_{54}$ is 222.8 ± 0.5 °C. Kinetic fragility is defined according to normalized Arrhenius plot (better known as Angell plot).[29] The kinetic fragility influences behavior of undercooled melts and its value lies usually between two limits, corresponding to a strong and fragile behavior. The value of the kinetic fragility for the studied $Ge_{18}Sb_{28}Se_{54}$ glass is 43.2 ± 0.4 that is approximately in the middle between two limits in Angell plot. Temperature dependence of viscosity of systems exhibiting this "intermediate" behavior can be typically

DOI: 10.1021/acs.jpcb.7b04429
J. Phys. Chem. B 2017, 121, 7978−7986

Table 1. Crystal Growth Rates in the $Ge_{18}Sb_{28}Se_{54}$ Bulk Glasses and Thin Films along with Viscosities in the $Ge_{18}Sb_{28}Se_{54}$ Bulk Material[a]

bulk glass				thin film				bulk material		
T (°C)	u (μm/min)			T (°C)	u (μm/min)			T (°C)	log (η/Pa·s)	
255.0	0.0071	±	0.0009	254.9	0.00572	±	0.00007	216.9	12.45	•
264.8	0.027	±	0.004	255.9	0.009	±	0.002	220.6	12.15	•
268.5	0.046	±	0.007	257.6	0.00755	±	0.00015	222.8	12.03	•
269.3	0.077	±	0.009	261.6	0.013	±	0.002	223.8	11.94	•
271.9	0.114	±	0.004	262.9	0.013	±	0.002	227.0	11.58	•
276.0	0.21	±	0.03	263.7	0.0142	±	0.0006	231.1	11.36	•
280.2	0.168	±	0.003	265.0	0.0157	±	0.0014	235.2	11.00	
280.3	0.26	±	0.04	265.9	0.021	±	0.002	238.4	10.65	
285.5	0.23	±	0.03	266.0	0.020	±	0.002	241.9	10.44	
290.0	0.44	±	0.08	267.9	0.016	±	0.002	244.5	10.24	
293.9	0.95	±	0.11	271.1	0.022	±	0.003	245.8	10.16	•
294.1	1.8	±	0.2	271.6	0.043	±	0.005	247.4	9.90	
299.8	2.0	±	0.3	276.5	0.043	±	0.003	251.4	9.65	
300.9	2.3	±	0.6	280.8	0.083	±	0.005	254.4	9.38	
303.9	3.6	±	0.4	283.8	0.102	±	0.003	258.6	9.03	
311.2	6.4	±	0.7	285.7	0.089	±	0.007	264.0	8.63	
315.8	13.3	±	1.2					267.3	8.45	
317.8	14	±	2					270.5	8.23	
319.7	25	±	2							
322.6	21.9	±	0.7							
326.0	25	±	3							
326.5	26	±	2							
328.6	38	±	5							
331.5	40	±	2							
342.5	110	±	16							
346.0	163	±	36							

[a]Temperature is constant within ±0.5 °C. Accuracy of the viscosity data is ±0.05 in log units. Viscosity values determined by penetration method with a hemispherical indenter are marked with •. Data without mark were measured using penetration method with a cylindrical indenter.

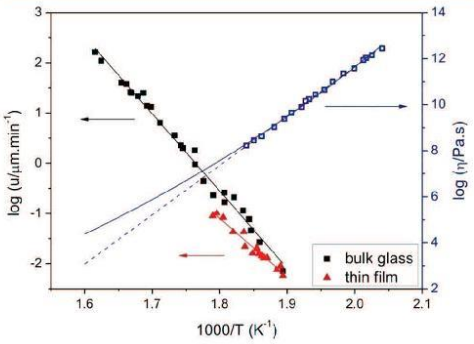

Figure 3. Temperature dependence of crystal growth rates for the $Ge_{18}Sb_{28}Se_{54}$ thin film and bulk glass along with temperature dependence of viscosity for the $Ge_{18}Sb_{28}Se_{54}$ bulk glass. The experimental viscosity data were fitted using Arrhenius (dashed line) and MYEGA (solid line) equations (see the text in the Discussion Section).

described by simple Arrhenius type equation in measurable region of undercooled melt and glass. On the other hand, the viscous behavior in a broad temperature interval, including region of melt, cannot be described by such a simple equation, and an equation with three or more parameters should be used (Figure 3; see the text in the Discussion Section).

Structure and Melting. The XRD analysis of fully crystallized sample of the bulk glass and thin film was performed. XRD patterns of fully crystallized samples are depicted in Figure 4. $Ge_{18}Sb_{28}Se_{54}$ crystalline phase has a complicated structure. Nevertheless, diffraction patterns reveal characteristic peaks of three phases, GeSe, $GeSe_2$, and Sb_2Se_3, which crystallize into an orthorhombic structure. It can be expected that the $Ge_{18}Sb_{28}Se_{54}$ crystalline phase is formed by

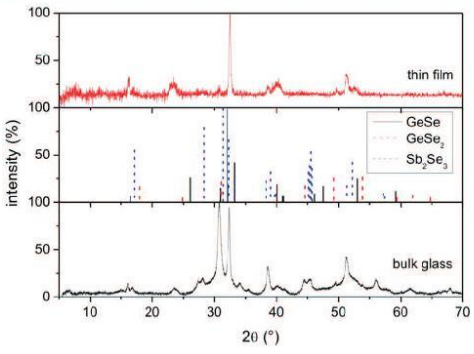

Figure 4. XRD patterns of fully crystallized $Ge_{18}Sb_{28}Se_{54}$ bulk glass and thin film. The positions and relative intensities of diffraction lines of possible formed phases are depicted.

DOI: 10.1021/acs.jpcb.7b04429
J. Phys. Chem. B 2017, 121, 7978−7986

mixed crystals of the found compounds. This crystalline phase has not been listed in the available databases. Similar findings have been published for Ge−Sb−Se system.[8,12,15,30,31]

Quite complex structure of the formed crystalline phase can be also assumed from the melting process shown in Figure 5.

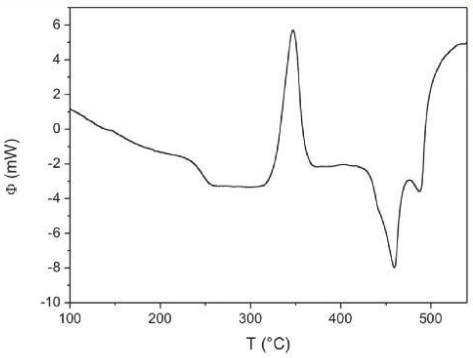

Figure 5. Crystallization and melting behavior in the $Ge_{18}Sb_{28}Se_{54}$ bulk glass followed by DSC at heating rate 10 °C/min.

The melting process in Ge−Sb−Se system exhibits a complex behavior according to available literature data.[3,8,14,15,32,33] Melting parameters of the $Ge_{18}Sb_{28}Se_{54}$ bulk glass were evaluated from the DSC measurements that were performed under nonisothermal conditions at a heating rate 10 °C/min. Figure 5 shows crystallization and melting of an amorphous sample. The crystallization, which occurs at ∼347 °C, is followed by the melting of one part of the material at ∼459 °C, and another part of the material melts at ∼487 °C. The temperature of melting was assumed as the onset of the first melting peak, T_m = 432.3 ± 1.2 °C.

■ DISCUSSION

The crystal growth kinetics was studied in the $Ge_{18}Sb_{28}Se_{54}$ bulk glasses and thin films. As can be seen in Figure 3, a simple exponential behavior of crystal growth rate on temperature can be assumed in a narrow temperature range. The values of activation energy of the crystal growth were estimated from the linearized dependence of log u on $1/T$: E_G = 294 ± 6 kJ/mol for bulk glass and E_G = 224 ± 12 kJ/mol for the thin film. Svoboda et al.[9] studied thin films of similar composition $Ge_{17}Sb_{23}Se_{60}$ using DSC, and the found value of the activation energy of crystallization was E_A = 299 ± 3 kJ/mol. The difference between the activation energy of $Ge_{18}Sb_{28}Se_{54}$ thin films and $Ge_{17}Sb_{23}Se_{60}$ thin films can be caused by the slightly different compositions or by the fact that the direct microscopic measurements observed the crystal growth and we obtain the activation energy of crystal growth, on the other hand, DSC measurements studied the overall nucleation−growth process. The difference in activation energies can be also explained by the different temperature regions where the studies were performed (microscopic measurements: 254−286 °C; DSC measurements: 310−340 °C). The dependence of log u on $1/T$ is, in fact, highly nonlinear in a wider temperature region.[23]

Crystal growth in amorphous materials can be described by different kinetic models.[16,34,35] One of the most important properties for evaluation and calculation of the crystal growth kinetic models is viscosity. The Figure 3 shows viscosity behavior of the $Ge_{18}Sb_{28}Se_{54}$ glass and undercooled melt. As was mentioned in Results Section, viscosity in measurable region of undercooled melt and glass exhibits an exponential Arrhenius type behavior. The highest temperature where the viscosity was measured reliably is 270 °C. The viscosity cannot be measured at higher temperatures due to the rapid crystallization of samples. Nevertheless, the crystal growth was studied almost up to 350 °C. According to the fragility of the studied system (m = 43.2), it is expected that the viscosity temperature dependence of undercooled melt can hardly exhibit Arrhenius type behavior at this temperature. It is typical for nonstrong systems that their viscosity dependences show non-Arrhenius behavior in a broad temperature interval.[29] Large extrapolation of viscosity into the immeasurable region by use of Arrhenius type equation can hence cause the distortion of estimated viscosity values. Therefore, it is necessary to estimate viscosity values as accurate as possible. The best way how to obtain viscosity values in immeasurable region of undercooled melt is the interpolation between measurable regions of undercooled melt and melt. The viscosities for the $Ge_{18}Sb_{28}Se_{54}$ melt were not reported yet, and measuring of chalcogenide melt viscosities is generally very difficult due to their high chemical reactivity and strong volatility. When viscosities in melt of the studied material are not available, there is another possibility to extrapolate viscous behavior into the undercooled melt region using three-parameter viscosity equations. A simplistic application of these equations can provide unrealistic estimation of viscosity values in some cases, especially if there is no fixed viscosity point in high temperature region. Such fixed point can be the viscosity at infinite temperature. According to the Angell plot, all viscosity dependencies presumably converge to one point at infinite temperature, i.e., 10^{-5} Pa·s. In compliance with measurements of temperature dependencies of viscosity in different materials, it is obvious, that the viscosity value of 10^{-5} Pa·s at infinite temperature is a simplification of the Angell plot. The viscosity behavior seems to be more complex. On the other hand, there is probably some, relatively narrow, viscosity interval of infinite temperature viscosities. According to Nemilov, the interval is in range of $10^{-3.5}$ to $10^{-5.5}$ Pa.s.[36] However, according to our experience, the fixation of viscosity to log η_0 = −5 at infinite temperature provides reasonable results with acceptable error limits. It is probably the best way how to estimate viscosities in immeasurable region of undercooled melt if viscosity of melt is not available. We used well-known MYEGA (Mauro, Yue, Ellison, Gupta, Allan) equation[37] for our extrapolation:

$$\log \eta = \log \eta_0 + \frac{K}{T} \cdot \exp\left(\frac{C}{T}\right) \tag{2}$$

This equation contains three parameters (η_0, K, C). Main advantage of this equation, according to the authors, is ability to better describe extreme behavior of melts at very high temperatures and glasses at very low temperatures. Extrapolation of measured data for $Ge_{18}Sb_{28}Se_{54}$ by MYEGA equation with fixed viscosity at infinite temperature is plotted in Figure 3. The extrapolated Arrhenius type equation is also depicted for comparison. The significant differences between viscosity data estimated by both equations are apparent.

A reliable viscosity data and, especially, the extrapolation is important for further description and modeling of crystal growth in the studied $Ge_{18}Sb_{28}Se_{54}$ system. As was mentioned

DOI: 10.1021/acs.jpcb.7b04429
J. Phys. Chem. B 2017, 121, 7978−7986

earlier, the crystalline layer in the bulk glasses and crystals in the thin films grew linearly with time (Figure 2), which is a sign of crystal growth controlled by liquid-crystal interface kinetics. Three standard phenomenological models[16] are applicable for the description of the crystal growth: normal growth model, screw dislocation growth model and 2D surface nucleated growth model. Jackson[17] proposed a simple way to determine an appropriate crystal growth model based on the dependence of reduced crystal growth rate U_R on undercooling ΔT ($\Delta T = T_m - T$). This dependence results in a shape of horizontal line for the normal growth model, a straight line with a positive slope for the screw dislocation growth model, or a curve with increasing positive slope for the 2D surface nucleated growth model. Reduced crystal growth rate is given by

$$U_R = \frac{u\eta}{1 - \exp\left(-\frac{\Delta G}{RT}\right)} \quad (3)$$

,where u is crystal growth rate measured at temperature T, η is viscosity given by MYEGA equation (eq 2), R is universal gas constant, and ΔG is change of Gibbs free energy between undercooled melt and crystalline phase. The Gibbs free energy between undercooled melt and crystalline phase ΔG can be calculated from the heat capacity difference between undercooled melt and crystalline phase. The heat capacity data are not available for many systems. Nevertheless, the ΔG can be easily expressed by the most widely used Turnbull's approximation[38] ($\Delta G = \Delta H_m \Delta T / T_m$), which is usually sufficient for calculating U_R and crystal growth models.[23]

The reduced crystal growth rate can be calculated using eq 3 in the case of knowledge of crystal growth rates u at different temperatures T (Table 1), temperature dependence of viscosity η (Table 1), enthalpy of melting ΔH_m, and temperature of melting T_m of the crystalline phase. Temperature dependence of viscosity was studied only in the bulk samples, nevertheless, it is assumed that the viscosity behavior in thin films and bulks is similar.[39] Melting process in Ge−Sb−Se system is very complicated and even a slight change of composition substantially influences melting behavior, especially the melting enthalpy.[3] Relatively complex melting of the $Ge_{18}Sb_{28}Se_{54}$ material is shown in Figure 5. The melting is immediately followed by evaporation and the melting enthalpy can be influenced by the evaporation. This can cause a significant distortion of the melting enthalpy value. Therefore, in calculations, the melting enthalpy is replaced by the enthalpy of crystallization, which corresponds directly to the studied crystal growth process. Similar assumption was made by Barták et al.[15] in the study of crystal growth in the $Ge_2Sb_2Se_5$ bulk glass. The enthalpy of crystallization was found to be $\Delta H_c = -40 \pm 4$ J/g, and the temperature of melting was found to be $T_m = 432.3 \pm 1.2$ °C.

Experimental crystal growth, viscosity, and melting data were used to calculate the reduced crystal growth rates U_R. The plot of U_R vs ΔT for the $Ge_{18}Sb_{28}Se_{54}$ bulk glass and thin film is depicted in Figure 6 along with characteristic standard deviations of the U_R for the bulk glass and the thin film. The standard deviations of the U_R were calculated using the error propagation model. Taking into account standard deviations of the U_R, the dependence of the reduced crystal growth rate on undercooling does not show clearly which crystal growth model is appropriate for the description of the crystal growth in the studied bulk glasses and thin films. The studied temperature region is quite short and more data on crystal growth in a wider

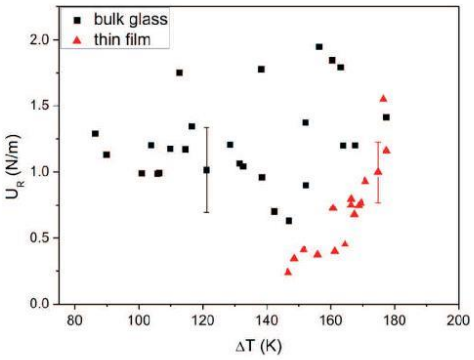

Figure 6. Dependence of the reduced crystal growth rate U_R on undercooling ΔT for the $Ge_{18}Sb_{28}Se_{54}$ bulk glass and thin film. The characteristic standard deviations of the U_R are shown.

temperature region are necessary to distinguish the crystal growth model. The crystal growth is too fast at high temperatures even for short times of annealing to be determined by the used techniques. Nevertheless, the dependence of U_R on ΔT (especially for the bulk glass) seems to be a cloud without any trend which could suggest the normal growth model. Previously published study on crystal growth in the $Ge_2Sb_2Se_5$ bulk glasses[15] showed screw dislocation growth model as the most probable. Therefore, the experimental crystal growth data in the $Ge_{18}Sb_{28}Se_{54}$ bulk glasses and thin films were fitted using the normal growth model and the screw dislocation growth model.

The normal growth model assumes a rough liquid-crystal interface on atomic scale where molecules can attach to the crystal at essentially any site.[16,34] The crystal growth rate of the standard normal growth model can be expressed by the following equation:

$$u = \frac{k_B T}{3\pi a_0^2 \eta}\left[1 - \exp\left(-\frac{\Delta G}{RT}\right)\right] \quad (4)$$

,where k_B is Boltzmann constant and a_0 is the mean interatomic distance in the interface layer. The screw dislocation growth model assumes a smooth liquid-crystal interface on atomic scale with dislocations on which crystals can grow.[16,34] The crystal growth rate can be expressed by equation:

$$u = \frac{\Delta T}{2\pi T_m}\frac{k_B T}{3\pi a_0^2 \eta}\left[1 - \exp\left(-\frac{\Delta G}{RT}\right)\right] \quad (5)$$

The standard growth models are based on the assumption that the Stokes−Einstein relation describes the transport process of the attachment of atoms to the growing crystal and the diffusion coefficient can be described by the inverse shear viscosity ($u \propto \eta^{-1}$).[40] It was shown that this assumption is not valid below 1.2 T_g where the crystal growth rate and viscosity can decouple. It was also shown in our previous published work[24] that the standard growth models do not describe the experimental growth data well if the decoupling of the crystal growth rate and viscosity occurs, and the correction of standard models is necessary. Ediger[20] proposed a simple way to test the decoupling which is based on a power law dependence of u_{kin} on the viscosity:

DOI: 10.1021/acs.jpcb.7b04429
J. Phys. Chem. B 2017, 121, 7978−7986

$$u_{kin} \propto \eta^{-\xi} \quad (6)$$

where u_{kin} is a kinetic part of crystal growth rate ($u_{kin} = u/[1 - \exp(-\Delta G/RT)]$) and the exponent $\xi < 1$ expresses the extent of decoupling between crystal growth rate and viscosity. The dependence of log u_{kin} vs log η for the $Ge_{18}Sb_{28}Se_{54}$ bulk glass and thin films, which yields a straight line with the slope ξ, is depicted in Figure 7. The kinetic exponent ξ is equal to 0.98 ± 0.02 for the bulk glass and to 0.67 ± 0.04 for the thin film. In the case of the bulk glass, the value of ξ is close to 1, so it seems, that the Stokes−Einstein relation is fulfilled near the melting point as well as below 1.2 T_g and the experimental crystal growth data can be described using standard crystal growth models. On the other hand, in the case of the thin films, the value of ξ is significantly smaller than 1 which is the sign of breakdown of the Stokes−Einstein relation and, therefore, for the description of the crystal growth in wide temperature region is necessary to use corrected crystal growth models. Taking into account the decoupling of the crystal growth and viscosity, the eq 4 or eq 5 is combined with eq 6 and the crystal growth rate of the corrected normal growth model and screw dislocation growth model can be expressed by the following equations, respectively:

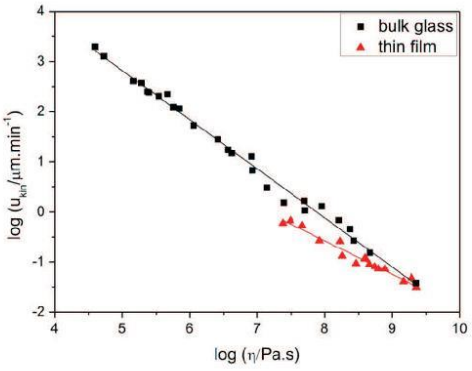

Figure 7. Dependence of kinetic part of the crystal growth rate u_{kin} on the viscosity η for the $Ge_{18}Sb_{28}Se_{54}$ bulk glass and thin film.

$$u = \frac{k_B T}{3\pi a_0^2 \eta^{\xi}}\left[1 - \exp\left(-\frac{\Delta G}{RT}\right)\right] \quad (7)$$

$$u = \frac{\Delta T}{2\pi T_m}\frac{k_B T}{3\pi a_0^2 \eta^{\xi}}\left[1 - \exp\left(-\frac{\Delta G}{RT}\right)\right] \quad (8)$$

Figure 8 shows the experimental growth data along with the calculated growth models for the $Ge_{18}Sb_{28}Se_{54}$ bulk glass. Taking into account the shape of the dependence of reduced crystal growth rate on undercooling, previously studied $Ge_2Sb_2Se_5$ bulk glass, and the extent of decoupling of crystal growth rate and viscosity, experimental crystal growth data were fitted using the standard normal and screw dislocation model. It is apparent from Figure 8 that it is not possible to distinguish which model is better for description of crystal growth in this system. The calculated models mainly differ in the region closed to the melting where the experimental growth data cannot be obtained reliably. Only one fitting parameter a_0 (the interatomic distance in the interface layer) is needed for both models which was found to be 0.109 Å for the normal growth model and 0.039 Å for the screw dislocation growth model. For both calculated parameters, the standard deviation was statistically negligible below 1.2×10^{-5} Å.

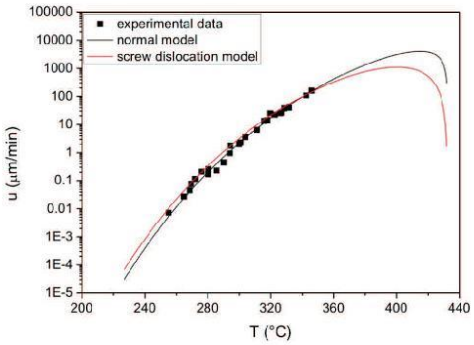

Figure 8. Temperature dependence of crystal growth rates in the $Ge_{18}Sb_{28}Se_{54}$ bulk glass fitted using the standard normal growth model and the standard screw dislocation growth model.

Figure 9 shows experimental growth data along with calculated standard and corrected growth models for the $Ge_{18}Sb_{28}Se_{54}$ thin films. The experimental growth data were also fitted using the normal and screw dislocation growth model. Taking into account the extent of decoupling of the crystal growth rate and viscosity, the standard growth models are not appropriate for description of the crystal growth, and it is necessary to use corrected growth models which can be seen in Figure 9. As in case of the bulk glasses, it is not possible to distinguish which corrected model is the appropriate one. Nevertheless, from Figure 9 it is apparent, that without the viscosity correction ($u \propto \eta^{-\xi}$), the standard crystal growth models cannot describe the experimental data well. Using the correction, both growth models (normal and screw dislocation) describe the experimental data sufficiently, the parameters a_0 of

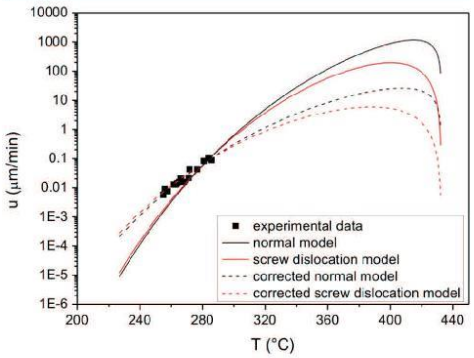

Figure 9. Temperature dependence of crystal growth rates in the $Ge_{18}Sb_{28}Se_{54}$ thin films fitted using the standard normal and screw dislocation growth models (solid lines), and the corrected normal and screw dislocation growth models (dashed lines).

DOI: 10.1021/acs.jpcb.7b04429
J. Phys. Chem. B 2017, 121, 7978−7986

the models can be evaluated 9.199 ± 0.006 Å for the corrected normal growth model and 1.698 ± 0.001 Å for the corrected screw dislocation growth model.

The parameter a_0 is usually assigned to the mean interatomic distance in the interface layer, which is equivalent to the jump distance, or to the crystal lattice parameter or the unit distance advanced by the interface.[16,19,34,35] In the case of the bulk glass studied in this work, both models can describe the experimental data equally within the experimental errors. The parameters a_0 found for the normal and screw dislocation growth model are more than ten times lower than covalent radii of the component elements in Ge−Sb−Se glasses.[41] Focusing on the crystal growth and evaluation of crystal growth models in the thin films of the studied samples, the kinetic growth models corrected for the decoupling provide better description of the experimental data and the evaluated parameters a_0 give more meaningful values. The value 1.698 Å evaluated from the screw dislocation growth model correspond to 2/3 of the nearest neighbor bond length found for $Ge_2Sb_2Se_5$ glass.[31] On the other hand, the parameter a_0 = 9.199 Å from the normal growth model might correspond to lattice parameter, which could be close to those expected for $Ge_2Sb_2Se_5$.[31] Nevertheless, it needs to be considered if the parameters a_0 for the thin films samples have the same meaning even when the correction for viscosity is used ($u \propto \eta^{-\xi}$).

As was shown in last paragraph, all the calculated growth models can be used for description of crystal growth in the $Ge_{18}Sb_{28}Se_{54}$ bulk glasses and thin films within experimental errors. Nevertheless, it is not possible to distinguish which model, normal or screw dislocation, is better for extrapolation into the higher temperature region to describe the crystal growth near the melting point. Without growth data from the temperature region near to the melting it is uneasy to distinguish which model is appropriate within the current knowledge of crystal growth in amorphous materials.

■ CONCLUSION

The isothermal crystal growth kinetics in the $Ge_{18}Sb_{28}Se_{54}$ bulk glasses and thin films was directly studied using optical, infrared, and scanning electron microscopy. The study of temperature dependence of viscosity and melting behavior were performed using thermomechanical analysis and differential scanning calorimetry, respectively.

In the case of the bulk glass, the crystal growth starts on the surface of a sample and continues with the formation of the compact crystalline layer. The needle-shape crystals which grew from randomly distributed nuclei were formed in thin films. Both types of crystals grew linearly with time indicating crystal growth controlled by liquid-crystal interface kinetics. The activation energies of crystal growth in the $Ge_{18}Sb_{28}Se_{54}$ bulk glasses and thin films were estimated.

Viscosity data were measured in the region of the undercooled melt and glass in the range of $10^8 - 10^{12.5}$ Pa·s. Simple Arrhenius equation was used to fit the experimental data. The apparent activation energy of viscous flow E_η was found to be 410 ± 4 kJ/mol. The fragility index of the studied $Ge_{18}Sb_{28}Se_{54}$ bulk glass is m = 43.2 ± 0.4. The viscosity behavior in the wide temperature region, including the region of melt, is not possible to describe using Arrhenius equation and the equation with three parameters should be used. The extrapolation of viscosity from undercooled melt region was performed using the MYEGA equation.

Melting process in Ge−Sb−Se system, which was measured under nonisothermal conditions, is very complicated. The temperature of melting was found as the onset of the first melting peak, T_m = 432.3 ± 1.2 °C.

The extent of decoupling between the crystal growth rate and viscous flow was tested. The exponent ξ was found to be 0.98 ± 0.02 for the bulk glass. This value is close to 1, therefore the standard growth models are appropriate for description of crystal growth in this system. On the other hand, the exponent ξ for the thin films was found to be much smaller than 1 (ξ = 0.67 ± 0.04). For the thin films, it was shown that the kinetic models corrected for the decoupling provide better description of the experimental data, and more realistic value of the parameter describing the mean interatomic distance in the crystal−liquid interface layer where the crystal growth takes place.

The growth, melting, and viscosity data were combined and the most probable growth models were calculated. Taking into account the dependence of reduced crystal growth rate on undercooling and the results from the previously studied $Ge_2Sb_2Se_5$ system, the normal and screw dislocation growth models were used for fitting the experimental growth data. Both models and their parameters were discussed within the current knowledge of crystal growth.

■ AUTHOR INFORMATION

Corresponding Author

*j-bartak@seznam.cz.

ORCID

Jaroslav Barták: 0000-0001-8675-1144

Notes

The authors declare no competing financial interest.

■ ACKNOWLEDGMENTS

The authors would like to express their gratitude for financial support from the Czech Science Foundation under grant no. 16-10562S and the International Cooperative Graduate Program between University of Pardubice and NIMS.

■ REFERENCES

(1) Savage, J. A.; Webber, P. J.; Pitt, A. M. Assessment of Ge-Sb-Se glasses as 8 to 12μm infra-red optical materials. *J. Mater. Sci.* **1978**, *13* (4), 859−864.

(2) Choi, D. Y.; Madden, S.; Rode, A.; Wang, R.; Luther-Davies, B. Fabrication of low loss Ge33As12Se55 (AMTIR-1) planar waveguides. *Appl. Phys. Lett.* **2007**, *91* (1), 011115.

(3) Bordas, S.; Clavaguera-mora, M. T.; Legendre, B. Phase diagram of the ternary system Ge-Sb-Se. *Thermochim. Acta* **1982**, *56* (2), 161−182.

(4) Sharma, P.; Rangra, V. S.; Katyal, S. C.; Sharma, P. Far-infrared study of amorphous Ge0.17Se0.83-xSbx chalcogenide glasses. *J. Alloys Compd.* **2009**, *480* (2), 934−937.

(5) Hosni, H. M.; Fayek, S. A.; El-Sayed, S. M.; Roushdy, M.; Soliman, M. A. Optical properties and DC electrical conductivity of Ge28-xSe72Sbx thin films. *Vacuum* **2006**, *81* (1), 54−58.

(6) Wei, W. H.; Wang, R. P.; Shen, X.; Fang, L.; Luther-Davies, B. Correlation between structural and physical properties in Ge-Sb-Se glasses. *J. Phys. Chem. C* **2013**, *117* (32), 16571−16576.

(7) Giridhar, A.; Narasimham, P. S. L.; Mahadevan, S. Electrical properties of Ge-Sb-Se glasses. *J. Non-Cryst. Solids* **1980**, *37* (2), 165−179.

(8) Svoboda, R.; Brandova, D.; Malek, J. Crystallization behavior of GeSb2Se4 chalcogenide glass. *J. Non-Cryst. Solids* **2014**, *388*, 46−54.

DOI: 10.1021/acs.jpcb.7b04429
J. Phys. Chem. B 2017, 121, 7978−7986

(9) Svoboda, R.; Prikryl, J.; Bartak, J.; Vlcek, M.; Malek, J. Crystallization behaviour of Ge17Sb23Se60 thin films. *Philos. Mag.* **2014**, *94* (12), 1301−1310.
(10) Svoboda, R.; Malek, J. Particle size influence on crystallization behavior of Ge2Sb2Se5 glass. *J. Non-Cryst. Solids* **2012**, *358* (2), 276−284.
(11) Wei, W. H.; Fang, L.; Shen, X.; Wang, R. P. Crystallization kinetics and thermal stability in Ge-Sb-Se glasses. *Phys. Status Solidi B* **2013**, *250* (1), 59−64.
(12) Shaaban, E. R.; Tomsah, I. B. I. The effect of Sb content on glass-forming ability, the thermal stability, and crystallization of Ge-Se chalcogenide glass. *J. Therm. Anal. Calorim.* **2011**, *105* (1), 191−198.
(13) Vazquez, J.; Barreda, D. G. G.; Lopez-Alemany, P. L.; Villares, P.; Jimenez-Garay, R. Levels of thermal stability in some glassy alloys of the Ge-Sb-Se system by differential scanning calorimetry. *J. Alloys Compd.* **2005**, *390* (1−2), 94−99.
(14) Svoboda, R.; Malek, J. Thermal behavior of Se-rich Ge2Sb2Se(5-y)Tey chalcogenide system. *J. Alloys Compd.* **2015**, *627*, 287−298.
(15) Barták, J.; Koštál, P.; Podzemná, V.; Shánělová, J.; Málek, J. Crystal growth kinetics and viscous behavior in Ge2Sb2Se5 undercooled melt. *J. Phys. Chem. B* **2016**, *120* (32), 7998−8006.
(16) Uhlmann, D. R. Crystal growth in glass forming system. In *Advances in Nucleation and Crystallization in Glasses*; Hench, L. L., Freiman, S. W., Eds.; American Ceramics Society: OH, 1972; pp 91−115.
(17) Jackson, K. A.; Uhlmann, D. R.; Hunt, J. D. On the nature of crystal growth from the melt. *J. Cryst. Growth* **1967**, *1*, 1−36.
(18) Ngai, K. L.; Magill, J. H.; Plazek, D. J. Flow, diffusion and crystallization of supercooled liquids: Revisited. *J. Chem. Phys.* **2000**, *112* (4), 1887−1892.
(19) Nascimento, M. L. F.; Ferreira, E. B.; Zanotto, E. D. Kinetics and mechanisms of crystal growth and diffusion in a glass-forming liquid. *J. Chem. Phys.* **2004**, *121* (18), 8924−8928.
(20) Ediger, M. D.; Harrowell, P.; Yu, L. Crystal growth kinetics exhibit a fragility-dependent decoupling from viscosity. *J. Chem. Phys.* **2008**, *128* (3), 034709.
(21) Nascimento, M. L. F.; Zanotto, E. D. Does viscosity describe the kinetic barrier for crystal growth from the liquidus to the glass transition? *J. Chem. Phys.* **2010**, *133* (17), 174701.
(22) Schmelzer, J. W. P.; Abyzov, A. S.; Fokin, V. M.; Schick, C.; Zanotto, E. D. Crystallization in glass-forming liquids: Effects of decoupling of diffusion and viscosity on crystal growth. *J. Non-Cryst. Solids* **2015**, *429*, 45−53.
(23) Barták, J.; Martinková, S.; Málek, J. Crystal growth kinetics in Se−Te bulk glasses. *Cryst. Growth Des.* **2015**, *15* (9), 4287−4295.
(24) Martinkova, S.; Bartak, J.; Malek, J.; Segawa, H. Crystal growth in Se70Te30 thin films followed by SEM and in situ XRD. *J. Appl. Phys.* **2016**, *120* (14).145301 10.1063/1.4964425
(25) Málek, J.; Barták, J.; Shánělová, J. Spherulitic crystal growth velocity in selenium supercooled liquid. *Cryst. Growth Des.* **2016**, *16* (10), 5811−5821.
(26) Douglas, R. W.; Armstrong, W. L.; Edward, J. P.; Hall, D. A penetration viscometer. *Glass Technol.* **1965**, *6* (2), 52−55.
(27) Málek, J.; Shánělová, J. Viscosity of germanium sulfide melts. *J. Non-Cryst. Solids* **1999**, *243* (2−3), 116−122.
(28) Kostal, P.; Malek, J. Viscosity of Se-Te glass-forming system. *Pure Appl. Chem.* **2015**, *87* (3), 239−247.
(29) Angell, C. A. Formation of Glasses from Liquids and Biopolymers. *Science* **1995**, *267* (5206), 1924−1935.
(30) Milliron, D. J.; Raoux, S.; Shelby, R.; Jordan-Sweet, J. Solution-phase deposition and nanopatterning of GeSbSe phase-change materials. *Nat. Mater.* **2007**, *6* (5), 352−356.
(31) Matsunaga, T.; Kojima, R.; Yamada, N.; et al. Structural analysis of GeSbTeSe phase-change materials. *Library of EPCOS* **2009**, 99−104.
(32) Svoboda, R.; Malek, J. Thermal behavior of Se-rich GeSb2Se(4-y)Tey (glassy) system. *J. Alloys Compd.* **2016**, *670*, 222−228.
(33) Svoboda, R.; Malek, J. Amorphous-to-crystalline transition in Te-doped Ge2Sb2Se5 glass. *J. Therm. Anal. Calorim.* **2014**, *117* (3), 1073−1083.
(34) Kirkpatrick, R. J. Crystal Growth from the Melt: A Review. *Am. Mineral.* **1975**, *60*, 798−814.
(35) Jackson, K. A.; Uhlmann, D. R.; Hunt, J. D. On the nature of crystal growth from the melt. *J. Cryst. Growth* **1967**, *1* (1), 1−36.
(36) Nemilov, S. V. Interrelation between shear modulus and the molecular parameters of viscous flow for glass forming liquids. *J. Non-Cryst. Solids* **2006**, *352* (26−27), 2715−2725.
(37) Mauro, J. C.; Yue, Y. Z.; Ellison, A. J.; Gupta, P. K.; Allan, D. C. Viscosity of glass-forming liquids. *Proc. Natl. Acad. Sci. U. S. A.* **2009**, *106* (47), 19780−19784.
(38) Turnbull, D. Formation of crystal nuclei in liquid metals. *J. Appl. Phys.* **1950**, *21*, 1022−1028.
(39) Stephens, R. B. Viscosity and structural relaxation rate of evaporated amorphous selenium. *J. Appl. Phys.* **1978**, *49* (12), 5855−5864.
(40) Gutzow, I. S.; Schmelzer, J. W. P. *The Vitreous State: Thermodynamics, Structure, Rheology, and Crystallization*; Springer: Berlin Heidelberg, 2013.
(41) Gunasekera, K.; Boolchand, P.; Micoulaut, M. Elastic phases of GexSbxSe100−2x ternary glasses driven by topology. *J. Phys. Chem. B* **2013**, *117* (34), 10027−10034.

DOI: 10.1021/acs.jpcb.7b04429
J. Phys. Chem. B 2017, 121, 7978−7986

PAPER V

CRYSTAL GROWTH & DESIGN

Article

pubs.acs.org/crystal

Crystal Growth Velocity in As_2Se_3 Supercooled Liquid

Jiří Málek,[†] Jana Shánělová,[*,†] Simona Martinková,[†] Petr Pilný,[†] and Petr Koštál[‡]

[†]Department of Physical Chemistry, Faculty of Chemical Technology, University of Pardubice, Studentská 573, Pardubice 532 10, Czech Republic

[‡]Department of Inorganic Technology, Faculty of Chemical Technology, University of Pardubice, Doubravice 41, Pardubice 532 10, Czech Republic

ABSTRACT: The crystal growth velocity of spherulitic As_2Se_3 in a supercooled melt of the same composition was studied by optical microscopy and thermoanalytical methods in isothermal and nonisothermal conditions. The time dependence of crystal size is linear, which suggests the crystal growth is controlled by interface kinetics. Crystal growth velocity was determined as the slope of these linear dependences. The experimental results presented in this paper considerably extend the previously reported range of crystal growth velocity. All isothermal crystal growth velocity data can be well described by the standard two-dimensional surface nucleated growth model (2Dsg) including crystal growth viscosity decoupling ($\xi = 0.647$). The activation energy of crystal growth for microscopic experiments is in a good agreement with values obtained from thermoanalytical experiments, and the ratio of the activation energy of crystal growth and the activation energy of viscous flow well corresponds to an independently determined decoupling parameter. The same model successfully describes also crystalline layer thickness and growth pattern at the amorphous As_2Se_3 surface in nonisothermal conditions.

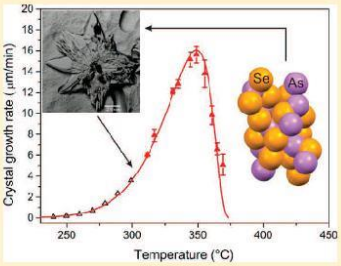

INTRODUCTION

Chalcogenide glasses are known as excellent optical materials in the infrared spectral region (3−12 μm) for more than 60 years. These glasses can be easily molded with high precision to aspheric or diffractive lenses and are now produced industrially, reducing the price of infrared optical systems used in night vision cameras, e.g., in the automotive industry.[1] Especially, arsenic−selenium glasses are resistant to devitrification and can easily be drawn into optical fibers transparent in the mid-infrared spectral region.[2,3] Such fibers are investigated as a potential for medical applications and bio-optical sensors based on monitoring the response of living cells to toxins by detecting change in their IR spectrum.[4] Important issues, unfortunately often overlooked in the literature, are chemical and phase purity of chalcogenides[5] as well as melt processing and homogenization.[6] The chalcogenide glasses are very sensitive to moisture and oxygen impurities, causing that the transparency window is partially closed due to the strong absorption in the 3−12 μm spectral region. Therefore, industrial chalcogenide glass production takes place in vacuum sealed quartz glass ampules, which considerably increases production cost. Recently, a new route to synthesize As_2Se_3 glass under argon that does not require sealing of reaction container has been described.[7]

Glass transformation, structural relaxation, and viscosity of supercooled liquid were studied by several authors.[8,9] However, one of the most important properties of amorphous material is its long-term stability and resistance to crystallization. The crystallization kinetics characterized by isothermal differential scanning calorimetry (DSC) and microscopy was thoroughly investigated by Henderson and Ast.[10] These authors proposed the Johnson−Mehl−Avrami kinetic model with kinetic exponent $m = 4.5$ for the description of isothermal crystallization data obtained by DSC. This model was also confirmed by others, however, with a different kinetic exponent, reflecting dimensionality of crystal growth[11] and the influence of mechanically induced defects.[12] Recently, a quadratic approximation of the nucleation−growth process was also reported.[13] The nucleation process was studied by DSC,[14,15] and the crystal growth kinetics was also monitored by thermomechanical analysis (TMA).[16] Apart from the thermoanalytical experiments represented by DSC and TMA, there is a notable crystal growth measurement reported by Henderson and Ast.[10] However, these crystal growth data were compared with DSC just in terms of activation energy[10,16] and any attempt to apply quantitative models of crystal growth data has not been made.

In this paper, we considerably extend previous[10] isothermal crystal growth velocity measurement of As_2Se_3 to higher temperatures, including the region close to the melting point. All of these isothermal experimental data are then well described by a two-dimensional surface nucleation growth model involving temperature dependent As_2Se_3 viscosity data. It is shown that this model successfully describes also development of crystalline layer thickness and growth pattern at the amorphous sample surface in nonisothermal conditions.

Received: July 19, 2017
Published: August 8, 2017

DOI: 10.1021/acs.cgd.7b01001
Cryst. Growth Des. 2017, 17, 4990−4999

MATERIALS AND METHODS

Arsenic selenide glass was prepared from high purity elements (selenium: 5N, Sigma-Aldrich, arsenic: 6N, ESPI Metals) by the conventional melt-quenching method. Stoichiometric amounts of polycrystalline arsenic and selenium pellets were placed into a carefully washed and dried quartz glass ampule (16 mm diameter, 1 mm wall thickness). The ampule was then evacuated to a pressure of 10^{-3} Pa and sealed. The sealed ampule was annealed in a rocking furnace at 750 °C for 24 h. The glass was then prepared by a rapidly quenching the ampule in the air. Then, the ampule was opened and the as-prepared As_2Se_3 glass ingot was broken into small pieces. These samples were used for isothermal crystal growth studies. The As_2Se_3 glass samples for nonisothermal crystal growth and nucleation studies were also prepared from high purity elements by the conventional melt-quenching method. The difference was in the size of the quartz glass ampule (4 mm inner diameter). The glass ingot was sectioned by a diamond saw to cylindrical samples with a diameter of 4 mm and height of 1 and 2 mm. Some of these samples were polished to optical quality. The composition of prepared bulk glasses was confirmed by an energy dispersive X-ray (EDX) microanalyzer IXRF Systems (detector GRESHAM Sirius 10) coupled with a scanning electron microscope (JEOL JSM-5500 LV). The amorphous nature of bulk glasses was verified using X-ray diffraction analysis (Bruker AXS X-ray diffractometer D8 Advance, Cu Kα (40 kV, 30 mA)).

Thin films were prepared by thermal deposition on microscopy glass substrates. Bulk glass, which was prepared by a conventional melt-quenching method, was used as starting material for the preparation of thin films. The glass substrates were rotated by means of a planetary rotation system during deposition to ensure homogeneity in the film thickness. Deposition rate was measured using a quartz microbalance technique. Final thickness of the thin films was 1 μm. The composition of prepared thin films was confirmed by an energy dispersive X-ray (EDX) microanalyzer IXRF Systems (detector GRESHAM Sirius 10) coupled with scanning electron microscope (JEOL JSM-5500 LV). The crystal growth in thin films was studied under nonisothermal conditions.

Crystalline As_2Se_3 was prepared by a slow cooling of the melt in an evacuated quartz ampule from 750 to 380 °C for 3 days. The ampule was then maintained at 380 °C for 1 day and then slowly cooled to 355 °C. After annealing for 3 days at this temperature, the ampule was slowly cooled to 340 °C and then rapidly quenched to room temperature. The cooling rate during the cooling steps was set approximately to −5 K/day. In this way, we were able to prepare a fully crystallized ingot of As_2Se_3. This material was composed of a large array of single sheet crystals that were used for single crystal X-ray diffraction analysis as well as for the determination of melting enthalpy (DSC measurements).

The isothermal crystal growth kinetics was studied by an Olympus BX51 optical microscope equipped with a DP72 camera and by an Olympus BX51 optical microscope equipped with the infrared XM10 camera, both in the reflection mode. The As_2Se_3 bulk samples were placed in a preheated computer-controlled furnace (within ±0.5 °C). The time needed for thermal equilibration of the specimen was estimated to be less than 2 min. Samples were first nucleated at a temperature of 233 °C for 6 h to be sure that crystals grew from preexisting nuclei. Immediately after thermal treatment at selected temperatures for various times, the samples were quickly cooled down and thoroughly analyzed by optical microscopy. This system exhibits only surface crystallization, so the samples were partitioned to follow crystal growth. The presence of bulk crystallization was not observed. The thickness of the surface crystalline layer was recorded and measured. The time evolution of the thickness of surface crystalline layers was measured at selected temperatures, and crystal growth velocities were obtained from the slopes of these dependences. The morphology of the formed crystals was observed using a scanning electron microscope (JEOL JSM-7500 F; 1 kV, gentle beam mode).

The nonisothermal crystal growth in As_2Se_3 thin films and bulk samples was studied by a thermomechanical analyzer (TMA CX 03; RMI, Czech Republic). More details about specification of this instrument are described elsewhere.[9] The temperature was calibrated on melting of pure metals (Ga, In, Sn, Pb, Zn, Al). The temperature was constant within ±0.2 °C. The nonisothermal experiments were performed in the temperature range from 233 to 374 °C at heating rates of 0.1, 0.5, 1, 1.5, 2, and 3 K/min. The force of 10 mN was applied. The sample was first nucleated at a temperature of 233 °C for 1 h and then heated to the selected temperature at various defined heating rates. After heat treatment in a TMA furnace, the sample was cooled down in the air in order to avoid further crystal growth, and sectioned (in case of bulk sample), and the crystalline layer or formed crystals in thin film were observed using an optical microscope (Olympus BX 51 with DP 72 camera). The thickness of the surface crystalline layer (bulk samples) or the length of crystal's long axis (thin films) was measured.

The same TMA instrument was also used for nucleation experiments. The cylindrical samples sandwiched between two synthetic sapphire plates were nucleated in the TMA furnace at a temperature of 233 °C for different times. The force of 10 mN was applied. Then, the samples were quenched to room temperature (RT) in the air. The quenched-in nuclei were then visualized by nonisothermal thermal treatment in the DSC (hermetically sealed Al sample pans, heating from 230 to 360 °C, heating rate 1 K/min). After heat treatment in TMA and DSC, the samples were observed using an optical microscope. The formed crystals were counted at the surface as well as within the fresh fracture of the bulk sample.

A SenSys-Evo DSC (Setaram) equipped with a 3D Calvet sensor was used for the measurement of melting enthalpy of the crystalline As_2Se_3 sample. Dry nitrogen was used as the purge gas at a rate of 100 cm^3/min. For temperature calibration of the calorimeter, high purity melting standards were used (In, Zn). The heat flow calibration was improved using the Joule effect method in the whole temperature range. The pieces of crystalline bulk sample (~75 mg) were placed in closed aluminum pans and used for the measurement. During the DSC measurements, the sample was heated to 420 °C (above melting point) at a heating rate of 1 K/min.

X-ray diffraction analysis of the As_2Se_3 single crystal sheet (approximately 0.211 mm × 0.120 mm × 0.011 mm) was performed by a Bruker D8-Venture diffractometer equipped with a Mo (Mo/Kα radiation; λ = 0.71073 Å) microfocus X-ray (IμS) source, a Photon CMOS detector, and an Oxford Cryosystems cooling device. Full sets of diffraction data for As_2Se_3 were collected at 150(2) K. The frames were integrated with the Bruker SAINT software package using a narrow-frame algorithm. Data were corrected for absorption effects using the Multi-Scan method (SADABS). Obtained data were treated by XT-version 2014/5 and SHELXL-2014/7 software implemented in the APEX3 v2016.5-0 (Bruker AXS) system.[17]

RESULTS

Nucleation in arsenic selenide glasses appears to be a quite complicated heterogeneous process that takes place at the sample surface well above the glass transition temperature. Nucleation density depends on many factors such as surface roughness, surface tension, particle size distribution, thermal history, etc. The nucleation process exhibits a significantly long time lag (hours to days) and stochastic behavior even in well prepared glass with minimum defects and stresses. On the other hand, the nucleation can be accelerated by mechanical grinding or contact with other materials. To minimize the time lag and stochastic effects, we measured the nucleation process at 233 °C by using cylindrical samples sandwiched between two synthetic sapphire plates in the TMA instrument with an applied force of 10 mN. Quenched nuclei created at this temperature after different periods of time were subsequently visualized by nonisothermal thermal treatment from 230 to 360 °C at a heating rate of 1 K/min. Figure 1 shows the number of nuclei per unit area (nuclei density) in As_2Se_3 as a function of nucleation time.

DOI: 10.1021/acs.cgd.7b01001
Cryst. Growth Des. 2017, 17, 4990−4999

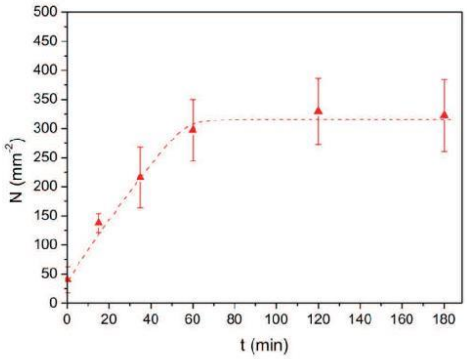

Figure 1. Time dependence of nuclei density in As_2Se_3 at 233 °C. Dotted line is drawn as a guide to the eye.

Every point in Figure 1 corresponds to about 10 independent measurements. It is seen that the steady state number of nuclei 316 ± 64 mm^{-2} is achieved after 60 min. The same steady state was observed also for small pieces of bulk sample; nevertheless, in this case, it took a considerably longer time (about 6 h) for most of the samples. The nucleation rate determined at 233 °C is 5.0 ± 0.7 mm^{-2}·min^{-1}. This temperature is close to the maximum nucleation rate in As_2Se_3 reported by Holubová et al.,[14] though their nucleation rate data are relative.

As_2Se_3 crystallizes as relatively open spherulitic arrays of individual crystallites as shown in Figure 2. A typical faceted

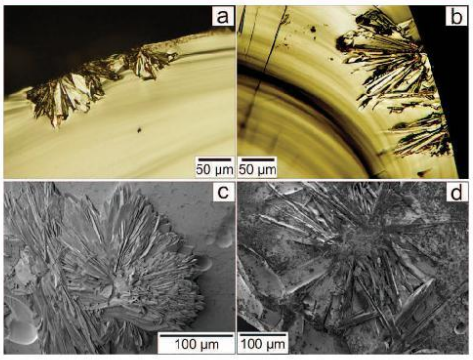

Figure 2. Morphology of As_2Se_3 crystals grown in a supercooled liquid of the same composition. Optical microscopy of fractured samples: (a) T = 311 °C; t = 15 min, (b) T = 365 °C; t = 15 min. SEM microscopy of etched surface of sample: (c) T = 311 °C; t = 30 min, (d) T = 365 °C; t = 30 min.

triangular "arrow-like" morphology, described previously by Henderson and Ast,[10] was observed below 350 °C (Figure 2a,c). A more open "rodlike" morphology was observed at higher temperatures where individual crystals exhibit a relatively high degree of correlation in crystallite orientation (Figure 2b,d).

Figure 3 shows the time dependence of crystal size measured as the thickness of the formed crystalline layer (spherulitic

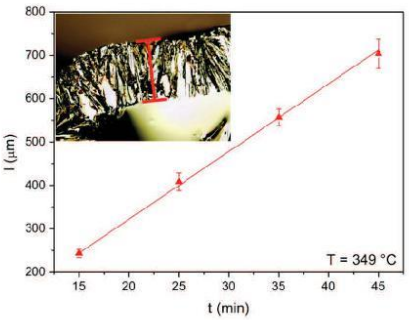

Figure 3. Time dependence of the thickness of crystalline layer grown in As_2Se_3 supercooled melt at a temperature of 349 °C.

radius). Every point in this figure corresponds to a mean value of 20−40 measurements of the thickness of the crystalline layer in different places of the sample. Typical standard deviations are shown as error bars for all data points. The linear behavior of this dependence is typical for crystal growth controlled by interface kinetics.

Crystal growth velocity u was determined as the slope of the linear fit illustrated in Figure 3. Experimental crystal growth velocity data for As_2Se_3 determined in this way are summarized in Table 1. These results considerably extend the previously measured range of crystal growth velocity reported by Henderson and Ast.[10]

Table 1. Crystal Growth Velocities in As_2Se_3 Glass

T (°C)	u (μm/min)
311.3	6.0 ± 0.2
317.0	7.9 ± 0.6
331.0	12.1 ± 0.3
335.0	12.8 ± 0.4
344.4	15.2 ± 0.7
349.0	15.6 ± 0.8
355.2	13.8 ± 1.3
361.0	9.8 ± 0.9
364.9	6.6 ± 0.6
369.0	5.1 ± 1.0

Figure 4 shows combined data sets on a logarithmic scale. The data of Henderson and Ast[10] were adjusted by a factor of $^1/_2$ as these authors measured spherulitic diameter and not radius.

The crystal growth velocity has been measured in a broad range of temperatures, from 240 °C to the melting point, over 3 orders of magnitude. Maximum growth velocity of the As_2Se_3 supercooled melt is about 15.6 μm/min. Figure 4 shows also DSC data in the whole temperature range at a slow scanning rate of 1 K/min. The enthalpy change obtained by integration of measured heat flow over the whole melting peak was found to be 86.3 J/g. This is a considerably lower value than the melting enthalpy of the completely crystallized As_2Se_3 sample obtained by a slow cooling of the melt, which was determined by high precision calorimetry ΔH_m = 106.9 ± 0.7 J/g at T_m = 375.5 °C. Therefore, it seems that the As_2Se_3 supercooled melt cannot completely crystallize even during slow heating in the

DOI: 10.1021/acs.cgd.7b01001
Cryst. Growth Des. 2017, 17, 4990−4999

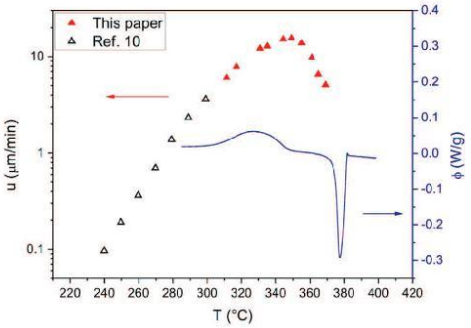

Figure 4. Temperature dependence of isothermal crystal growth velocity of As_2Se_3 and nonisothermal DSC curve measured at 1 K/min.

DSC experiment. This probably explains the quite wide scatter of melting enthalpy/crystallization enthalpy values of As_2Se_3 obtained from heating experiments found in the literature.[11,14,15,18] Also, the determination of melting point from the onset of DSC melting peak is not so accurate. Therefore, the melting point was checked by optical microscopy in a quasi-isothermal experiment (0.5 °C increase every 30 min) in the same computer-controlled furnace used for growth experiments. The complete melting was observed at 374.4 °C. This temperature was used as the melting point in all the following calculations of crystal growth models.

The crystal data for the unit cell of an As_2Se_3 single crystal are summarized in Table 2 (standard errors in parentheses refer

Table 2. Crystal Data for As_2Se_3 Prepared by Slow Cooling of the Melt

space group: $P2_1/n$
a = 4.2700(10) Å
b = 9.887(2) Å
c = 12.082(3) Å
β = 90.441(9)°
Z = 4
V_{cell} = 510.1(2) Å^3

to the last digit). These results are in very good agreement with previously reported crystallographic results by Stergiou and Rentzeperis.[19] Only negligible differences observed for these structures were found in a slight shortening of all unit cell length parameters by ~0.05 Å, probably caused by the cell volume contraction with lowering the temperature of measurement to 150 K used in our experimental setup.

The structure of crystalline As_2Se_3 is visualized in Figures 5 and 6 where the covalently bonded monolayer and weakly bonded bilayer are presented, showing mutual connectivity of building blocks with essential interatomic distances. It can be suggested that the crystal growth takes place from left to right within the monolayer (Figure 5), propagating in a layer-by-layer way. These layered structures are bound together by weaker van der Waals forces as shown in Figure 6. It indicates the brittleness of sheet-like crystals and their ability to form more complex spherulitic structures. As the interlayer interatomic distances are shorter than the sum of covalent radii for both Se-

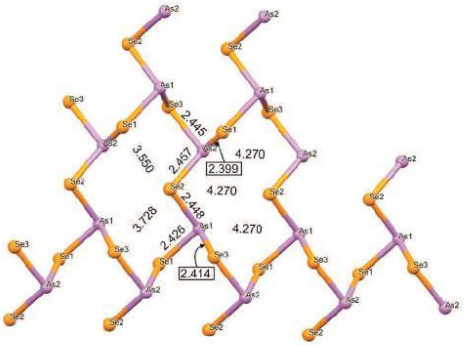

Figure 5. Projection of covalently bonded monolayer of As_2Se_3 along the b axis.

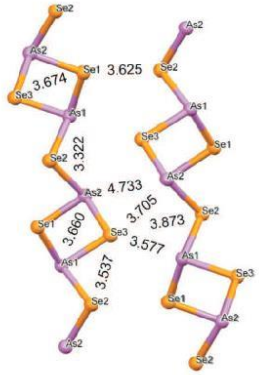

Figure 6. Projection of weakly bonded bilayer of As_2Se_3 along the a axis.

Se and As-Se, it can be speculated about the ordering of substructures based on noncovalent contacts of a pair of selenium atoms by chalcogen and arsenic selenium by pnictogen bonds.

DISCUSSION

Viscosity Scaling of Crystal Growth. The isothermal crystal growth velocity in supercooled liquid can be expressed as the product of the molecular growth rate at the crystal–liquid interface u_{kin} and the probability that the newly formed molecular layer is retained in the growing crystal.[20−22] This probability is typically expressed as $[1 - \exp(-\Delta G/RT)]$, where ΔG is the Gibbs energy difference between crystalline and supercooled liquid phase. By definition ΔG is given by

$$\Delta G = \Delta H - T\Delta S \quad (1)$$

This can be expanded by using the well-known expression for ΔH and ΔS by the integration heat capacity difference between the supercooled melt and crystalline phase $\Delta C_p = C_p^m - C_p^\sigma$. However, it is not so easy to obtain reliable values of ΔC_p due to sublimation of crystalline As_2Se_3 and the volatility of its melt.

DOI: 10.1021/acs.cgd.7b01001
Cryst. Growth Des. 2017, 17, 4990−4999

The inset of Figure 7 shows nearly all available heat capacity data[18,23−26] for this material, clearly showing this difficulty.

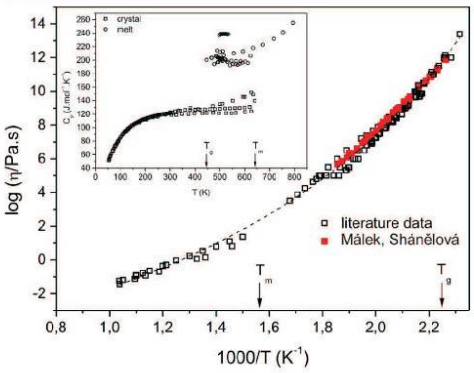

Figure 7. Temperature dependence of viscosity (Malek and Shanelova,[9] other literature[10,28−37]) and heat capacity[18,23−26] (inset) of As_2Se_3. Dashed line was calculated by VFT (eq 4).

In this case, we should use an approximation for ΔG. The expression of Thomson and Spaepen[27] is likely to be a reasonable approximation for chalcogenides even for higher supercoolings

$$\Delta G \cong \frac{\Delta H_m \Delta T}{T_m}\left(\frac{2T}{T_m + T}\right) \quad (2)$$

where ΔH_m is the melting enthalpy, T_m is the melting temperature, and $\Delta T = T_m - T$ is the supercooling.

For classical crystal growth mechanisms, the transport process in the vicinity of the crystal−liquid interface is similar to self-diffusion. The temperature dependence of the self-diffusion coefficient is not always available, so it is usually replaced by the inverse shear viscosity η^{-1} according to the Stokes−Einstein equation. Ediger et al.[22] reported u_{kin} scaling with viscosity $\sim \eta^{-\xi}$ for several inorganic and organic materials with the exponent ξ smaller than unity:

$$u_{kin} = \frac{u}{1 - \exp(-\Delta G/RT)} \propto \eta^{-\xi} \quad (3)$$

Figure 7 shows the temperature dependence of dynamic viscosity summarizing previously published data of supercooled liquid As_2Se_3[9,10,28−34] and kinematic viscosity of liquid As_2Se_3[35−37] converted using density taken from ref 38. All data can be well approximated by the Vogel−Fulcher−Tamman (VFT) equation:

$$\log(\eta/Pa{\cdot}s) = A + \frac{B}{T - T_0} \quad (4)$$

where $A = -5.78 \pm 0.18$, $B = 2965 \pm 96$ K, and $T_0 = 276 \pm 4$ K.

Figure 8 shows the u_{kin} plot in log−log format calculated from crystal growth velocity by eqs 2 and 3, as a function of As_2Se_3 supercooled liquid viscosity (eq 4). Nearly identical dependence is obtained for the simplest approximation of $\Delta G \cong (\Delta H_m/T_m)\Delta T$ that is attributed to Turnbull.[39] A key parameter in this approximation as well as in eq 2 is the melting

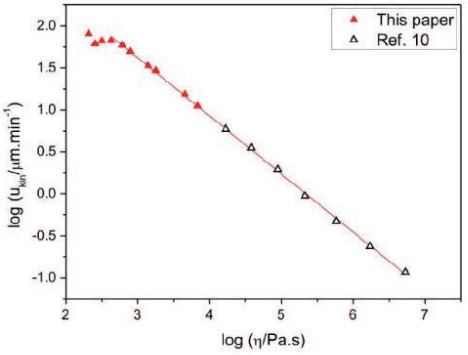

Figure 8. Viscosity scaling of crystal growth velocity of As_2Se_3 corrected for thermodynamic driving force.

entropy of As_2Se_3. The value obtained by high precision calorimetric measurement ($\Delta S_m = \Delta H_m/T_m = 7.68 \pm 0.05\ R$) is very similar to the value $\Delta S_m = 7.6\ R$ reported by Myers and Felty[40] that is also indirectly supported by a thermodynamic study by O'Hare et al.[18] A linear dependence corresponding to a power law anticipated by eq 3 is observed in nearly the whole range, except for the vicinity of the melting point. The slope corresponding to the kinetic exponent $\xi = 0.692 \pm 0.005$ departs significantly from 1. Ediger et al.[22] demonstrated that, for numerous organic and inorganic glasses, the exponent ξ is linearly correlated with fragility m of supercooled liquid near the glass transition ($\xi = 1.1-0.005{\cdot}m$). Fragility of the As_2Se_3 melt reported by Málek and Shánělová[9] is $m \cong 38$, which is an intermediate value between the strong and fragile pattern. According to this correlation, it would provide an estimation of $\xi \cong 0.91$ that is, however, considerably higher than the experimental value.

Spherulitic Growth Morphology. Spherulites are polycrystalline aggregates composed by highly anisometric crystallites that grow independently by *noncrystallographic branching* of their single crystalline progenitor.[41] Spherulitic crystal growth in As_2Se_3 glass has been reported by Henderson and Ast[10] and it is also shown in Figure 2. These crystalline aggregates are composed of thin plates showing triangular "arrow-like" morphology for intermediate and high supercoolings ($\Delta T \geq 30$ K). The thickness of crystallites is practically constant during the growth; however, the apex angle increases slightly with temperature.[10] A more open "rodlike" morphology was observed at lower supercoolings ($\Delta T \leq 25$ K) as shown in Figure 2b,d. The spherulitic growth habitat is maintained and the long axis of crystallites is oriented along the radial axis of spherulites for both growth morphologies.

The crystal structure of As_2Se_3 is composed of trigonal pyramids $AsSe_3$ linked together with common Se atoms to form infinite covalently bonded sheets oriented along the b axis (see Figure 5). As has been mentioned earlier, the crystal growth takes place from left to right within these sheets (monolayers). These sheets are bound together by weaker van der Waals type forces forming the above-mentioned thin-plate crystallites. Henderson and Ast[10] also confirmed by TEM that the crystal growth on an atomic level takes place by addition of As_2Se_3 molecules to the edges of sheetlike structures, gradually

DOI: 10.1021/acs.cgd.7b01001
Cryst. Growth Des. 2017, 17, 4990−4999

forming layered crystallites that are aggregated to a macroscopic spherulitic structure. However, the growth on an atomic scale can be treated to a good approximation as two-dimensional faceted growth of crystals of approximately constant thickness.[10] According to the theory of Jackson, Uhlmann, and Hunt,[20] faceted crystal growth might be also expected from the relatively high melting entropy of As_2Se_3 (ΔS_m = 7.68 ± 0.05 R).

It is interesting to compare spherulitic growth morphology in As_2Se_3 glass and pure amorphous selenium.[42] In both materials, the spherulites are composed by thin plate crystallites. In both cases, there are two distinct spherulitic morphologies, typical for low and higher supercoolings. However, the spherulites grown in As_2Se_3 glass do not exhibit a banded structure composed of twisted lamellae. Another striking difference is related to the compactness and roughness of the spherulitic structure. The spherulites formed in pure amorphous selenium exhibit a compact structure and a nearly smooth surface. The agreement of crystallization enthalpy and melting enthalpy clearly indicates full crystallization with no amorphous phase retained within spherulitic lamellae. Although the structure of As_2Se_3 spherulites seems to be compact with a rather rough surface and several authors[10,14,15] reported full crystallization, there is a clear difference between crystallization and melting enthalpy that does indicate some uncrystallized amorphous phase likely retained in spherulitic structure.

Isothermal Crystal Growth Velocity. The relaxation in As_2Se_3 supercooled liquid is relatively fast,[9] not affecting significantly crystal growth velocity. It seems, therefore, that standard methods of description of crystal growth kinetics can be used. As has been anticipated earlier, the growth of As_2Se_3 crystals in a supercooled liquid of the same composition is controlled by crystal−liquid interface kinetics. There are the phenomenological models suitable for the description of such a process: (i) normal growth, (ii) screw dislocation growth, and (iii) two-dimensional surface nucleated growth.[20,21] For molecularly complex liquids, it is usually assumed that reorientation of the molecule or breaking bonds between atoms at the crystal−liquid interface should precede the incorporation of the molecule into the crystal. Such reorientation and bond breaking actually controls the crystal growth velocity u. It should involve similar molecular motions as in a highly viscous liquid. Usually, it is assumed that the temperature dependence of the interface process can be represented by supercooled melt viscosity η through the Stokes−Einstein equation. Jackson et al.[20] have shown that the growth model can be assessed from the reduced growth rate U_R given by the following equation

$$U_R = \frac{u \cdot \eta}{1 - \exp(-\Delta G/RT)} \tag{5}$$

where T is the temperature at which the crystal growth rate u and viscosity η are known, and ΔG is expressed by eq 2, where $\Delta H_m/T_m$ = 7.68 R.

The $U_R(\Delta T)$ plot provides information about the fraction of preferred growth sites at the interface. Therefore, for the normal growth, it should be a constant, i.e., a horizontal line; for screw dislocation growth, where the interface site factor is linearly dependent on supercooling, this plot should be a straight line of positive slope; and for two-dimensional surface nucleated growth, this plot should be a curve with increasing positive slope passing through the origin. Figure 9 shows the $U_R(\Delta T)$ plot calculated by eq 5, for crystal growth velocities

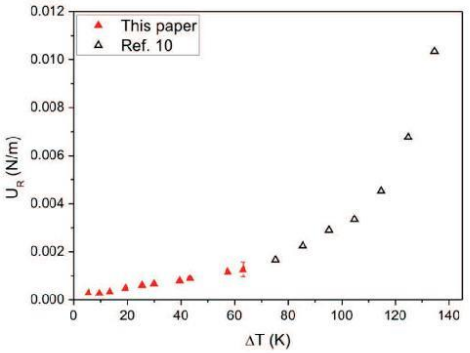

Figure 9. Reduced crystal growth velocity dependence on supercooling.

reported in this paper as well as for data previously reported by Henderson and Ast.[10] Both data sets clearly show the positive curvature that indicates the standard two-dimensional surface nucleated growth model (2Dsg). In this case, the growth velocity should be expressed as[20,21]

$$u = \frac{C}{\eta}\exp\left(-\frac{B}{T\Delta T}\right) \tag{6}$$

where B and C are constants. From a logarithmic form of eq 6, it is expected that the dependence of $\ln(u \cdot \eta)$ versus $1/(T\Delta T)$ should be linear. Figure 10a shows that this is not the case for

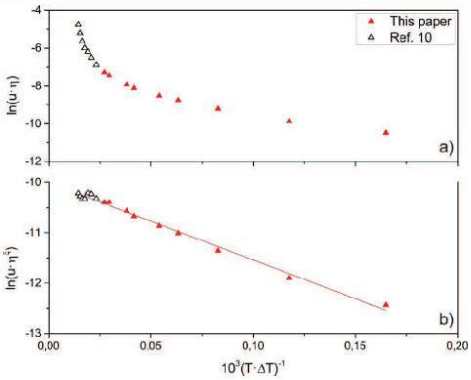

Figure 10. Plot of logarithm (growth velocity × viscosity) versus $1/(T\Delta T)$ for crystal growth of As_2Se_3: (a) uncorrected data, (b) data corrected for the crystal growth viscosity decoupling.

both As_2Se_3 crystal growth velocity data sets. The linear dependence is restored when the crystal growth viscosity decoupling is introduced in the 2Dsg model:

$$u = \frac{C}{\eta^{\xi}}\exp\left(-\frac{B}{T\Delta T}\right) \tag{7}$$

In this case, the logarithm of crystal growth velocity is a linear combination of the logarithm of viscosity and $1/(T\Delta T)$:

DOI: 10.1021/acs.cgd.7b01001
Cryst. Growth Des. 2017, 17, 4990−4999

$$\ln u = \ln C - \xi \ln \eta - \frac{B}{T\Delta T} \quad (8)$$

On the basis of this equation, the parameters $B = (15.36 \pm 0.60) \times 10^3$ K^2 and $\ln(C/\mathrm{N{\cdot}m^{-1}}) = -10.005 \pm 0.098$ and $\xi = 0.647 \pm 0.008$ were obtained by least-squares fit in three dimension space. The last point measured at 369 °C was outlying, and it was excluded from regression.

Figure 10b shows the best linear $\ln(u{\cdot}\eta^{\xi})$ versus $1/(T\Delta T)$ dependence that is obtained for $\xi = 0.647$. This value is slightly lower than ξ extracted from the viscosity scaling of crystal growth velocity of As_2Se_3 corrected for thermodynamic driving force mentioned earlier.

The parameter B is given by[20]

$$B = \frac{\pi\lambda V_m \sigma_E^2}{3k\Delta S_m} \quad (9)$$

where λ is a molecular diameter, and V_m is the molar volume. The parameter σ_E is the solid−liquid interface energy of the nucleus that should be equivalent to the crystal-melt surface tension, provided that there is not significant change in surface structure associated with deformation. Assuming from crystal data that $V_{cell} = 510 \times 10^{-30}$ m^3 and $Z = 4$ (Table 2), we can estimate the molecular diameter as $\lambda = (6V_{cell}/\pi Z)^{1/3} \cong 6.425 \times 10^{-10}$ m. Then, we can estimate the solid−liquid interface energy from eq 9 as $\sigma_E = 16$ mJ·m^{-2}. This appears to be physically meaningful in comparison with experimentally observed behavior of supercooled melt at the As_2Se_3 surface and the reported values of solid−liquid interface energy of pure selenium,[39,43] 28 and 21 mJ·m^{-2}. The value of surface tension of the As_2Se_3 liquid measured by a silica capillary method, recently reported by Mishinov et al.,[44] is considerably higher, ~90 mJ·m^{-2}, in the temperature range of measurable crystal growth. Such a significant difference is in qualitative agreement with our wetting experiments of As_2Se_3 liquid at the quartz glass and As_2Se_3 crystal surfaces.

Figure 11 shows the crystal growth velocity of As_2Se_3 prediction for the 2Dsg model (solid line) calculated by eqs 4 and 7 using founded parameters. It is evident that there is a satisfactory agreement between the 2Dsg model prediction and experimental data reported in this paper as well as for the data reported earlier by Henderson and Ast.[10] This model is consistent with the expected two-dimensional faceted growth of crystals of approximately constant thickness anticipated by Henderson and Ast.[10]

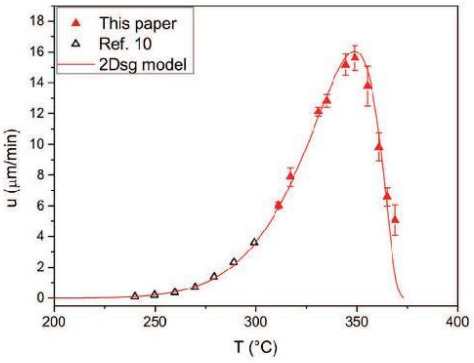

Figure 11. Temperature dependence of crystal growth velocity in As_2Se_3 glass calculated by eqs 7 and 4.

Nonisothermal Crystal Growth. The 2Dsg model used for the successful description of isothermal As_2Se_3 crystal growth velocity data in the previous section can also be used in nonisothermal conditions. The change of the crystalline layer thickness dl at temperature T is given by

$$\mathrm{d}l = u(T){\cdot}\mathrm{d}t = u(T){\cdot}\frac{\mathrm{d}T}{\beta} \quad (10)$$

where dT is a change of temperature, β is a linear heating rate, and $u(T)$ is given by eq 7. Let us suppose that an initial thickness of the crystalline layer is zero ($l_0 = 0$) at sufficiently low temperature (e.g., 150 °C in the glass transition range) and a temperature step is small enough. Then, the differential eq 10 can be solved by the Euler method assuming the viscosity given by eq 4 and $u(T)$ by eq 7 with parameters (ξ, B, C) obtained by least-squares fitting of isothermal data. Figure 12 shows the $l(T)$ dependence calculated in this way for heating rate $\beta = 1.5$ K/min (full line).

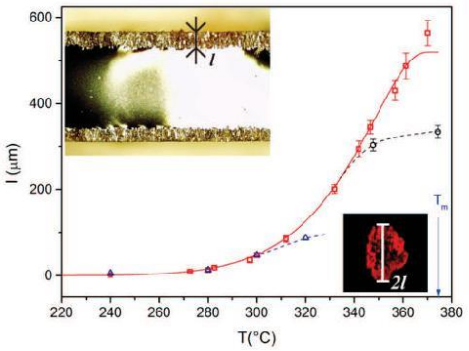

Figure 12. Temperature dependence of crystalline layer thickness in As_2Se_3 glass under nonisothermal conditions ($\beta = 1.5$ K/min) calculated by eqs 10, 7, and 4 (full line). Experimental data (points) were determined by a direct optical measurement on bulk samples (upper inset) and thin film (lower inset). Squares correspond to the bulk samples with initial height of 2 mm, circles correspond to the bulk sample with initial height of 1 mm, and triangles correspond to the thin film (1 μm). Dashed lines are plotted as guides to the eye.

There is a good agreement between these curves and experimental data obtained for the same heating rate (points) up to about 300 °C. At higher temperature, however, we should take into account that the sample thickness limits crystal size even for this relatively slow heating rate. This is shown in Figure 12 for thin film (triangles) and for the $l_0 = 1$ mm thick sample (circles). The crystalline layer growing in a sufficiently thick sample of $l_0 = 2$ mm (squares) can fully develop in the whole temperature range up to the melting point. Here, the sample deformation caused by viscous flow at higher temperature should be taken into account.

Figure 13 shows similar $l(T)$ dependences calculated by eqs 10, 7, and 4 for different heating rates within $0.1 \leq \beta \leq 3$ K/min. These results clearly show that the 2Dsg model provides a

DOI: 10.1021/acs.cgd.7b01001
Cryst. Growth Des. 2017, 17, 4990−4999

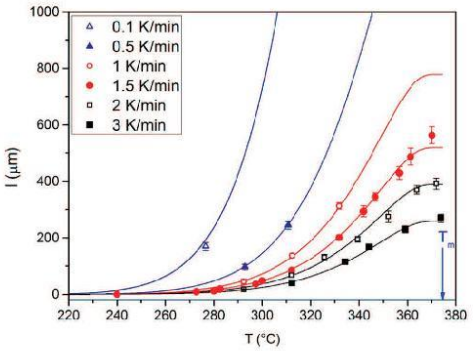

Figure 13. Temperature dependences of crystalline layer thickness in As_2Se_3 glass under nonisothermal conditions calculated by eqs 10, 7, and 4 for different heating rates (full lines). Experimental data (points) correspond to the bulk samples with initial height of 2 mm.

consistent description of As_2Se_3 crystal growth kinetics both for isothermal and for nonisothermal conditions.

The same nonisothermal model expressed can also be used for the description of growth pattern at the sample surface. For the steady state number of nuclei 316 ± 64 mm^{-2} formed after 60 min annealing at 233 °C (see Figure 1), assuming their random distribution at the sample surface, the most probable growth pattern at the sample surface can be calculated by eq 10. Figure 14 compares the result of such calculation for the

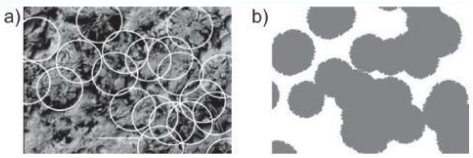

Figure 14. (a) SEM photograph of nucleated sample surface (etched) after nonisothermal heat treatment from 233 to 295 °C at heating rate 1.5 K/min. (b) The growth pattern calculated by eq 10 for the same thermal history assuming 5% variation in growth rate of individual crystals.

growth of these nuclei after nonisothermal heat treatment from 233 to 295 °C at a heating rate of 1.5 K/min with the SEM picture of etched sample surface after the same thermal treatment. It is seen that the 2Dsg model prediction is in good agreement with the experiment.

Activation Energy of Crystal Growth. Crystallization behavior is very often studied by a calorimetric method such as DSC. Most of the papers related to crystallization of glassy As_2Se_3 found in the literature are based exclusively or partly[10] on DSC. A key parameter elucidated from kinetic analysis of these data is the apparent activation energy that is essential for the description of experimental data by phenomenological approaches such as the Johnson−Mehl−Avrami (JMA) model.[45−48] The apparent activation energy E_a is usually determined by a well-known Kissinger method[49] from the temperature shift of the maximum of the DSC peak (T_p) with heating rate (β):

$$\frac{\mathrm{d}\ln(\beta/T_p^2)}{\mathrm{d}(1/T_p)} = -\frac{E_a}{R} \tag{11}$$

Svoboda[12] reported an averaged value of $E_a \cong 105$ kJ·mol^{-1} determined in this way for crystallization of slowly cooled and hyperquenched bulk and powdered samples of As_2Se_3 glass. Very similar values were also found by isothermal DSC crystallization experiments by Thornburg and Johnson[50] (∼120 kJ·mol^{-1}), Henderson and Ast[10] (∼125 kJ·mol^{-1}), and Černošková et al.[11] (∼101 kJ·mol^{-1}). In these studies, the JMA model was assumed where we can expect that nucleation effects do not play an important role and the apparent activation energy might be associated entirely with the crystal growth kinetics.

In a relatively narrow temperature range of DSC experiments, the crystal growth velocity can be described by a simple exponential function of temperature that should be linear in log scale. The activation energy of crystal growth then corresponds to the slope of such linear dependence:

$$\frac{\mathrm{d}\log(u)}{\mathrm{d}(1/T)} = -\frac{E_G}{2.303 \cdot R} \tag{12}$$

Figure 15 shows our experimental data for As_2Se_3 crystal growth velocity as well as the data reported by Henderson and

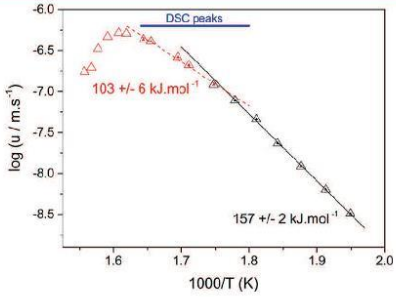

Figure 15. Determination of activation energy of As_2Se_3 crystal growth by eq 12 in two different temperature ranges. The marked region corresponds to the temperature range where nonisothermal DSC peaks are observed.

Ast.[10] In the high temperature range matching DSC experiments, the crystal growth data can be approximated by the dashed line with slope $E_G = 103 \pm 6$ kJ·mol^{-1}. This value is not so different from E_a determined from DSC experiments taking into account different types of measurements and experimental uncertainties involved.

At lower temperatures, the log u vs $1/T$ dependence can be approximated by the full line with slope $E_G = 157 \pm 6$ kJ·mol^{-1}. A very similar value was reported by Černošková et al.[11] (∼152 kJ·mol^{-1}) for isothermal DSC experiments in the same temperature range. Zmrhalová et al.[16] reported also a similar value of apparent activation energy (∼162 kJ·mol^{-1}) elucidated from interesting experiments where the sample deformation controlled by viscous flow and crystal growth is being monitored by thermomechanical analysis. Therefore, it seems that the apparent activation energy determined by DSC and TMA methods in fact corresponds to the value of activation energy of As_2Se_3 crystal growth E_G.

DOI: 10.1021/acs.cgd.7b01001
Cryst. Growth Des. 2017, 17, 4990−4999

The activation energy of viscous flow, defined as the slope of the linear plot in a narrow temperature range, is

$$\frac{\mathrm{d}\log(\eta)}{\mathrm{d}(1/T)} = \frac{E_\eta}{2.303 \cdot R} \quad (13)$$

By using eq 4 for As_2Se_3 VFT parameters, we can estimate the activation energy of viscous flow in the same low temperature range as $E_\eta = 233 \pm 3$ kJ·mol^{-1}. It can easily be shown that, for relatively high entropy of melting ($\Delta S_m = 7.56\ R$) and higher supercoolings ($\Delta T > 80$ K), the exponential term in eq 3 can be neglected. In a narrow temperature range, the decoupling parameter ξ then can be expressed by combining eqs 3, 12, and 13 as follows:

$$\xi = -\frac{\mathrm{d}\log(u)}{\mathrm{d}\log(\eta)} \cong \frac{E_G}{E_\eta} \quad (14)$$

The decoupling parameter calculated in this way for low temperature data is $\xi = 157/233 = 0.67$. This value agrees within the combined error limits with the value determined from log u_{kin} vs log η ($\xi = 0.692$) and by least-squares fit of eq 8 in three dimensional space ($\xi = 0.647$), which was also confirmed by fitting the $u(T)$ experimental data as described earlier.

CONCLUSIONS

The crystal growth velocity of spherulitic As_2Se_3 in a supercooled melt of the same composition was studied by optical microscopy and thermoanalytical methods in isothermal and nonisothermal conditions. It is shown that As_2Se_3 crystallizes as relatively open spherulitic arrays showing two different faceted growth morphologies. The time dependence of crystal size corresponding to both of these morphologies is the same, and its linearity suggests the crystal growth is controlled by interface kinetics. Crystal growth velocity was determined as the slope of these linear dependences. The experimental results presented in this paper considerably extend the previously reported range of crystal growth velocity.

All isothermal crystal growth velocity data can be well described by the standard two-dimensional surface nucleated growth model (2Dsg) including crystal growth viscosity decoupling ($\xi = 0.647$). The solid−liquid interface energy extracted from this model is in reasonable agreement with reported values for amorphous selenium as well as with qualitative microscopic wetting experiments. The 2Dsg model has been successfully applied for the description of crystal growth kinetics as well as the growth pattern at the sample surface in nonisothermal conditions. It is shown that the activation energy of crystal growth from microscopic experiments is in a good agreement with values obtained from thermoanalytical experiments. The ratio of the activation energy of crystal growth and the activation energy of viscous flow well corresponds to the decoupling parameter confirmed from the logarithmic crystal growth velocity vs viscosity dependence of all experimental data.

AUTHOR INFORMATION

Corresponding Author

*E-mail: jana.shanelova@upce.cz. Tel.: 00420466037346.

ORCID

Jana Shánělová: 0000-0001-5517-7434

Notes

The authors declare no competing financial interest.

ACKNOWLEDGMENTS

This work has been supported by the Czech Science Foundation under grant No. 16-10562S. The authors are indebted to Dr. Veronika Podzemná for SEM measurement and Prof. Aleš Růžička for X-ray diffraction analysis of As_2Se_3 single crystal.

REFERENCES

(1) Lucas, P.; Coleman, G. J.; Jiang, S. B.; Luo, T.; Yang, Z. Y. Chalcogenide glass fibers: Optical window tailoring and suitability for bio-chemical sensing. *Opt. Mater.* **2015**, *47*, 530−536.

(2) Yang, G.; Rouxel, T.; Troles, J.; Bureau, B.; Boussard-Pledel, C.; Houizot, P.; Sangleboeuf, J. C. Viscosity of As2Se3 Glass During the Fiber Drawing Process. *J. Am. Ceram. Soc.* **2011**, *94* (8), 2408−2411.

(3) Deng, D. H.; Liu, L.; Tuan, T. H.; Kanou, Y.; Matsumoto, M.; Tezuka, H.; Suzuki, T.; Ohishi, Y. Mid-infrared supercontinuum covering 3−10 mu m using a As2Se3 core and As2S5 cladding step-index chalcogenide fiber. *J. Ceram. Soc. Jpn.* **2016**, *124* (1), 103−105.

(4) Lucas, P.; Solis, M. A.; Le Coq, D.; Juncker, C.; Riley, M. R.; Collier, J.; Boesewetter, D. E.; Boussard-Pledel, C.; Bureau, B. Infrared biosensors using hydrophobic chalcogenide fibers sensitized with live cells. *Sens. Actuators, B* **2006**, *119* (2), 355−362.

(5) Snopatin, G. E.; Shiryaev, V. S.; Plotnichenko, V. G.; Dianov, E. M.; Churbanov, M. F. High-purity chalcogenide glasses for fiber optics. *Inorg. Mater.* **2009**, *45* (13), 1439−1460.

(6) Ravindren, S.; Gunasekera, K.; Tucker, Z.; Diebold, A.; Boolchand, P.; Micoulaut, M. Crucial effect of melt homogenization on the fragility of non-stoichiometric chalcogenides. *J. Chem. Phys.* **2014**, *140* (13), 134501.

(7) Guillevic, E.; Zhang, X. H.; Adam, J. L.; Ma, H. L.; Lucas, J.; Tariel, H. Fabrication of highly homogeneous As2Se3 glass under argon flow. *J. Non-Cryst. Solids* **2011**, *357* (15), 2897−2902.

(8) Kasap, S. O.; Tonchev, D. Glass transformation in vitreous As2Se3 studied by conventional and temperature-modulated differential scanning calorimetry. *J. Mater. Res.* **2001**, *16* (8), 2399−2407.

(9) Malek, J.; Shanelova, J. Structural relaxation of As2Se3 glass and viscosity of supercooled liquid. *J. Non-Cryst. Solids* **2005**, *351* (43−45), 3458−3467.

(10) Henderson, D. W.; Ast, D. G. Viscosity and Crystallization Kinetics of As2Se3. *J. Non-Cryst. Solids* **1984**, *64* (1−2), 43−70.

(11) Cernoskova, E.; Holubova, J.; Cernosek, Z. Crystallization kinetics of glassy As2Se3. *J. Therm. Anal. Calorim.* **1999**, *56* (1), 423−428.

(12) Svoboda, R.; Malek, J. Non-isothermal crystallization kinetics of As2Se3 glass studied by DSC. *Thermochim. Acta* **2014**, *579*, 56−63.

(13) Chovanec, J.; Chromcikova, M.; Pilny, P.; Shanelova, J.; Malek, J.; Liska, M. As2Se3 melt crystallization studied by quadratic approximation of nucleation and growth rate temperature dependence. *J. Therm. Anal. Calorim.* **2013**, *114* (3), 971−977.

(14) Holubova, J.; Cernosek, Z.; Cernoskova, E. A detailed study of isothermal crystallization of As2Se3 undercooled liquid. *J. Therm. Anal. Calorim.* **2013**, *114* (3), 997−1002.

(15) Svoboda, R.; Malek, J. Nucleation in As2Se3 glass studied by DSC. *Thermochim. Acta* **2014**, *593*, 16−21.

(16) Zmrhalova, Z.; Pilny, P.; Svoboda, R.; Shanelova, J.; Malek, J. Thermal properties and viscous flow behavior of As2Se3 glass. *J. Alloys Compd.* **2016**, *655*, 220−228.

(17) Sheldrick, G. M. Crystal structure refinement with SHELXL. *Acta Crystallogr., Sect. C: Struct. Chem.* **2015**, *71*, 3−8.

(18) O'Hare, P. A. G.; Lewis, B. M.; Susman, S.; Volin, K. J. Standard Molar Enthalpies of Formation and Transition at the Temperature 298.15 K and Other Thermodynamic Properties of the Crystalline and Vitreous Forms of Arsenic Sesquiselenide (As2Se3) - Dissociation Enthalpies of As-Se Bonds. *J. Chem. Thermodyn.* **1990**, *22* (12), 1191−1206.

DOI: 10.1021/acs.cgd.7b01001
Cryst. Growth Des. 2017, 17, 4990−4999

(19) Stergiou, A. C.; Rentzeperis, P. J. The crystal structure of arsenic selenide, As2Se3. *Z. Kristallogr.* **1985**, *173* (3−4), 185−191.
(20) Jackson, K. A.; Uhlmann, D. R.; Hunt, J. D. On the nature of crystal growth from the melt. *J. Cryst. Growth* **1967**, *1* (1), 1−36.
(21) Kirkpatrick, R. J. Crystal Growth from the Melt: A Review. *Am. Mineral.* **1975**, *60*, 798−814.
(22) Ediger, M. D.; Harrowell, P.; Yu, L. Crystal growth kinetics exhibit a fragility-dependent decoupling from viscosity. *J. Chem. Phys.* **2008**, *128* (3), 034709.
(23) Blachnik, R.; Hoppe, A. Glass-Transition and Specific-Heats in the Systems P-S, P-Se, As-S and As-Se. *J. Non-Cryst. Solids* **1979**, *34* (2), 191−201.
(24) Schnaus, U. E.; Moynihan, C. T.; Gammon, R. W.; Macedo, P. B. The Relation of Glass Transition Temperature to Vibrational Characteristics of Network Glasses. *Phys. Chem. Glasses* **1970**, *11* (6), 213−218.
(25) Tarasov, V. V.; Zhdanov, V. M.; Mal'tsev, A. K.; Dembovskii, S. A. Dynamics of the vibrations of selenium and arsenic triselenide in crystalline and glassy states from low-temperature specific heat data. *Zh. Fiz. Khim.* **1969**, *43* (2), 467−471.
(26) Blachnik, R.; Hoppe, A.; Wickel, U. The Systems Arsenic-Sulfur and Arsenic-Selenium and the Thermodynamical Data of Their Compounds. *Z. Anorg. Allg. Chem.* **1980**, *463* (4), 78−90.
(27) Thompson, C. V.; Spaepen, F. Approximation of the free-energy change on crystallization. *Acta Metall.* **1979**, *27* (12), 1855−1859.
(28) Chernov, A. P.; Dembovskii, S. A.; Machova, V. I. Viscosity and Structure of As_2X_3-AsI_3 glasses (Russ.). *Izv. Akad. Nauk SSSR, Neorg. Mater.* **1970**, *6* (4), 823−825.
(29) Nemilov, S. V.; Petrovskii, G. T. Study of Viscosity of Glassy System Se-As (Russ.). *J. Appl. Chem.-USSR* **1963**, *36*, 977−981.
(30) Kunugi, M.; Ota, R.; Suzuki, M. Viscosity of glasses in the system As-Se, As-Se-S, As-Se-Te and As-Se-Tl (jpn.). *J. Soc. Mater. Sci., Jpn.* **1970**, *19* (197), 145−150.
(31) Orlova, G. M.; Udalov, S. S.; Manachova, E. N. Elastic and Thermal Properties of AsSe-TlSe and As_2Se_3-Tl_2Se Glasses (Russ.). *Fiz. Khim. Stekla* **1985**, *11* (2), 215−218.
(32) Webber, P. J.; Savage, J. A. Measurement of the Viscosity of Chalcogenide Glasses by a Parallel Plate Technique. *J. Mater. Sci.* **1981**, *16* (3), 763−766.
(33) Musgraves, J. D.; Wachtel, P.; Novak, S.; Wilkinson, J.; Richardson, K. Composition dependence of the viscosity and other physical properties in the arsenic selenide glass system. *J. Appl. Phys.* **2011**, *110* (6), 063503−6.
(34) Webber, P. J.; Savage, J. A. Some physical properties of Ge-As-Se infrared optical glasses. *J. Non-Cryst. Solids* **1976**, *20*, 271−283.
(35) Kolomiets, B. T.; Pozdnev, V. P. Viscosity of As_2Se_3-As_2Te_3 glassy semiconductors (Russ.). *Sov. Phys.-Sol. State* **1960**, *2*, 28−34.
(36) Tverjanovich, A. S.; Skorobogatova, I. Viscosity of As_2Se_3-Tl_2Se melts (Russ.). *Fiz. Khim. Stekla* **1990**, *16* (3), 369−373.
(37) Kadoun, A.; Chaussemy, G.; Fornazero, J.; Mackowski, J. M. Kinematic Viscosity of As_xSe_{1-x} Glass Forming Liquids. *J. Non-Cryst. Solids* **1983**, *57* (1), 101−108.
(38) Ananichev, V. A.; Demidov, A. I.; Kudryavtsev, A. N. Coefficient of thermal expansion and density of glassy melts of the systems As_2S_3-$TlAsS_2$ and As_2Se_3-$TlAsSe_2$. *Fiz. Khim. Stekla* **1985**, *11* (2), 224−227.
(39) Turnbull, D. Formation of crystal nuclei in liquid metals. *J. Appl. Phys.* **1950**, *21*, 1022−1028.
(40) Myers, M. B.; Felty, E. J. Heats of fusion of A2B3 compounds As2S3, As2Se3, As2Te3, and Sb2S3. *J. Electrochem. Soc.* **1970**, *117* (6), 818−820.
(41) Shtukenberg, A. G.; Punin, Y. O.; Gunn, E.; Kahr, B. Spherulites. *Chem. Rev.* **2012**, *112* (3), 1805−1838.
(42) Malek, J.; Bartak, J.; Shanelova, J. Spherulitic Crystal Growth Velocity in Selenium Supercooled Liquid. *Cryst. Growth Des.* **2016**, *16* (10), 5811−5821.
(43) Kelton, K. F. Crystal nucleation in liquids and glasses. *Solid State Phys.* **1991**, *45*, 75−177.
(44) Mishinov, S. V.; Churbanov, M. F.; Shiryaev, V. S.; Snopatin, G. E. Wetting, surface tension, and work of adhesion of As2S3 and As2Se3 glass melts to quartz glass. *Glass Phys. Chem.* **2016**, *42* (6), 542−546.
(45) Johnson, W. A.; Mehl, R. F. Kinetics in processes of nucleation and growth. *Trans. AIME* **1939**, *135* (8), 416−458.
(46) Avrami, M. Kinetics of Phase Change. I General Theory. *J. Chem. Phys.* **1939**, *7* (12), 1103−1112.
(47) Avrami, M. Kinetics of Phase Change. II Transformation-Time Relations for Random Distribution of Nuclei. *J. Chem. Phys.* **1940**, *8* (2), 212−224.
(48) Avrami, M. Granulation, Phase Change, and Microstructure Kinetics of Phase Change. III. *J. Chem. Phys.* **1941**, *9* (2), 177−184.
(49) Kissinger, H. E. Reaction kinetics in differential thermal analysis. *Anal. Chem.* **1957**, *29* (11), 1702−1706.
(50) Thornburg, D. D.; Johnson, R. I. Thermal-analysis of bulk amorphous arsenic triselenide. *J. Non-Cryst. Solids* **1975**, *17* (1), 2−8.

DOI: 10.1021/acs.cgd.7b01001
Cryst. Growth Des. 2017, 17, 4990−4999